PhD Thesis

Role of CGI-58 in macrophages and Autophagy in lipase-deficient macrophages

submitted by
Mag. rer. nat.
Madeleine GÖRITZER

for the Academic Degree of
Doctor of Philosophy
(PhD)

at the

Medical University of Graz
Institute of Molecular Biology and Biochemistry

under the Supervision of
ao. Univ. Prof.^{in} Mag.^{a} Dr.^{in} rer. nat. Dagmar Kratky

2015

„Wichtig ist, dass man nicht aufhört zu fragen."

Albert Einstein

Für mich

Declaration

I hereby declare that this thesis is my own original work and that I have fully acknowledged by name all of those individuals and organizations that have contributed to the research for this thesis. Due acknowledgement has been made in the text to all other material used.

Throughout this thesis and in all related publications I followed the guidelines of "Good Scientific Practice".

Please note that parts of this thesis have already been published or accepted for publication:

Deletion of CGI-58 or adipose triglyceride lipase differently affects macrophage function and atherosclerosis

Goeritzer M, Schlager S, Radovic B, Madreiter CT, Rainer S, Thomas G, Lord CC, Sacks J, Brown AL, Vujic N, Obrowsky S, Sachdev V, Kolb D, Chandak PG, Graier W, Sattler W, Brown JM, Kratky D.

Journal of Lipid Research. 2014. 55: 2562-2575

Active autophagy but not lipophagy in macrophages with defective lipolysis

Goeritzer M*, Vujic N*, Schlager S., Chandak PG, Korbelius M, Gottschalk B, Leopold C, Obrowsky S, Rainer S, Doddapattar P, Aflaki E, Wegscheider M, Sachdev V, Graier WF, Kolb D, Radovic B†, Kratky D†.

Biochimica et Biophysica Acta (BBA) - Molecular and Cell Biology of Lipids.

In press, *equal contribution, †equal corresponding authors

Graz, June 2015

_____

Madeleine Göritzer

Acknowledgement

First of all I would like to thank Dagmar Kratky for giving me the possibility to do my PhD under her great supervision. Thank you so much for your support and for being just like you are. You are the only PI I know who is always there for her students.

I would like to thank all our current and former lab members, especially: Silvia Rainer for being a very good friend. Thank you for your great help during my PhD. Without you nothing would work in the lab. Nemanja Vujic for being a great seatmate. We always had a lot of fun. Stefanie Schlager for being a good friend. It was always nice to share a room with you. Sascha Obrowsky, you always came once a day to visit me in the lab and we also always had a lot of fun. Thank you, Melanie Korbelius and Christina Leopold for your friendship and for your nice self-made presents and cakes. Thank you, Anton Ibovnik, you were always there when help was needed. Thank you, Isabella Hindler, for taking care of my mice. Thank you, Prakash Chandak, Prakash Doddapattar, Martin Wegscheider, Jay Patankar, Branislav Radovic, Vinay Sachdev, Sabrina Rexeis and Madalina-Cristina Duta-Mare.

Furthermore, I would like to thank our collaborators Mark J. and Amanda Brown, Wolfgang Sattler and Helga Reicher, my thesis committee members Günter Hämmerle and Juliane Bogner-Strauss, as well as my mentor Dagmar Kolb for their support and fruitful discussions. I also would like to thank Christoph Binder and Miranda van Eck for giving me the chance to work in their labs for my research stay abroad. Thank you, Sabrina Gruber, for helping me with experiments and for nice discussions during lunch.

Of course, I thank a lot our funding sources, the FWF, the SFB Lipotox and the Medical University of Graz, as well as the DK-Program “Metabolic and Cardiovascular Disease”. I also would like to thank Karin Osibow, the administrator of this DK-Program, for all her help and for organizing courses, stays abroad and much more.

Finally, I would like to thank my family, especially my parents and Markus, for always encouraging me and being there for me during my PhD studies.

Table of Contents

Abbreviations

A0	ATGL-knockout
A0H0	ATGL-HSL-double knockout
ABCA1	ATP-binding cassette transporter A1
ABCG1	ATP-binding cassette transporter G1
ABHD5	α/β-hydrolase domain containing 5
AEC	3-Amino-9-ethylcarbazole
Ai	Atglistatin (ATGL-inhibitor)
Aox	Fatty acyl-CoA oxidase
ApoB	Apolipoprotein B
ApoE	Apolipoprotein E
APS	Ammonium persulfate
Arg-1	Arginase-1
ASO	Antisense oligonucleotide
ATF4	Activating transcription factor 4
ATF6	Activating transcription factor 6
ATGL	Adipose triglyceride lipase
ATP	Adenosine triphosphate
AV	Autophagic vacuole
AVd	Degradative autophagic vacuole
Baf	Bafilomycin A1
BAT	Brown adipose tissue
Bax	Bcl-2-associated X protein
Bcl-XL	B-cell lymphoma extra large
BSA	Bovine serum albumin
CAD	Coronary artery disease
Ccl5	Chemokine (C-C motif) ligand 5
Cd36	Cluster of differentiation 36

CDS	Chanarin-Dorfman syndrome
CE	Cholesteryl ester
CGI-58	Comparative gene identification-58
CHOP	CCAAT/enhancer-binding protein homologous protein
Complex III	Ubiquinol-cytochrome C reductase
Complex Va	ATP5A
COX4	Cyclooxygenase 4
Cpt1α	Carnitine palmitoyl-transferase 1α
Cq	Chloroquine
CXCL-1	CXC-chemokine ligand 1
DC	Dendritic cell
DEPC	Diethyl pyrocarbonate
DG	Diglyceride
DGAT1	acyl-CoA:diacylglycerol acyltransferase 1
DGAT2	acyl-CoA:diacylglycerol acyltransferase 2
DKO	Double knock-out
DMEM	Dulbecco's modified eagle medium
DTT	Dithiothreitol
E. coli	*Escherichia coli*
EC	Endothelial cell
EDTA	Ethylendiaminetetraacetic acid
eIF2α	Translation initiation factor 2α
ELISA	Enzyme Linked Immunosorbent Assay
Emr1	EGF-like module-containing mucin-like hormone receptor-like 1
ER	Endoplasmic reticulum
ERAD	ER-associated degradation
Erdj4	ER DnaJ-like 4
FA	Fatty acid

FFA	Free fatty acid
FAME	Fatty acid methyl ester
FAO	Fatty acid oxidation
FC	Free cholesterol
FCCP	*p*-trifluoromethoxyphenylhydrazone
FCS	Fetal calf serum
GAPDH	Glycerinaldehyd-3-phosphat-Dehydrogenase
GC	Gas chromatography
GF	growth factor
GM-CSF	Granulocyte-macrophage colony stimulating factor
Gro-1	Chemokine (C-X-C motif) ligand 1
Grp78/BIP	Immunoglobulin heavy chain binding protein
H0	HSL-knockout
HBSS	Hank's Balanced Salt Solution
HDL	High-density lipoprotein
HF/HCD	High-fat/high-cholesterol diet
HFD	High-fat diet
Hi	76-0079 (HSL-Inhibitor)
HL	Hepatic lipase
HMGCoAR	3-hydroxy-3-methylglutaryl-coenzyme A
HPF	High-pressure freezing
HPRT	Hypoxanthine-guanine phosphoribosyltransferase
Hsc70	Chaperone protein heat shock protein 70
HSL	Hormone-sensitive lipase
IDL	Intermediate-density lipoproteins
IFN-γ	Interferon-γ
IL-10	Interleukin-10
IL-1β	Interleukin-1β

IL-6	Interleukin-6
i.p.	Intraperitoneally
IRE1α	Inositol-requiring kinase 1
KD	Knockdown
LAL	Lysosomal acid lipase
LAMP-2A	Lysosomal-associated membrane protein-2A
LC3	Microtubule-associated protein light chain 3
LC3-I	Cytosolic LC3
LC3-II	Membrane-bound LC3
LD	Lipid droplet
Ldlr	Low-density lipoprotein receptor
LPA	Lysophosphatidic acid
LPAAT	Lysophosphatidic acid acyltransferase activity
LPDS	Lipoprotein-deficient serum
LPL	Lipoprotein lipase
LPS	Lipopolysaccharide
MAM	mitochondrial-associated membranes
Mcad	Medium chain acyl-CoA dehydrogenase
Mcl-1	Myeloid cell leukemia 1
Mcp-1	Monocyte chemoattractant protein-1
Mcp-2	Monocyte chemotactic protein-2
M-CSF	Macrophage colony-stimulating factor
MFI	Mean fluorescence intensity
MG	Monoacylglycerol
MGL	Monoacylglycerol lipase
MMP	Matrix metalloproteinase
MoMa-2	Monoclonal antibody to macrophages-2
Mrc-1	Mannose receptor, C type 1
mRNA	Messenger RNA

NLSD	Neutral lipid storage disease
NLSDI	Neutral lipid storage disease with ichthyosis
NLSDM	Neutral lipid storage disease with cardiac myopathy
OA	Oleic acid
OCR	Oxygen consumption rate
OCT	Optimal cutting temperature
oxLDL	Oxidized LDL
P/S	Penicillin/streptomycin
PA	Phosphatidic acid
PBS	Phosphate buffered saline
Pdi	Protein disulfide isomerase
PERK	Double-stranded RNA-activated protein kinase-like endoplasmic reticulum kinase
PI	Propidium iodide
PKA	Protein kinase A
PPARα	Peroxisome proliferator-activated receptor alpha
qPCR	Quantitative real time PCR
RCT	Reverse cholesterol transport
RER	Rough endoplasmic reticulum
RIPA	Radioimmunoprecipitation assay
ROS	Reactive oxygen species
RT	Room temperature
SAA	Serum amyloid A
SAP	Serum amyloid P component
SD	Standard deviation
SDS	Sodium dodecyl sulfate
SDS-PAGE	SDS-polyacrylamide gel electrophoresis
SEM	Standard error of mean
SER	Smooth endoplasmic reticulum

SM	Skeletal muscle
SMC	Smooth muscle cell
SRA	Scavenger receptor A
SrB1	Scavenger receptor class B type 1
SREBP2	Sterol-regulatory element-binding protein 2
TC	Total cholesterol
TEMED	Tetramethylethylenediamine
TG	Triglyceride
TLC	Thin layer chromatography
TNFα	Tumor necrosis factor α
UPR	Unfolded-protein response
Vlcad	Very long chain acyl-CoA dehydrogenase
VLDL	Very low-density lipoprotein
WAT	White adipose tissue
WBC	White blood cell
WTD	Western type diet
XBP1	X-box-binding protein 1
XBP1s	Spliced XBP1

Abstract

Cellular triglyceride (TG) stores are efficiently hydrolyzed by adipose triglyceride lipase (ATGL). Its co-activator comparative gene identification-58 (CGI-58) strongly increases ATGL-mediated TG catabolism in cell culture experiments. In humans, mutations of CGI-58 cause Chanarin-Dorfman-Syndrome resulting in ichthyosis and TG accumulation in essentially all tissues. Since CGI-58 knockout (*-/-)* mice die soon after birth due to a severe skin barrier defect we generated myeloid-specific CGI-58 (macCGI-58)*-/-* mice to elucidate the consequences of CGI-58 deficiency in murine macrophages. These mice are viable with no apparent changes in skin phenotype. CGI-58-/- macrophages accumulate intracellular TG-rich lipid droplets (LDs) and have decreased phagocytic capacity, comparable to ATGL-/- macrophages. In contrast to ATGL-/- macrophages, however, CGI-58-/- macrophages have intact mitochondria and show no indications of mitochondrial apoptosis and endplasmic reticulum (ER) stress. Another notable difference is the fact that CGI-58-/- macrophages adopted an M1-like phenotype *in vitro*.

Finally, we investigated atherosclerosis susceptibility in macCGI-58/ApoE-double knockout (DKO) animals. In response to high fat/high cholesterol diet feeding, DKO animals showed comparable plaque formation in aortic root sections as observed in ApoE*-/-* mice. In agreement, antisense oligonucleotide-mediated knockdown of CGI-58 in low-density lipoprotein receptor-/- mice did not alter atherosclerosis burden in the aortic root.

These results suggest that (despite comparable TG accumulation by ATGL and CGI-58 deficiency) macrophage function and atherosclerosis susceptibility differ fundamentally in these two animal models with disturbed TG homeostasis.

During autophagy, autophagosomes fuse with lysosomes to degrade damaged organelles and misfolded proteins. Breakdown products are released into the cytosol and contribute to energy and metabolic building block supply, especially during starvation. Lipophagy has been defined as the autophagy-mediated degradation of LDs by lysosomal acid lipase. Most organs and cells, including

macrophages, lacking ATGL accumulate TGs, resulting in reduced intracellular free fatty acid concentrations. Macrophages deficient in hormone-sensitive lipase (*H0*) do not accumulate TG albeit reduced *in vitro* TG hydrolase activity. We hypothesized that autophagy is activated in lipase-deficient macrophages to counteract their energy deficit. We therefore generated mice with loss of both ATGL and HSL (*A0H0*). Macrophages from *A0H0* mice showed 73% reduced neutral TG hydrolase activity, resulting in TG-rich LD accumulation. Increased expression of cathepsin B, accumulation of LC3-II, reduced expression of p62, and increased DQ-BSA dequenching suggest intact autophagy and functional lysosomes in *A0H0* macrophages. Markedly decreased acid TG hydrolase activity and lipid flux independent of bafilomycin A1 treatment, however, argue against effective lysosomal degradation of LDs in *A0H0* macrophages. We conclude that autophagy of proteins and cell organelles but not of LDs is active as a compensatory mechanism to circumvent and balance the reduced availability of energy substrates in *A0H0* macrophages.

Zusammenfassung

Zelluläre Triglyzerid (TG)-Speicher werden effizient von der Adipose Triglyzerid Lipase (ATGL) abgebaut. Ihr Co-Aktivator „comparative gene identification-58“ (CGI-58) steigert den Abbau von TG durch ATGL in Zellkultur-Experimenten. In Menschen verursacht eine Mutation von CGI-58 das Chanarin-Dorfman-Syndrom, welches zu Ichthyose und zu einer TG Akkumulierung in sämtlichen Geweben führt. Da CGI-58-/- Mäuse kurz nach der Geburt aufgrund eines schweren Hautbarrieredefekts sterben, generierten wir myeloid-spezifische CGI-58-/- (macCGI-58) Mäuse um die Konsequenzen von CGI-58-Defizienz in Makrophagen von Mäusen zu untersuchen. Diese Mäuse sind lebensfähig und weisen keine sichtbaren Veränderungen der Haut auf. CGI-58-/- Makrophagen akkumulieren intrazellulär TG-reiche Lipidtropfen und zeigen eine verringerte Phagozytose-Fähigkeit, welche mit denen von ATGL-/- Makrophagen vergleichbar ist. Im Gegensatz zu ATGL-/- Makrophagen haben CGI-58-/- Makrophagen jedoch intakte Mitochondrien. Außerdem fanden wir keine Anzeichen von mitochondrialer Apoptose oder ER Stress. Ein weiterer bemerkenswerter Unterschied ist auch der M1-Phänotyp, den CGI-58-/- Makrophagen *in vitro* aufweisen.

Ferner untersuchten wir die Atherosklerose-Suszeptibilität in macCGI-58/ApoE-doppelknockout (DKO) Mäusen. Nach Fütterung einer fett- und cholesterinreichen, zu Atherosklerose-führenden Diät, zeigten DKO- und ApoE-/- Mäuse eine vergleichbare Plaqueentwicklung in der Aortenwurzel. Dementsprechend führte auch ein durch „antisense oligonucleotide“ Behandlung herbeigeführter Knockdown von CGI-58 in „low-density lipoprotein receptor-/-“ Mäusen zu keinem Unterschied der Atherosklerosesuszeptibilität.

Diese Resultate weisen darauf hin, dass sich (trotz vergleichbarer TG Akkumulierung durch ATGL und CGI-58-Defizienz) die Makrophagenfunktion und Atherosklerosesuszeptibilität in diesen zwei Tiermodellen mit gestörter TG Homöostase wesentlich voneinander unterscheiden.

Als Autophagie wird die Fusion von Autophagosomen und Lysosomen bezeichnet um beschädigte Organelle oder falsch gefaltete Proteine abzubauen. Abbauprodukte werden ins Zytosol abgegeben und tragen speziell im Falle eines geringeren Nährstoffangebots zur Energie- und metabolischen Bausteinversorgung bei. Lipophagie bezeichnet den Autophagie-mediierten Abbau von Lipidtropfen durch die lysosomale saure Lipase. Die meisten Organe und Zellen (inklusive Makrophagen), denen die ATGL fehlt, akkumulieren TG, woraus eine geringere intrazelluläre freie Fettsäurekonzentration resultiert. Makrophagen, denen die hormonsensitive Lipase (HSL) fehlt (*H0*), akkumulieren trotz geringerer *in vitro* TG Hydrolaseaktivität keine TG. Wir vermuteten, dass Autophagie in lipase-defizienten Makrophagen aktiviert wird um dem Energiedefizit entgegenzuwirken. Um dies heraufzufinden generierten wir ATGL- und HSL-defiziente Mäuse (*A0H0*). Makrophagen von *A0H0*-Mäusen zeigten eine um 73% reduzierte neutrale TG Hydrolaseaktivität, die zu einer TG-reichen Lipidtropfen-Akkumulierung führte. Eine erhöhte Cathepsin B Expression, eine Akkumulierung von LC3-II Protein, eine reduzierte Proteinexpression von p62 und ein erhöhtes DQ-BSA Dequenching weisen auf eine intakte Autophagie sowie auf funktionelle Lysosomen in *A0H0*-Makrophagen hin. Eine deutlich verminderte saure TG Hydrolaseaktivität und ein von der Bafilomycin A1 Behandlung unabhängiger Lipidfluss argumentieren jedoch gegen einen effektiven lysosomalen Abbau von Lipidtropfen in *A0H0*-Makrophagen. Daraus schließen wir, dass Autophagie von Proteinen und Zellorganellen, aber nicht Autophagie von Lipidtropfen, ein aktiver, kompensatorischer Mechanismus in *A0H0*-Makrophagen ist um die reduzierte Energieverfügbarkeit zu verhindern oder auszugleichen.

1. Introduction

1.1 Lipolysis

All organisms use fatty acids (FAs) for energy substrates or as precursors for membrane and signaling lipids. [reviewed in (1)] Excessive cellular concentrations of FAs are toxic to cells and tissues. Due to their amphipathic nature, FAs act as detergents, damage cell and organelle membranes, and perturb the cellular acid/base homeostasis. To avoid lipotoxicity, FAs are esterified with glycerol to form triglycerides (TGs), which are stored in lipid droplets (LDs). (2, 3) TGs are not capable of traversing biological membranes, and need to be cleaved by TG hydrolases, the so called “lipases”, before moving in or out of cells. This process is generally named “lipolysis”. Furthermore, there are known two different types of lipolysis: **intravascular lipolysis,** which degrades lipoprotein-associated TGs to FAs for their subsequent uptake by parenchymal cells (4) and **intracellular lipolysis,** which generates FAs and glycerol for their release (in case of white adipose tissue) or use by cells (in case of other tissues). (5)

1.1.1 Intravascular lipolysis

Intravascular lipolysis is the hydrolysis of TG carried out within plasma lipoproteins. Dietary lipids are packed into chylomicrons by intestinal enterocytes. These chylomicrons enter the lymphatics and quickly reach the bloodstream. Chylomicrons transport TGs to adipose tissue for storage and to vital tissues [heart, skeletal muscle (SM)] for use as energy fuel. The liver secretes very low-density lipoprotein (VLDL) which serves to redistribute TGs to adipose tissue, heart, and muscle. Lipoprotein lipase (LPL) hydrolyzes TG in VLDLs and chylomicrons on the luminal face of capillaries. LPL products, FAs, and monoacylglycerols (MGs), traverse the endothelium and are taken up by the underlying parenchymal cells (adipocytes and myocytes). MGs are further hydrolyzed by monoglyceride lipase (MGL), generating FAs and glycerol. FAs generated by LPL are re-esterified to TG or oxidized. Glycerol is resecreted and transported to the liver. (2, 6)

1.1.2 Intracellular lipolysis

Intracellular lipolysis of TGs in cytoplasmic LDs fulfills two important functions. In white adipose tissue (WAT), lipolysis generates FAs and glycerol that are released into the blood for transport to other tissues, for instance to heart and SM, liver and brown adipose tissue (BAT). This release of FAs and glycerol during fasting is exclusively happening in WAT. Other tissues do not release the products of TG hydrolysis, but use them for lipid synthesis or oxidation. The main enzymes in intracellular lipolysis are the same in adipose and non-adipose tissues. [reviewed in (1)] Adipose triglyceride lipase (ATGL) is responsible for TG hydrolysis (7-9), hormone-sensitive lipase (HSL) for diglyceride (DG) hydrolysis to MGs (5, 10), and MGL catalyzes the last step ending in the formation of glycerol and FA. HSL exhibits broader substrate specificity, also hydrolyzing TGs, cholesteryl esters (CEs), MGs, and retinyl esters in addition to DGs (Fig. 1). (5)

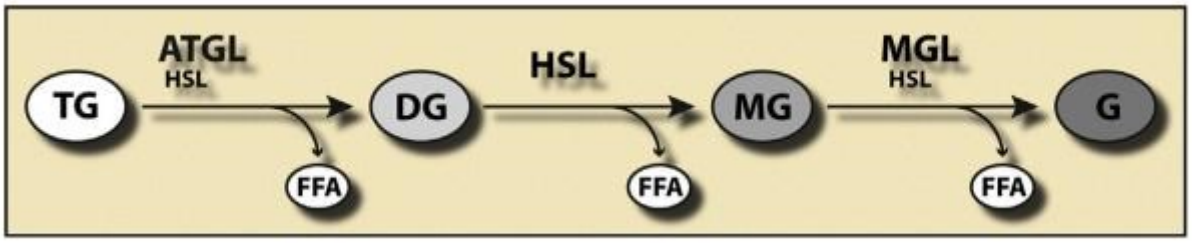

Figure 1: Breakdown of triglycerides during lipolysis. (11)

1.1.2.1 HSL

The enzyme responsible for DG hydrolysis is activated by catecholamines via phosphorylation by cAMP-dependent protein kinase A. (12) HSL-knockout (-/-) mice are viable and have reduced WAT. (13) Male mice are not fertile. (10) HSL was shown to be expressed in macrophages and foam cells. Interestingly, although HSL-/- macrophages lack CE hydrolase activity, there is no change in CE concentrations. (14) HSL overexpression in macrophages led to decreased CE concentrations due to a clearly enhanced CE hydrolase activity. (15) HSL was long thought to be the major enzyme responsible for complete lipolysis. (5) However, the finding that HSL-/- mice accumulate DG, but not TG in WAT clearly indicated that there must be another enzyme responsible for TG hydrolysis. (16) HSL was also shown to play a role in atherosclerotic plaque formation. Low-

density lipoprotein receptor (Ldlr)-/- mice transplanted with HSL-/- bone marrow showed increased plaque formation due to increased ACAT-1 activity, which led to CE accumulation in macrophages. (17)

1.1.2.2 ATGL

ATGL, first described in 2004, catalyzes the initial step of TG hydrolysis, converting TGs to DGs. (7-9) Efficient ATGL enzyme activity requires the co-activator comparative gene identification-58 (CGI-58). (18) ATGL hydrolyzes TGs selectively at the sn-2 position of the glycerol backbone. However, upon stimulation of the enzyme by CGI-58 [which increases the activity of ATGL up to 20-fold (18)], the stereo/regioselectivity of ATGL broadens to the sn-1 position, leading to increased FA release. (19) How ATGL is co-activated by CGI-58 is still elusive. It could be that CGI-58 affects substrate presentation, changes the conformation of ATGL or removes its substrate. However, it was found that both LD binding and ATGL binding are required for efficient ATGL activation by CGI-58. (20) Granneman *et al.* (21, 22) showed that the activation of ATGL is hormone-dependent. In unstimulated cells, CGI-58 is not available for ATGL activation since it is bound to perilipin-1. β-adrenergic stimulation leads to perilipin-1 phosphorylation by protein kinase A (PKA) and the dissociation of CGI-58, allowing CGI-58 to bind to and activate ATGL. Mutations in perilipin-1 prevent CGI-58 binding and lead to unrestrained lipolysis and partial lipodystrophy in humans. (23)

ATGL-/- mice show increased TG deposition in several tissues and exhibit mild obesity caused by enlarged adipose LDs. (24) Severe fat accumulation in the cardiac muscle in these mice leads to cardiac insufficiency and premature death. (25) When Ldlr-/- mice were transplanted with ATGL-/- bone marrow mice showed a decreased plaque formation compared to controls due to decreased plasma interleukin-6 (IL-6) and monocyte chemoattractant protein-1 (Mcp-1) concentrations, a reduced amount of macrophages in the plaque, and a reduced circulating white blood cell (WBC) number. (26)

The role of ATGL in macrophages has already been extensively studied. It was shown that ATGL-/- macrophages accumulate TGs, show a decreased TG hydrolase activity and phagocytic capacity, induce endoplasmic reticulum (ER) stress, are more apoptotic, and migrate less (Fig. 2). (27-31)

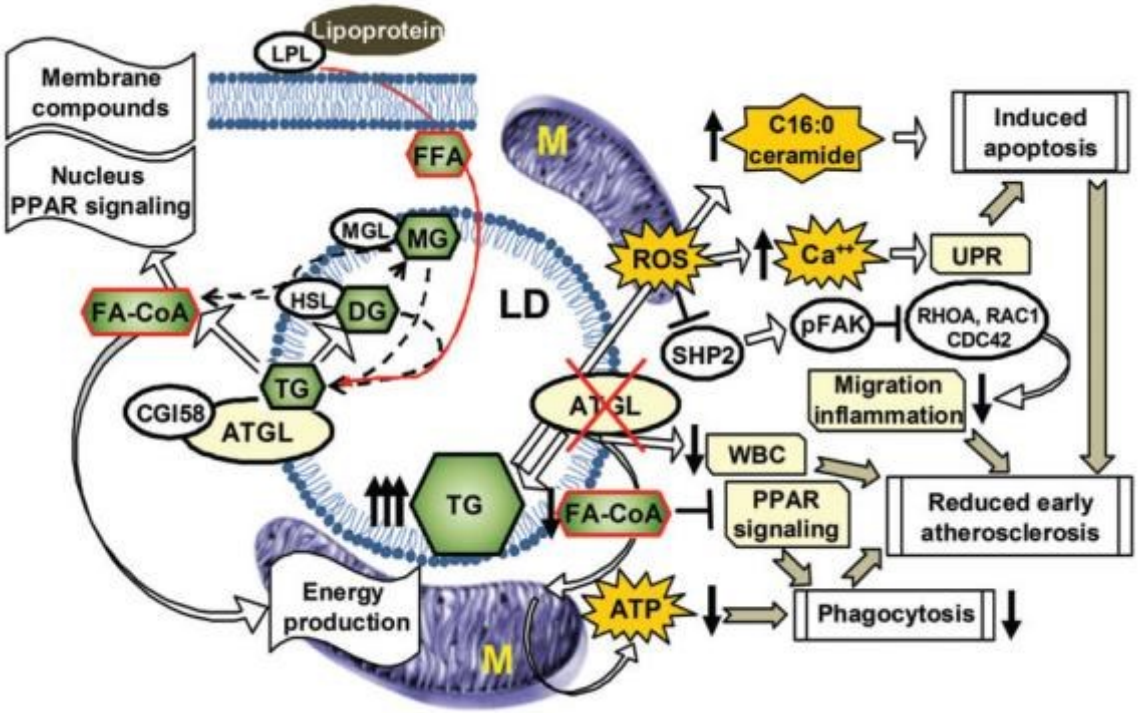

Figure 2: Role of ATGL in macrophages. Lack of ATGL in macrophages results in TG accumulation. Reduced free FA (FFA) levels lead to decreased peroxisome proliferator-activated receptor (PPAR) signaling, reduced ATP levels and impaired phagocytosis. Increased reactive oxygen species (ROS) levels due to Rac2 activation inactivate Src homology 2-containing phosphotyrosine phosphatase (SHP-2) resulting in sustained phosphorylation and activation of FAK, which in turn perturbs the disassembly of the cytoskeleton leading to enhanced cell spreading with concomitant impaired migration capacity. Moreover, ATGL deficiency results in ER Ca^{2+} depletion leading to elevated cytosolic Ca^{2+} levels, which induces the unfolded protein response (UPR). Increased C16:0 ceramide concentrations cause dysfunctional mitochondria and activate the mitochondrial apoptosis pathway. Reduced numbers of WBCs, decreased migration and inflammation, impaired phagocytosis, and induction of apoptosis lead to reduced atherosclerosis susceptibility. [reviewed in (31)]

1.1.2.3 CGI-58

Human and murine CGI-58, also annotated as α/β-hydrolase domain containing 5 (ABHD5), display 94% sequence identity and consist of 349 and 351 amino acids,

respectively. Murine CGI-58 contains a catalytic triad within the α/β-hydrolase domain, but the nucleophilic serine is replaced by an asparagine, which makes CGI-58 unable to hydrolyze lipids. (32) However, CGI-58 was shown to be the co-activator of ATGL. The N-terminal tryptophan-rich region of CGI-58 was discovered to be important for LD binding and ATGL activation. However, deletion of this N-terminal region abolished LD binding but did not affect its interaction with ATGL. It was suggested that CGI-58 might directly interact with the LD, thereby enabling access of ATGL to TG or promoting interaction of CGI-58 with ATGL at the LD. (20, 33) In 2008 and 2010, it was reported that CGI-58 obtains lysophosphatidic acid acyltransferase (LPAAT) activity (34, 35), this finding, however, was withdrawn when one of these groups published just recently that CGI-58 lacks LPAAT activity and stated that the identified activity was due to a bacterial contaminant. (36)

Whole body CGI-58-/- mice exhibit growth retardation, systemic TG accumulation in multiple tissues, and hepatic steatosis (Fig. 3). Furthermore, these mice die within 1 day after birth due to a severe skin barrier defect leading to rapid dehydration. This neonatal lethal skin barrier defect is linked to an impaired hydrolysis of epidermal TG. As a consequence, sequestration of FAs in TG prevents the synthesis of acylceramides, which are essential lipid precursors for the formation of a functional skin permeability barrier. This skin barrier defect uncovers an essential ATGL-independent role of CGI-58. (37)

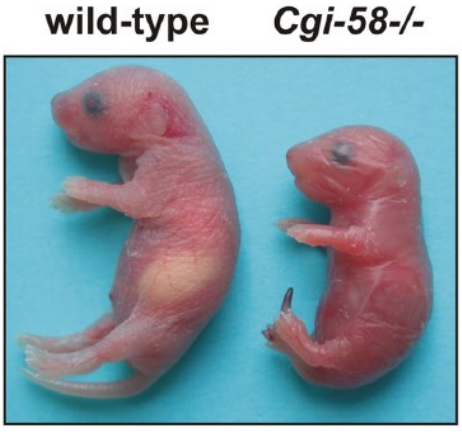

Figure 3: Photograph of a newborn wild-type and CGI-58-/- mouse. The CGI-58-/- mouse has a glossy and dry skin, smaller body size, and a necrotic tail tip. (37)

CGI-58 showed distinct roles in different tissues and cells. When mice were treated with CGI-58 antisense oligonucleotides (ASO) to silence CGI-58 expression and inhibit lipolysis in adipose tissue and liver, mice had smaller fat pads and were protected against diet-induced obesity. (38, 39) This finding suggests that there could be currently unknown compensatory mechanisms preventing fat accumulation in adipose tissue when CGI-58 is absent, for instance that the lack of CGI-58 also leads to a concomitant reduction in fat synthesis. (40) Interestingly, overexpression of CGI-58 in adipocytes did not lead to a distinct phenotype. Neither basal nor stimulated lipolysis was altered in adipocytes and also fat mass was identical compared to control mice. (41)

In cardiac muscle, CGI-58 deficiency results in an accumulation of fat leading to cardiomyopathy. Furthermore, a decreased expression of PPARα target genes, mitochondrial dysfunction, and inefficient FA oxidation was found. (42) CGI-58 mutations do not result in cardiomyopathy in humans. (40) In SM, there was also an excessive amount of fat when CGI-58 was missing. However, the running capacity, TG hydrolase activity, and fatty acid oxidation (FAO) rates of muscle-specific CGI-58-/- mice were comparable to control mice, suggesting that CGI-58 is not a major requirement for ATP production in SM. (42) In contrast, overexpression of CGI-58 in myotubes increased TG hydrolysis and FAO. (43) Recently, Xie *et al.* (44) showed that although muscle-specific CGI-58 deficiency causes cardiac dysfunction and fat deposition, it also results in improved insulin sensitivity in mice fed a high-fat diet.

CGI-58 overexpression or silencing in hepatoma cells altered VLDL packaging and secretion, leading to the question if CGI-58 has also a role in VLDL biogenesis. (45, 46) In liver, ASO-mediated knockdown (KD) of CGI-58 in mice led to a reduction in circulating TG levels, hepatic steatosis and reduction in hepatic VLDL release. However, ASO treatment also silences CGI-58 white adipose tissue, so decreased plasma TG and VLDL levels could origin from decreased FA delivery from adipose tissue to the liver. (38) Interestingly, studies in liver-specific CGI-58-/- mice argue against a role of CGI-58 in VLDL metabolism, since VLDL production and plasma TG levels were identical to control mice. However, these mice showed reduced hepatic TG hydrolase activity and FAO rates resulting in hepatosteatosis. (47) Moreover, although ASO-treated mice show hepatosteatosis and an

increased hepatocellular DG level, which is known to be a trigger of insulin resistance, mice remain insulin-sensitive. (48) Studies revealed that the intracellular compartmentation of DG is important. DG increased in the membrane fraction of high fat-fed mice leads to hepatic insulin resistance, whereas DG accumulation in LDs or lipid-associated ER does not. (49)

Intestine-specific CGI-58-/- mice showed reduced intestinal TG hydrolase activity and postprandial plasma TG concentrations (most probably due to the inhibition of the mobilization of cytosolic LD-associated TG for lipoprotein-mediated secretion), associated with an 4-fold increase in intestinal TG content and large cytosolic LD accumulation in enterocytes during the fasting state. (50)

The most severe phenotype is shown by the lack of CGI-58 in the skin in humans and in mice. CGI-58 deficiency causes nonbullous congenital ichthyosisform erythroderma, leading to a severe skin barrier defect. (51) This condition is characterized by the complete absence of covalently bound ω-(O)-acylceramides (52), which are important intermediates for the development of a functional cornified lipid envelope and the formation of an intact skin barrier. (53) The consequence of CGI-58 deficiency has also been described in colon cancer cells since it is known that the CGI-58 expression falls substantially and negatively correlates with malignant features. The data suggest that colon cancer cells develop aerobic glycolysis by suppressing CGI-58 mediated intracellular lipolysis. (54)

In the last years, several studies addressed the role of CGI-58 in macrophages. Miao *et al.* (55) showed that CGI-58-/- macrophages exhibit dysfunctional mitochondria due to defective PPARγ signaling. As a result, the ROS-inflammasome pathway was activated to promote insulin resistance in mice. Recently, the same group showed that over-nutrition leads to inhibition of CGI-58 expression in monocytes/macrophages through non-esterified FAs and perhaps lipopolysaccharide (LPS), leading to IL-1β secretion, which dampens insulin signaling. (56) Overexpression of CGI-58 in macrophages alleviates atherosclerotic lesion development in ApoE-/- mice since CGI-58 promotes cholesterol efflux and decreases serum tumor necrosis factor α (TNFα) and IL-6 levels. (57) CGI-58 is also expressed in many other cells and tissues including

brain, pancreas, testis, lung, kidney and stomach. (18, 58) However, its function in these tissues is still elusive.

1.1.2.4 Regulation of intracellular lipolysis

Lipolysis has been very well described in WAT. The most important mechanism regulating lipolysis involves the activation of ATGL by CGI-58 and the PKA–mediated phosphorylation of HSL and perilipin-1. (59) In the non-stimulated/basal state, CGI-58 is bound to perilipin-1 and not available for ATGL binding or activation and HSL resides in the cytosol. Upon β-adrenergic stimulation, PKA phosphorylates HSL, perilipin-1 as well as CGI-58 on multiple serines, which causes the translocation of HSL to the LD and the release of CGI-58, making it available for ATGL binding and activation. ATGL also translocates from the cytosol to the LD surface. (60) G0S2 was shown to be an ATGL inhibitor *in vitro* (Fig. 4). (11, 61) Most recently, Hofer *et al.* (62) demonstrated that adipocyte-type fatty acid-binding protein (A-FABP) and other members of the FABP family directly interact with CGI-58, thereby stimulating ATGL-catalyzed TG hydrolysis and enhancing the activity of PPARs.

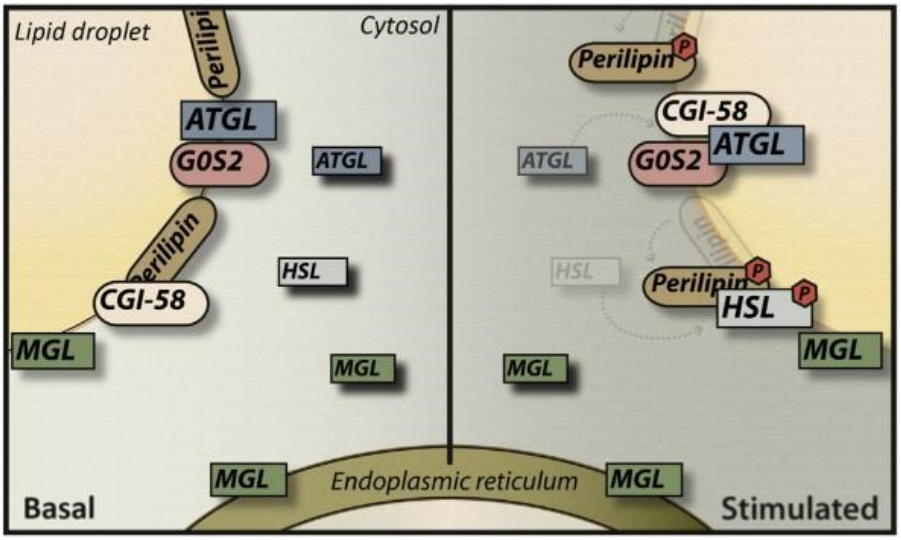

Figure 4: Intracellular localization of lipases and regulatory proteins in the basal and the stimulated state. (11) Explained in detail in the text.

1.2 Lipid droplets

LDs store neutral lipids, such as TGs, steryl esters, and retinyl esters. [reviewed in (3, 63, 64)] These stored lipids can be used in times of need to generate energy, membrane components, and signaling lipids. Impairment of this machinery, which degrades or generates LDs, has severe physiological consequences, demonstrating that LDs play a central role in cellular and organismal energy homeostasis, in particular, and overall lipid metabolism in general. [summarized in (63, 65-67)] LDs allow the cell to safely sequester otherwise toxic lipids, since FAs are amphiphatic molecules and can severely compromise membrane integrity. Once turned into TGs and incorporated into LDs, they are inert, stable, and harmless. This protective function is most probably the reason for the abundant accumulation of LDs in several disease states, which are characterized by aberrant lipid supply and metabolism, such as obesity, atherosclerosis, and fatty liver disease. [reviewed in (63, 67, 68)]

LDs contain a central core of hydrophobic neutral lipids and are surrounded by a single layer of amphipathic lipids and proteins. TGs in the hydrophobic core are generated by a biosynthetic pathway with the final step catalyzed by the acyl-CoA:diacylglycerol acyltransferases (DGAT)1 and DGAT2, which convert diacylglycerol and acyl-CoA (ultimately derived from FAs) into TGs. Both enzymes are located in the ER, where TGs accumulate at privileged sites that represent nascent LDs. Mature LDs are generated by continuous growth of these structures and finally become distinct from the ER via a process resembling budding. Whether this budding process is spontaneous or assisted by ER proteins is not known. Subsequent growth of LDs may take place by neutral lipid synthesis either at the ER or on the LD surface by a fusion mechanism that transfers lipid during homotypic LD-LD interaction. Neutral lipid addition to the LD core must be coupled with addition and remodeling of phospholipids (PLs), mostly phosphatidylcholine, at the LD surface to enable the coordinated expansion of the organelle. (6, 69, 70) LDs show a marked heterogeneity regarding size, cellular location, and associated protein composition within a given cell or between different tissues. (71)

Breakdown of TGs can occur by two different pathways, either by hydrolysis via neutral lipases or LD degradation by autophagy. During autophagy, LDs are taken up by autophagosomes, which fuse with lysosomes to form autolysosomes. The

hydrolytic enzymes delivered from the lysosome are then able to break down the autophagosome content. TGs are predominantly hydrolyzed by lysosomal acid lipase (LAL) (Fig. 5). [reviewed in (69)]

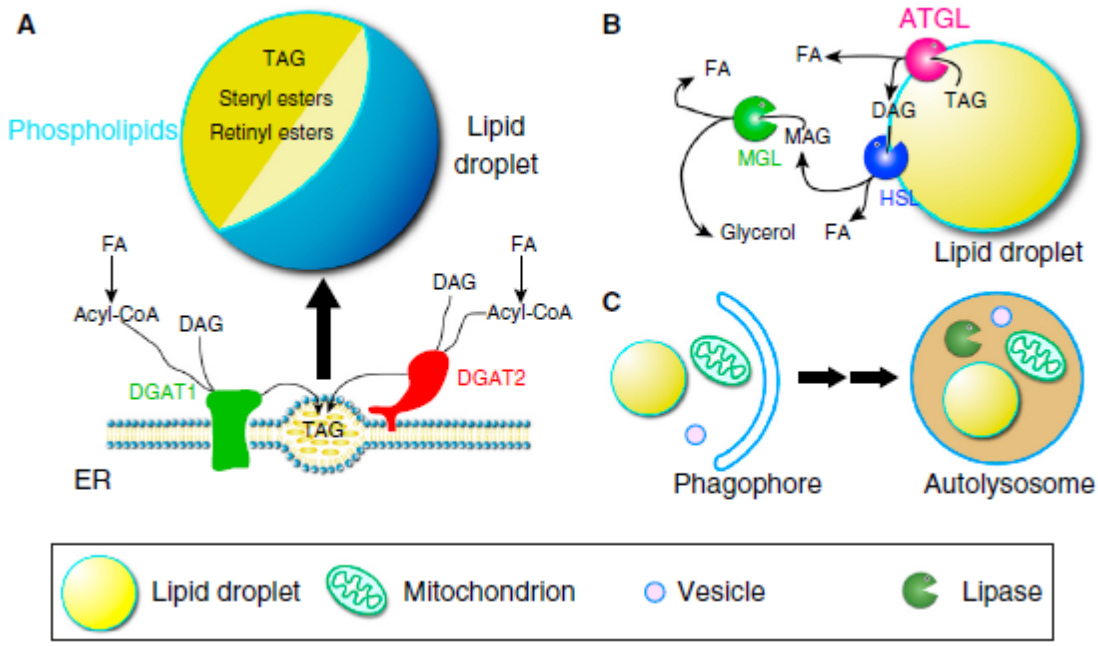

Figure 5: LD generation and breakdown. (A) LDs have a central core of neutral lipids and arise from the ER. (B) TG breakdown via cytoplasmic lipases. (C) TG breakdown via autophagy. (69)

1.3 Neutral lipid storage disease

In humans, mutations of ATGL or CGI-58 cause neutral lipid storage disease (NLSD). This disease defines a group of disorders characterized by the excessive accumulation of neutral lipids in multiple tissues, including skin, muscle, liver, central nervous system, and blood leukocytes. [summarized in (72)] One of the diagnostic characteristics of NLSD is the presence of lipid-containing vacuoles in leukocytes called “Jordans’ anomaly”. (73) However, mutations of ATGL or CGI-58 cause two different types of NLSD. Deficiencies of ATGL result in NLSD with cardiac myopathy (NLSDM) characterized also very frequently by skeletal myopathy and less frequently by hepatomegaly and liver steatosis. Mutations of CGI-58 cause NLSD with ichthyosis (NLSDI) (74), also designated as Chanarin-Dorfman syndrome (CDS), very often accompanied by hepatomegaly, liver steatosis, and neurological disorders, sometimes also by skeletal myopathy. True

null mutations of these two genes have not been investigated so far. [reviewed in (72)]

1.4 ER stress and mitochondria-dependent apoptosis

The ER is a membrane-bound organelle comprising of interconnected highly branched tubules, vesicles, and cisternae. It functions mainly in translocating and integrating proteins (secretory and membrane proteins, respectively), assisting their folding and transport (extracellular or to the cell membrane), lipid biosynthesis, and maintaining Ca^{2+} homeostasis. Furthermore, the ER is also a site for post-translational modification of proteins and is considered a signaling organelle. Ribosomes embedded on the rough ER (RER) are sites for protein synthesis and secretion. The smooth ER (SER) lacks bound ribosomes and is therefore inefficient in protein synthesis, but it is important for FA and PL synthesis, carbohydrate metabolism, lipid bilayer assembly, and regulation of Ca^{2+} homeostasis. [reviewed in (75)]

The role of the ER in the cell is determined by cell type, cell function, and cellular needs. For instance, liver cells are high in SER for drug detoxification, whereas plasma cells and other secretory cells are rich in RER to meet their secretory protein demand. The excursion of secretory or membrane proteins begins at the ER. The proteins in the ER are folded and modified by ER-resident chaperones and folding enzymes assisting in appropriate conformation and maturation. The folded proteins are transported to the Golgi via vesicular carriers and finally escorted to their destinations (plasma membrane, lysosomal membrane or loaded into granules for secretion). There are selective chaperones capable of tagging unassembled, misfolded or unfolded proteins, which facilitate their identification and translocation to the cytosol, where they are steered to the ubiquitin proteasome degradation system or eliminated by autophagic degradation. (76-78)

Accumulation of unfolded/misfolded/mutated proteins, disturbances in cellular redox regulation and endogenous ROS production, hypoxia, hyperglycemia, and hyperlipidemia, aberrations in Ca^{2+} regulation and viral infections act as stress signals and alter ER homeostasis making it dysfunctional. In response to these diverse signals, the ER elicits a protective or adaptive response called UPR aiming

to restore ER homeostasis or if the stress signal is severe and/or prolonged, ER triggers cell death pathways. (79-84)

The adaptive UPR comprises of signal transduction pathways initiated by ER UPR transmembrane proteins: inositol-requiring kinase 1 (IRE1α), activating transcription factor 6 (ATF6), and double-stranded RNA-activated protein kinase-like endoplasmic reticulum kinase (PERK) in an attempt to restore homeostasis and normal ER functions. [reviewed in (85)]

UPR transducers are negatively regulated by the chaperone Grp78/BIP (immunoglobulin heavy chain binding protein) in unstressed or healthy ER. However, an increase in unfolded proteins causes dissociation of Grp78/BIP, thereby releasing the inhibition and thus eliciting the response. Released ATF6 acts as a transcription factor, travels to the nucleus, and binds to ER stress response elements, thereby inducing the transcription of several genes like BIP, CCAAT/enhancer-binding protein homologous protein (CHOP) and X-box-binding protein 1 (XBP1). IRE1α is activated and undergoes homodimerization and autophosphorylation, which induces XBP1 mRNA splicing. Spliced XBP1 (XBP1s) translocates to the nucleus and regulates genes involved in UPR and ER-associated degradation (ERAD). The release of BIP activates the PERK pathway, which initiates a global translational arrest by phosphorylating the translation initiation factor 2α (eIF2α), thus decreasing ER protein load. ATF4 enters the nucleus and regulates expression of UPR target genes (Fig. 6). [reviewed in (85)]

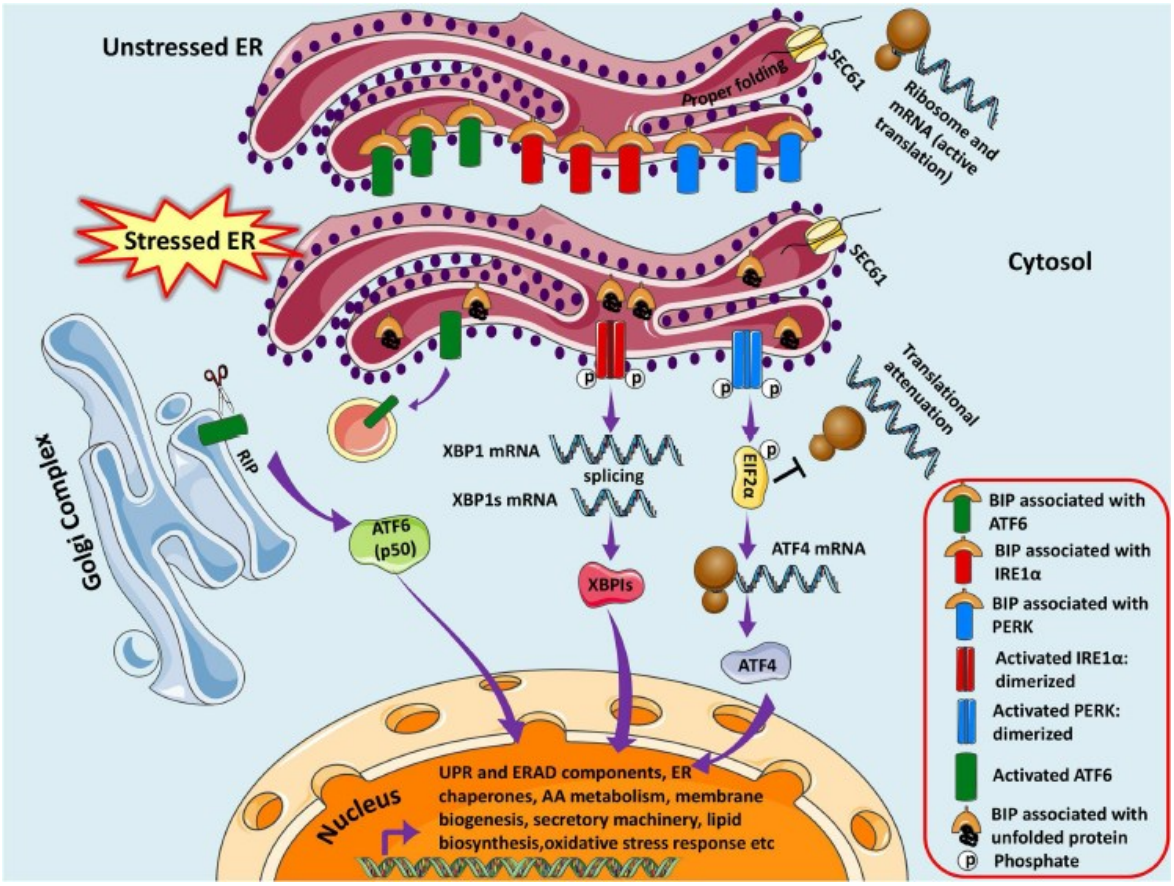

Figure 6: Unfolded protein response pathways. (85) Explained in detail in the text.

The ER is physically and functionally tightly interconnected with mitochondria. They are connected via mitochondrial-associated membranes (MAM), which participate in Ca^{2+} signaling, lipid transport, energy metabolism, and cell survival. Imbalances in Ca^{2+} homeostasis and ER stress affect this system. During Ca^{2+} overload, Ca^{2+} influx increases in mitochondria and ER, thereby causing changes in mitochondrial pH and ROS production accompanied by altered mitochondrial membrane potential and opening of permeability transition pore with subsequent release of cytochrome C. Ca^{2+}-induced ROS increase and ROS-mediated Ca^{2+} vulnerability create a self-amplifying loop. In the adaptive phase of UPR, ER-to-mitochondria Ca^{2+} transfer under regulation by MAM maintains mitochondrial metabolism and ATP production. However, severe ER stress induces mitochondrial Ca^{2+} overload, ROS accumulation, and ATP depletion and thus activates mitochondria-dependent apoptosis (Fig. 7). ROS are generated in the ER as part of an oxidative folding process. ROS can target ER resident proteins,

enzymes, chaperones and ER-based Ca^{2+} channels, leading to the release of calcium from the ER into the cytosol and ER stress signaling, which stimulates mitochondria metabolism to produce more ROS, further inducing inflammatory responses. [reviewed in (85, 86)]

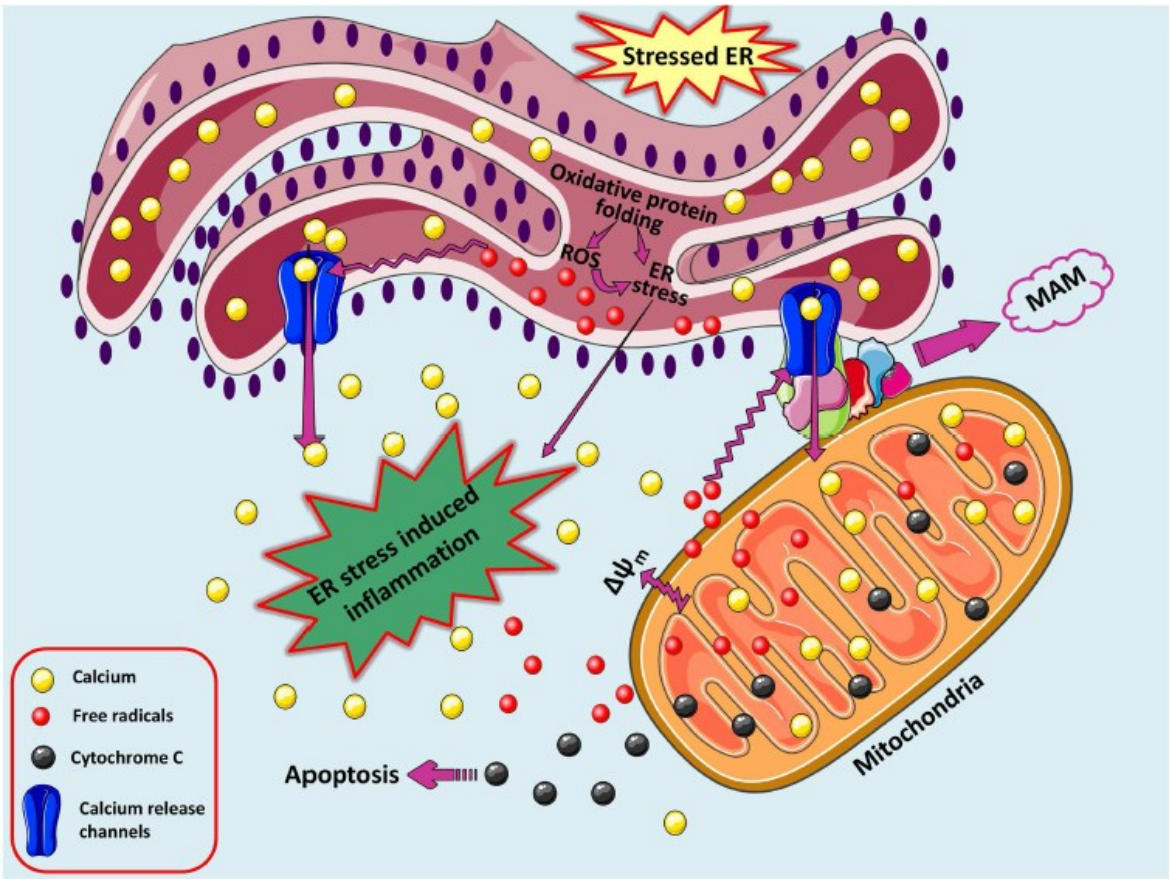

Figure 7: Loop of oxidative stress and ER stress leading to mitochondria-dependent apoptosis. During protein overload, ROS are generated in the ER, which can target ER resident proteins, enzymes, chaperones, and Ca^{2+} channels, leading to the release of Ca^{2+} from the ER into the cytosol and ER stress signaling. (85)

1.5 Phagocytosis

Phagocytosis is an early and fundamental step for the effective clearance of disease-causing agents and pathogens. Particulate targets typically have a size of >0.5 µm in diameter. Smaller particles are taken up via an actin-independent process called endocytosis. (87) Myeloid phagocytes include neutrophils, dendritic cells (DCs) and macrophages, however, the ability to engulf and kill pathogens is

considered as a major effector function of macrophages. In their phagocytic role, macrophages are part of the first line of innate immune defense. [reviewed in (88, 89)] The main mechanisms via which macrophages are able to internalize and clear microbial material occur through receptor-mediated phagocytosis. The process making use of different receptors, for instance Fc or scavenger receptors, ensure the uptake of particulate material into phagosomes followed by the delivery of lysosomes. (90) There are three types of phagocytosis: (i) opsonic phagocytosis, using Fc receptor-, complement receptor- and a5β1 integrin-mediated uptake, (ii) non-opsonic phagocytosis, when it comes to dectin 1-, macrophage receptor MARCO-, SRA- and aVβ5 integrin-mediated uptake, and (iii) triggered (non-specific) phagocytosis via toll-like receptors (Table 1).

Table 1: Types of phagocytosis. (89)

Type of phagocytosis	**Receptors**	**Ligands**
Opsonic phagocytosis	Fc receptor family (FcγRI, FcγRIIA)	Antibody-opsonized targets
	Complement receptors (CR1, CR3 and CR4)	Complement-opsonized targets
	A5β1 integrin	Fibronectin
Non-opsonic phagocytosis	Dectin 1	β-glucan
	Macrophage receptor MARCO	Bacteria (undefined specific ligand)
	SRA	Bacteria (diverse charged molecules)
	αVβ5 integrin	Apoptotic cells
Triggered (nonspecific) phagocytosis	Toll-like receptors	Various, including LPS and lipopeptides

Phagocytic leukocytes, especially macrophages, not only ingest and destroy invading pathogens, but are also charged with clearing dead and dying host cells. The process of engulfing apoptotic cells is called efferocytosis. The process of efferocytosis begins with the exposure of phosphatidylserine to the exofacial leaflet of the PL membrane by an apoptotic cell. Another early event is the release of chemokines, which attract macrophages to the site of cell death. Macrophages

respond with the increased expression of bridge molecules and receptors and engulf the apoptotic cell in a large spacious efferosome. Efferocytosis is important for the resolution of inflammation not only because it removes dead cells, relieves tissue congestion, and prevents release of phlogistic cellular contents, but also promotes tissue repair and wound healing (Fig. 8). [reviewed in (91)]

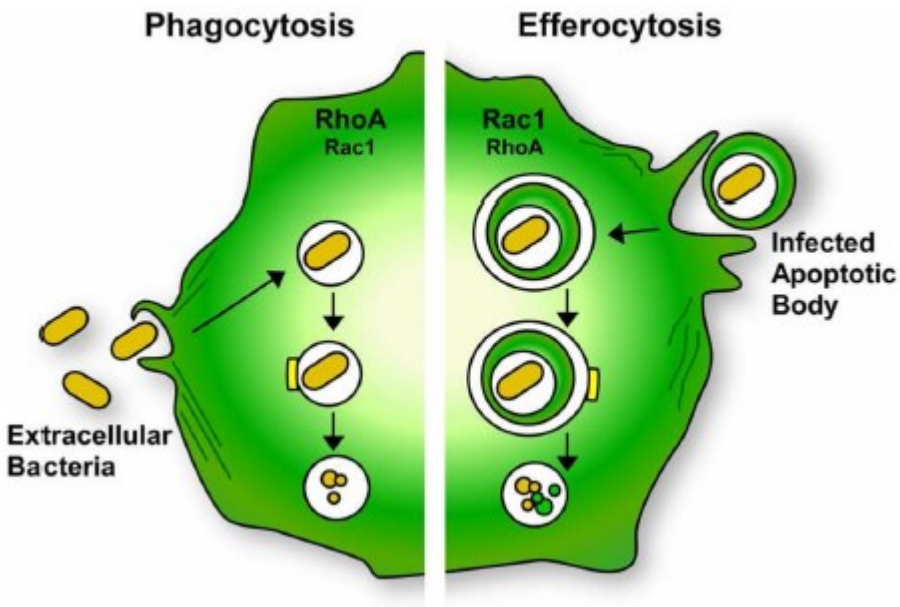

Figure 8: Efferocytosis is a distinct process from phagocytosis. In phagocytosis, increased levels of RhoA lead to actin polymerization and stress fiber formation, allowing receptor-mediated uptake of microbes. Fusion of actin projections leads to internalization of the bacteria in a phagosome, which undergoes stepwise maturation, leading to degradation of the pathogen. In efferocytosis, increased Rac1 levels result in the formation of lamellipodia and membrane ruffles upon actin polymerization, leading to the internalization of infected apoptotic bodies in an efferosome. The "double-wrapped" pathogen can be destroyed if the efferosome undergoes acidification, similar to the process of phagolysosome fusion. (91)

1.6 Autophagy

Macroautophagy, also called autophagy, is defined as a catabolic process maintaining cellular homeostasis in a lysosome-dependent manner. Lysosomes are intracellular degradation units of eukaryotic cells. The process of autophagy includes sequestration of misfolded or long-lived proteins and aggregates into double-bilayer vesicular compartments followed by their delivery to lysosomes for degradation. Macroautophagy of mitochondria is named mitophagy. [reviewed in

(92)] The final metabolites of lysosomal activity are then used to fulfil energy and new macromolecule needs of the cell. The autophagic process works like an intracellular recycling mechanism. Autophagy can be activated in response to various cellular stresses and often has a cytoprotective function. Nutrient deprivation, damaged or excessive organelles, accumulated misfolded proteins, ER stress, oxidative stress, certain toxins, radiation, and hypoxia can trigger autophagy. Autophagy is involved in a wide array of physiologic and pathologic pathways playing a role in cell survival, tumor suppression, lifespan extension, cell death, cell differentiation, organismal development, and immunity. [reviewed in (92)]

Three autophagy pathways have been described (Fig. 9).

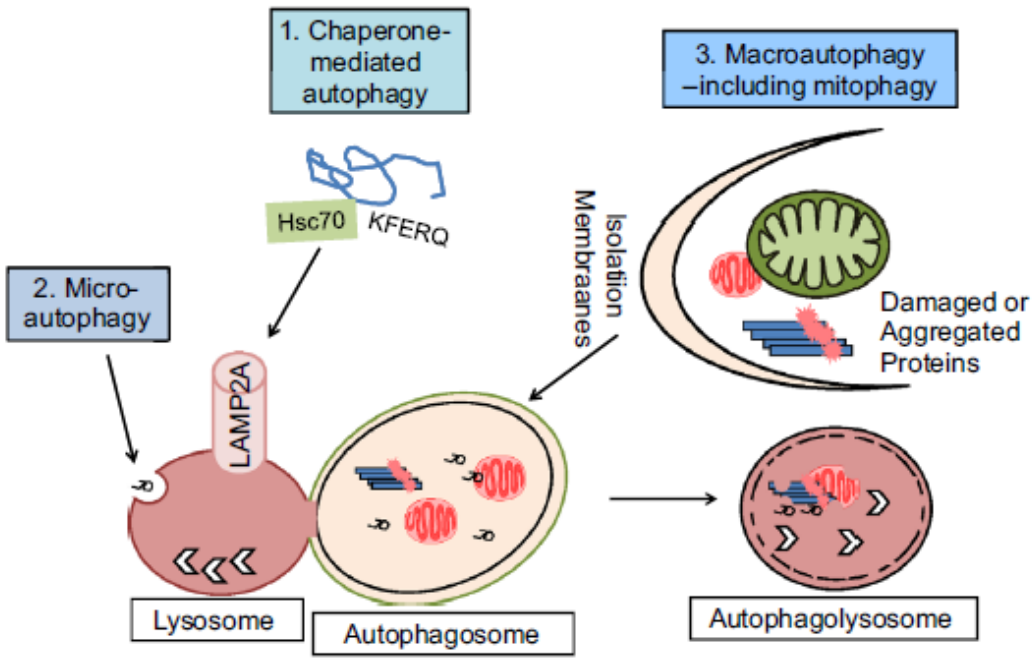

Figure 9: Autophagic and mitophagic degradation of organelles and proteins. Three major autophagy pathways have been described. 1. Chaperone-mediated autophagy involves Hsc70, recognizing target proteins which have a KFERQ consensus sequence, followed by binding to LAMP-2A, and transport of the targeted protein to the lysosome to be degraded. 2. Microautophagy is the invagination of lysosomal membranes to encircle cellular contents like proteins and lipids. 3. Macroautophagy involves the formation of a double-membrane structure to encircle proteins, lipids and organelles. Degradation of mitochondria via macroautophagy is termed mitophagy. Degradation of other cellular structures, such as fragments of the nucleus, LDs, peroxisomes, ribosomes, and ER, have been called, nucleophagy, lipophagy, pexophagy, ribophagy, and reticulophagy. (92)

The most extensively studied autophagy process is macroautophagy. The first step in autophagy is the formation of double-membrane vesicles called autophagosomes. Autophagy consists of four main steps: (i) initiation, (ii) elongation of autophagosomes, (iii) closure, and (iv) fusion with the lysosome. Autophagosomes emerge in the cytoplasm as autophagic phagophores, which often arise in the ER, the Golgi, mitochondria-ER contact sites, and the plasma membrane (Fig. 10). [reviewed in (93)]

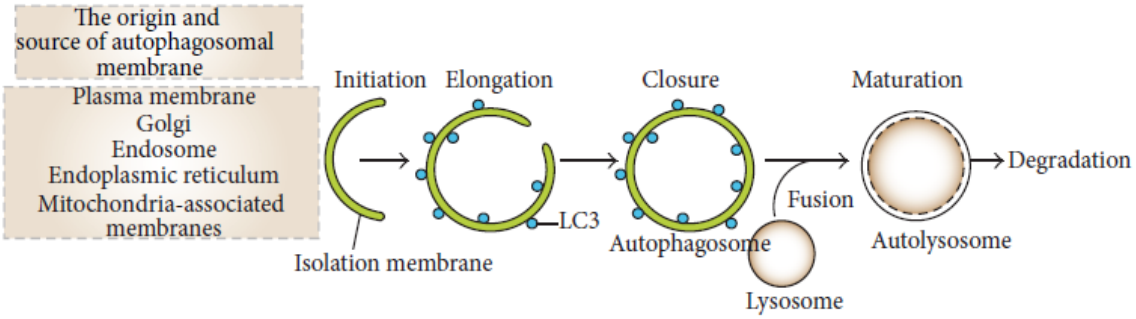

Figure 10: Process of autophagy. (93) Explained in detail in the text.

There are two important proteins which contribute to autophagy and are commonly used to monitor the process of autophagy. One is the cytosolic protein microtubule-associated protein light chain 3 (LC3-I), which is modified to its membrane-bound form (LC3-II) located on pre-autophagosomes and autophagosomes during autophagy. (94) The other one is p62, a chaperone that shuttles intracellular protein aggregates into autolysosomes for degradation. After engulfment by the autolysosome, the entire p62-protein aggregate is degraded. (95)

Another known autophagic process is chaperone-mediated autophagy, which involves the chaperone protein heat shock protein (Hsc70). Hsc70 recognizes target proteins which have a KFERQ consensus sequence and binds to lysosomal-associated membrane protein (LAMP-2A). Targeted proteins are transported to the lysosome and degraded (Fig. 9). [reviewed in (92)]

There is one more existing pathway, termed microautophagy, which is the invagination of lysosomal membranes to encircle cellular contents, such as proteins and lipids (Fig. 9). [reviewed in (92)]

Until recently, the breakdown of TGs and CEs of LDs was exclusively attributed to the actions of cytosolic lipases. However, in 2009, Singh *et al.* (96) demonstrated that LDs are engulfed into double-membrane vesicles and termed this process lipophagy. During lipophagy, portions of large LDs or entire small LDs are sequestered by an autophagosome. Autophagosomes fuse with lysosomes to form autolysosomes, in which the substrates of the autophagosome and the hydrolytic enzymes of the lysosome are mixed for cargo degradation. Lipid breakdown leads to release of FAs into the cytoplasm for mitochondrial β-oxidation and generation of ATP to maintain cellular energy homeostasis (Fig. 11). (97) The enzyme responsible for LD breakdown in lipophagy is lysosomal acid lipase (LAL). (98)

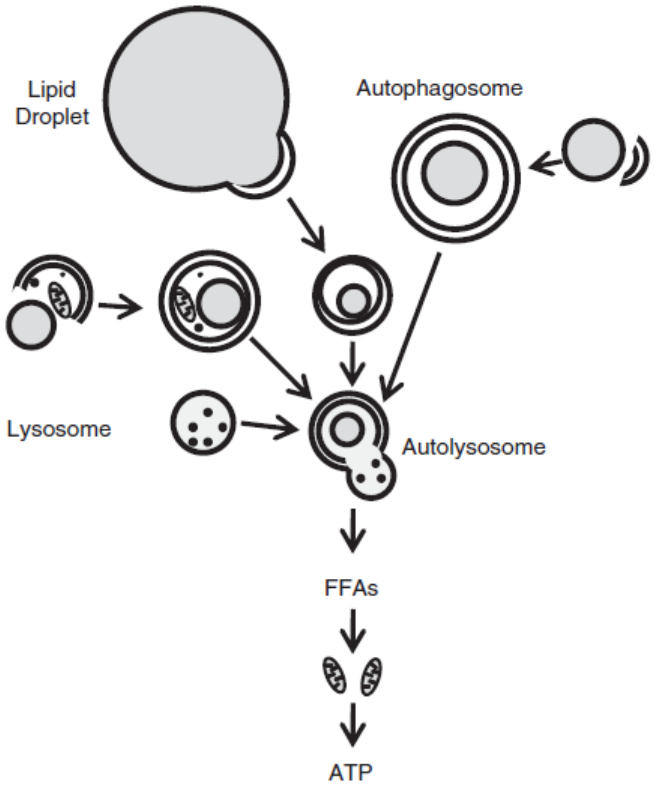

Figure 11: Process of LD breakdown by lipophagy. LDs and other cellular contents are engulfed into autophagosomes. Autophagosomes fuse with lysosomes to form autolysosomes in which enzymes and content of the autophagosome are mixed for cargo degradation. Lipid breakdown leads to the release of FFAs into the cytoplasm which serve to sustain rates of mitochondrial β-oxidation for generation of ATP. (97)

1.7 Atherosclerosis

Atherosclerosis is one of the leading causes of death arising from coronary artery disease (CAD), stroke, and peripheral vascular disease. Atherosclerosis is a chronic inflammatory disorder caused by lipids (particularly LDL) and leukocytes. The disease is likely to be initiated by the activation of the endothelium via the expression of adhesion molecules which in turn enables the adhesion of monocytes and T-cells to the endothelium and their transmigration into the intima. (99-101) Several risk factors for atherosclerosis have been identified and are generally classified as modifiable and non-modifiable factors. The latter include age, gender and genetic predisposition to hypercholesterolemia, hypertension, diabetes, and systemic inflammation. Modifiable risk factors are cigarette-smoking, diet rich in saturated fats, and a sedentary lifestyle. (102)

1.7.1 Lipid metabolism in atherosclerosis

Lipoprotein particles function as vehicles for the transport of insoluble lipids in the blood and are composed of a core region storing TGs and CEs, with a surrounding polar region consisting of PLs as well as apolipoproteins. Different forms of lipoproteins are involved in lipid trafficking with a considerable exchange of various apolipoproteins occurring between them. (102)

Chylomicrons primarily facilitate the transport of dietary TGs from the intestine to peripheral tissues. Non-esterified FAs and 2-MG produced by the digestion of TGs within chylomicrons by LPL are taken up by adipose tissue or SM for utilization or storage. (102) The liver can take up resulting chylomicron remnants via specific receptors and metabolize them. (103)

VLDLs are involved in the transport of TGs synthesized in the liver. Intermediate-density lipoproteins (IDLs) are produced following the digestion of TGs in VLDL by LPL und hepatic lipase (HL). Further processing and hydrolysis of TGs in IDL by HL results in the formation of LDL particles. (102)

LDL carries cholesterol from the liver to peripheral tissues. High plasma LDL levels are associated with a high risk for atherosclerosis as identified from numerous epidemiological studies and clinical trials. (102) LDL particles enter cells of

peripheral tissues predominantly via receptor-mediated endocytosis involving its cognate receptor Ldlr. The clearance of plasma LDL by Ldlr is crucial for limiting atherosclerosis, since LDL is subject to modification, particularly oxidation, and such modified LDL is taken up in an uncontrolled manner by scavenger receptors such as SRA and cluster of differentiation 36 (Cd36) by certain plaque-resident macrophages and smooth muscle cells (SMCs). (102, 104)

Since excess intracellular cholesterol is toxic, the cells established two main routes for its removal; either through enzymatic-driven conversion to a more soluble transportable form or through reverse cholesterol transport (RCT) (Fig. 12). Cholesterol can be enzymatically modified through a number of processes such as hydroxylation and esterification within the ER to produce oxysterols and sterol esters, respectively. Cholesterol esterification reduces its solubility and promotes storage within cytoplasmic LDs. RCT is the primary pathway for the removal of excess cholesterol, which involves lipid transporters such as ATP-binding cassette transporter (ABC)-A1 and -G1 that mediate the transfer of cholesterol from peripheral cells to selected extracellular acceptors such as high-density lipoproteins (HDL) and associated apolipoproteins. Cholesterol is then delivered to the liver for further conversion to bile salts in preparation for excretion. (102, 105)

The relationship between reduced plasma HDL levels and incidences of CAD has long been established as one of the major risk factors for the disease. HDL concentrations are often negatively affected by many other atherosclerotic risk factors such as gender, obesity, and exercise. Studies in both, animals and humans, have shown that raised plasma HDL levels are generally associated with protection against atherosclerosis. The anti-atherosclerotic effects are thought to mostly arise from the involvement of HDLs within RCT, however, it was also shown that HDL particles have additional protective properties like inhibition of lipoprotein oxidation, attenuation of the inflammatory response, endothelial cell (EC) protection and suppression of monocyte adhesion. [reviewed in (106)] Recent studies have shown that rather HDL composition than concentration is important for cardiovascular risk assessment. (107, 108)

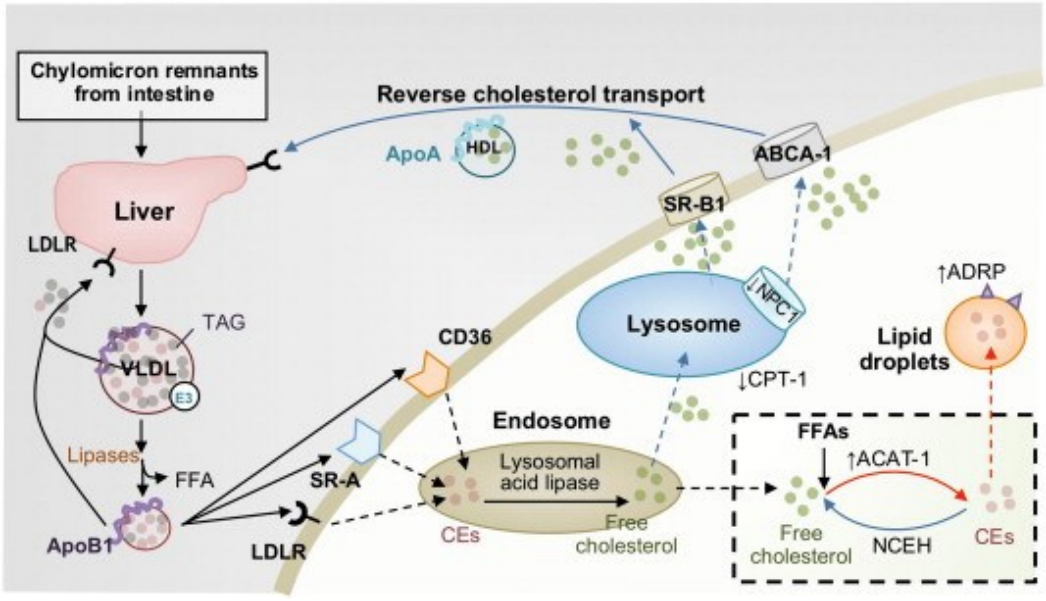

Figure 12: Scheme of cholesterol metabolism. Dietary lipids get absorbed in the intestine and transported by chylomicrons to peripheral tissues. After lipolysis, chylomicron remnants deliver dietary lipids to the liver. Liver-derived VLDLs containing Apolipoprotein (Apo) B and ApoE (E3) are then hydrolyzed to IDLs and on to LDLs. ApoB facilitates LDL binding to its cognate receptor Ldlr, which is then internalized and degraded in lysosomes. SRA and Cd36 facilitate the excessive, uncontrolled uptake of modified LDL particles into macrophages during the disease. Lysosomal acid lipases hydrolyze CEs to free cholesterol (FC) and FFAs. FC is either trafficked out of the cells for RCT through Abca1 and SrB1, or re-esterified to CEs for storage by the action of acyl-coenzyme A acyltransferase 1 (ACAT-1) within the ER, and then stored as LDs [regulated by adipocyte differentiation-related protein (ADRP)]. The accumulation of CEs depends on the hydrolysis of CEs [modulated by neutral cholesterol ester hydrolase (NCEH)] and FFA availability [regulated by carnitine palmitoyltransferase 1 (CPT-1)]. Intracellular trafficking of cholesterol is regulated by Niemann-Pick type C disease proteins (NPC)-1 and -2. (106)

1.7.2 Initiation and progression of atherosclerosis

Atherosclerotic plaques tend to develop within areas of curvature such as branching points, which are prone to disturbed laminar flow within large- and medium-sized arteries. (102, 109) In healthy states, the arterial endothelium is impermeable to large biomolecules such as LDL. However, physiological and pathophysiological changes can lead to an increase in the permeability of the endothelium. As a result, the expression of adhesion molecules on the cell surface increases and chemokines and growth factors (GFs) including macrophage colony-stimulating factor (M-CSF) are secreted. (109, 110) LDL particles containing ApoB diffuse between EC junctions, accumulate within the

subendothelial space, and become chemically modified and particularly oxidized (oxLDL). The presence of oxLDL in the intima aggravates surrounding cells and induces SMC mitogenesis. (102) Immune cells such as monocytes, neutrophils, T-cells, B-cells, DCs, and mast cells are recruited by chemokines released by activated ECs and SMCs. The leukocyte adhesion process consists of three different stages: rolling, activation, and arrest. (111-113) The rolling on the EC surface as well as the transmigration across the endothelium of mouse monocytes is dependent on the immobilization of chemokines, such as CXC-chemokine ligand (CXCL)-1 and CC-chemokine ligand (CCL)-5, and the expression of their surface receptors. (114) Once in the intima, monocytes differentiate into macrophages under the influence of M-CSF and granulocyte-macrophage colony-stimulating factor (GM-CSF). The formation of an intermediate plaque arises due to the migration and proliferation of SMCs into the inflamed area in response to GFs released from plaque-resident cells. (111-114) In later stages of the disease, the plaque is characterized by an abundance of disorganized cells, lipids, matrix components, and minerals. (102) First clinical symptoms may occur during this phase of the disease, since the intimal region is thickened and the area of the arterial lumen may be reduced in size. (102, 115, 116) At the last stage of the disease, the plaque contains fibrous material and show signs of calcification, ulceration, and hemorrhaging from small vessels, which grow in and are leaky. The thrombus may obstruct the lumen or may detach in form of an embolus and block blood flow leading to myocardial infarction. (102, 117)

1.7.3 The role of macrophages in atherogenesis

The development of atherosclerosis involves the activation of various cell types including ECs, SMCs, lymphocytes, monocytes, and macrophages in the intima of the arteries, which results in a local inflammatory response. (118) Increasing circulating LDL-cholesterol levels and the subsequent accumulation of oxLDL in the subendothelial space triggers the recruitment and retention of monocytes and lymphocytes in the arterial wall. Monocytes differentiate into macrophages, which scavenge lipoprotein particles and eventually become foam cells (Fig. 13). (119) Macrophage-derived foam cells secrete inflammatory molecules and factors, which further promote lipoprotein retention and sustain inflammation. (120, 121)

Atherogenesis is characterized by apopotosis of resident macrophages in the lipid core of the lesion. The clearance of apoptotic cells is mediated by phagocytes, mostly macrophages, which recognize and internalize dead cells in a process called efferocytosis. In early lesions, phagocytes clear apoptotic cells, avoiding further progression of atherosclerosis. In chronic, advanced lesions, efferocytosis is no longer sufficient to engulf all dead cells, and the accumulation of apoptotic debris results in the formation of a necrotic core, which triggers further inflammation, necrosis, and thrombosis. (122) Macrophages are crucial in the maintenance of efficient efferocytosis, thereby resolving inflammation and preventing the formation of a necrotic core within the plaque. (115)

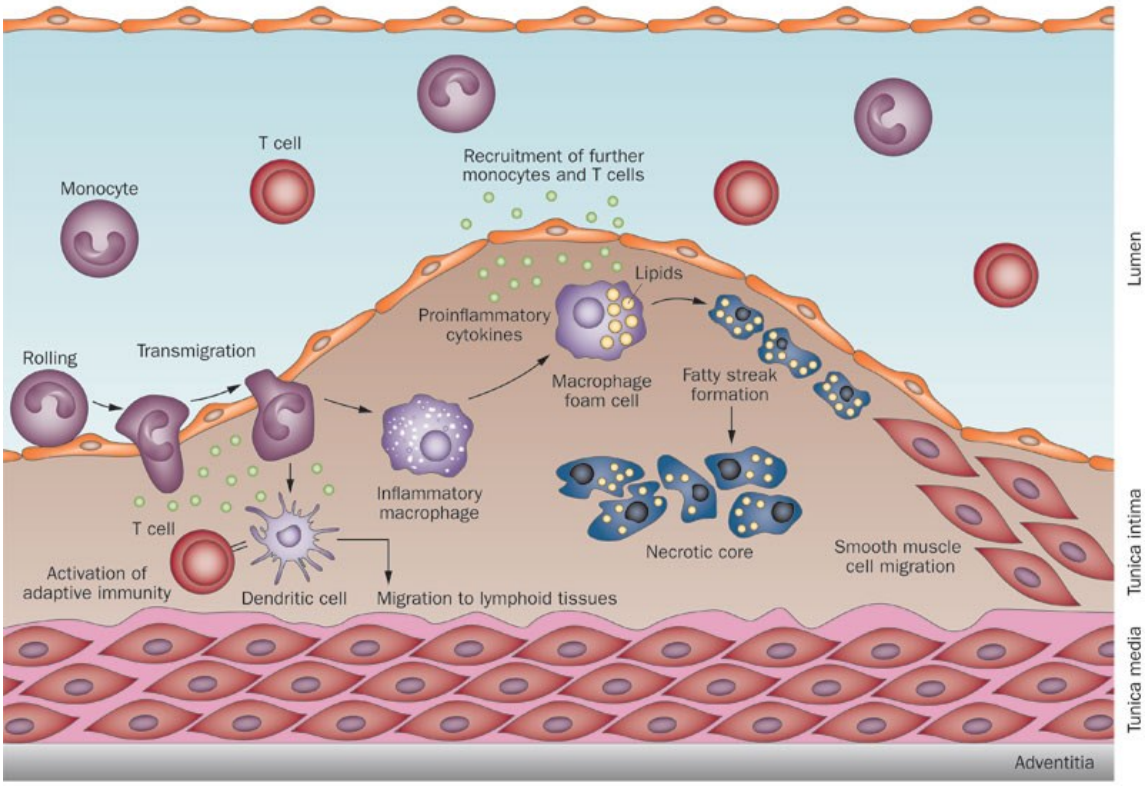

Figure 13: Role of monocytes/macrophages in atherogenesis. Endothelial cells become activated and facilitate the rolling, adhesion and transmigration of monocytes into the subendothelial space. Monocytes differentiate either into DCs, which are key players in activating adaptive immunity, or into macrophages, which secrete pro-inflammatory cytokines, thereby recruiting further immune cells and promoting inflammation. Lipoprotein particles are taken up by macrophages which can lead to fatty streak formation. Migration of SMCs from the tunica media into the tunica intima further promotes atherogenesis. Monocyte-derived cells turn this early lesion into an advanced atherosclerotic plaque containing a lipid-rich and macrophage-rich necrotic core that is finally destabilized, leading to plaque rupture. (123)

Macrophages in atherosclerotic lesions are continuously exposed to accumulating lipids and their oxidized derivatives. Cholesterol crystals that accumulate during early stages of atherosclerosis might be responsible for the inflammatory activation of macrophages. It was shown that cholesterol crystals that are present in the arteries of mice can act as an M1-polarizing stimulus. Moreover, an accumulation of oxidized lipoproteins can also direct human macrophages toward an M1 pro-inflammatory phenotype. The number of macrophages in atherosclerotic lesions gradually increases with plaque progression and severity, and is much higher in symptomatic than asymptomatic plaques. Macrophages which are located in the most unstable areas of the plaque mainly express M1 polarization markers, whereas macrophages present in the fibrous cap surrounding the necrotic core express both M1 and M2 markers. [reviewed in (124)] Moreover, unstable plaques are associated with a high proportion of macrophages to SMCs and a lipid-rich necrotic core. Macrophages induce the expression of matrix metalloproteinases (MMPs), which promote the degradation of collagen. MMPs are overexpressed in regions within the plaque that are prone to rupture and degrade connective tissue, which is detrimental to plaque stability. [reviewed in (106)]

1.7.4 Macrophage polarization

Based on the expression of several markers or the production of specific factors different classes of macrophages were defined. Classically activated M1 macrophages are typically induced by interferon (IFN)-γ, TNFα, or LPS recognition. These macrophages secrete pro-inflammatory cytokines like TNFα, IL-6, and IL-1β. (125, 126) M1 macrophages participate in the removal of pathogens during infection through the activation of the NADPH oxidase system and the subsequent generation of ROS. Chronic M1 macrophage activation can therefore mediate ROS-induced tissue damage and impair wound healing. (127)

To protect against such tissue damage, the inflammatory response is temporally counterbalanced by regulatory mechanisms driven by alternatively activated M2 macrophages. (128) Three subclasses of M2 macrophages have been identified: M2a macrophages induced by IL-4 and IL-13; M2b macrophages induced by

immune complexes in combination with IL-1β or LPS; and M2c macrophages induced by IL-10, transforming growth factor-β (TGF-β), or glucocorticoids. (129) All M2 macrophages have an anti-inflammatory cytokine profile characterized by a high production of IL-10 in humans and arginase I in mice. (128-130) Interestingly, M2b macrophages also produce high levels of pro-inflammatory cytokines like IL-1, IL-6, and TNFα. (131)

In haemorrhagic zones of human atherosclerotic lesions, macrophages display the M(Hb) phenotype. M(Hb) macrophages are induced *in vitro* by haemoglobin–haptoglobin complexes and characterized by the production of anti-inflammatory factors. (132)

Haem induces macrophage polarization toward the Mhem phenotype. Mhem macrophages are characterized by increased expression of haem oxygenase I and are protected from oxidative stress and lipid accumulation. (133)

Mox macrophages are triggered by oxidized PLs. Compared with M1 and M2 macrophages, Mox macrophages show reduced phagocytic and chemotactic capacities. In advanced atherosclerotic lesions of mice, Mox macrophages comprise approximately 30% of the total macrophage number. Whether Mox macrophages are also present in human atherosclerotic lesions is not known. (134)

In humans, CXCL4 induces the M4 macrophage phenotype, which, despite displaying characteristics of the M1 and M2 phenotype, completely lacks the capacity for phagocytosis. M4 macrophages have been found in human atherosclerotic plaques, suggesting a potential role for this macrophage phenotype in atherosclerosis. (135)

Macrophages are remarkably plastic and are able to switch from one phenotype to another depending on the environmental cues encountered. (136, 137) Interestingly, polarization to the M4 phenotype seems to be irreversible. (138)

1.7.5 Atherosclerotic mouse models

Advances in murine models capable of developing advanced atherosclerotic lesions have markedly facilitated our understanding of the molecular basis of this disease, particularly by using ApoE-/- and Ldlr-/- mice. (139, 140) ApoE is produced within the liver and by macrophages and is a component of lipoprotein particles where it functions as a ligand for lipoprotein receptors. ApoE-/- mice are highly hypercholesterolemic and develop spontaneous atherosclerotic lesions that can be additionally induced by challenging mice with a high fat diet. (141)

Ldlr-/- mice are mildly hypercholesterolemic due to defective clearance of plasma LDL and develop atherosclerotic lesions accompanied with increased levels of plasma cholesterol and raised amounts of pro-atherogenic lipoproteins on a high fat diet. Bone marrow transplantations are often used to investigate whether a given phenotype is governed by hematopoietic or non-hematopoietic cells. (140)

However, the use of mouse models has some key limitations, since the disruption of genes for ApoE or Ldlr may affect other crucial cellular processes. For instance, ApoE also functions as an anti-oxidant and modulator of immune responses. (142) Moreover, it is known that the expression profiles of several tissues show different RNA expressions in humans and mice. Importantly, mice have a distinct lipoprotein profile from humans and the majority of plasma cholesterol is carried on HDL particles, whereas in humans 75% cholesterol is carried on LDL particles. Despite some disadvantages, the usage of mouse models has greatly progressed our understanding of the disease. Many advantages such as environmental conditions and dietary intake, which can be carefully controlled, the short generation time of mice, and the evaluation of disease progression undertaken within a reasonable time frame makes the use of mouse models indispensable for atherosclerosis research. [reviewed in (106)]

2. Aim of the studies

CGI-58 is the co-activator of ATGL. The aims of the first part of my thesis were to investigate the role of CGI-58 in macrophage function and atherogenesis. We therefore generated mice with a myeloid specific knock-out of CGI-58 by using the cre/loxP sytem. We hypothesized that the lack of CGI-58 in macrophages leads to the inhibition or reduction of TG hydrolysis via ATGL and could hence affect foam cell formation and atherogenesis, as well as cell death and inflammation in macrophages. Furthermore, we aimed to elucidate whether CGI-58 has ATGL-independent functions.

In the second part of my thesis, I investigated the contribution of ATGL and HSL to TG hydrolysis in murine macrophages. ATGL and HSL were reported to be the major enzymes in adipose tissue TG metabolism. Macrophages from *A0* and *H0* mice show markedly reduced neutral TG hydrolase activity. We generated *A0H0* mice and determined whether additional lipase(s) might be involved in the catalytic breakdown of TG in macrophages. To circumvent the lack of FAs for energy production, we expected that macrophages lacking ATGL and HSL induce autophagy.

3. Materials and Methods

3.1 Diethyl pyrocarbonate water

Diethyl pyrocarbonate (DEPC, 400 µl) was dissolved in ddH_2O (400 ml), kept stirring under the hood overnight, and then autoclaved.

3.2 Thioglycolate medium (3%)

Agar (0.7 g), L-cystein (0.25 g), glucose (6 g), peptone 140 (17 g), peptone 110 (3 g), sodium chloride (2.5 g), sodium sulfate (0.1 g), and sodium thioglycolate (0.5 g) were dissolved in ddH_2O (1000 ml) and boiled. The mixture was allowed to cool down at room temperature (RT) and stored in aliquots (15 ml and 50 ml) at -20°C.

3.3 PBS (10x)

NaCl (80 g), KCl (2 g), KH_2PO_4 (2 g), and $NaHPO_4x2H_2O$ (14.3 g) were filled up to 1000 ml with ddH_2O.

3.4 Western blot buffers and reagents

3.4.1 Acrylamide

Acrylamide (30 g) and bisacrylamide (0.8 g) were filled up to 100 ml with ddH_2O.

3.4.2 10x running buffer

Glycine (150.1 g), sodium dodecyl sulfate (SDS) (10 g) and Tris (30.3 g) were dissolved in ddH_2O (1000 ml).

3.4.3 Separating gel buffer

SDS (10%, 4 ml) and Tris (18.2 g) were dissolved in ddH_2O (80 ml), adjusted to pH 8.8, and filled up to a total volume of 100 ml with ddH_2O.

3.4.4 Stacking gel buffer

Tris (6 g) was dissolved in ddH_2O (90 ml), adjusted to pH 6.8 with HCl, and filled up to a total volume of 100 ml with ddH_2O.

3.4.5 SDS sample buffer

SDS (2.15 g) and Tris (0.76 g) were dissolved in ddH_2O (45 ml), adjusted to pH 6.8 with HCl and glycerol (80%, 10 ml) and a small amount of bromophenol blue were added.

3.4.6 SDS running buffer

Tris (30.3 g), glycine (150.1 g), and SDS (10 g) were filled up to 1000 ml with ddH_2O.

3.4.7 10x blotting buffer

Ethylendiaminetetraacetic acid (EDTA) (1 mg/ml), glycine (30 g), and Tris (12.1 g) were dissolved in ddH_2O (1000 ml).

3.4.8 10x washing buffer

NaCl (90 g), Tween 20 (5 g), Tris-HCl (pH 7.4, 1 M, 100 ml) were dissolved in ddH_2O (1000 ml).

3.4.9 Separating gel (SDS-gel, 12.5%)

Reagents	Volume (µl)
Acrylamide	3583
Separating gel buffer	217
ddH_2O	213
Tetramethylethylenediamine (TEMED)	4.4
Ammonium persulfate (APS), 10%	76
Total volume	4093.4

3.4.10 Separating gel (SDS-gel, 15%)

Reagents	Volume (µl)
Acrylamide	4300
Separating gel buffer	217
ddH_2O	213
TEMED	4.4
APS, 10%	76
Total volume	4810.4

3.4.11 Stacking gel (SDS-gel, 12.5% or 15%)

Reagents	Volume (µl)
Acrylamide	250
Stacking gel buffer	385
ddH_2O	885
TEMED	3.8
APS, 10%	38
Total volume	1561.8

3.5 Preparation of acetylated LDL

Native LDL (3.2 ml) was mixed with an equal volume of saturated NaCl and kept on ice under continuous stirring. Diethyl ether (5.4 µl) was added dropwise every 3 min until a total volume of 57.76 µl was added. After adding diethyl ether for the third time, PBS (10x, 100 µl) was added to avoid precipitation. The mixture was kept on ice under continuous stirring for 45 min. Acetylated LDL (acLDL) was dialyzed with sterile PBS (2-3 hours, 4°C). Total cholesterol (TC) concentration was determined enzymatically.

3.6 Phosphatidylcholine/phosphatidylinositol preparation

Phosphatidylcholine (20 mg/ml in toluene) was mixed with phosphatidylinositol (20 mg/ml in toluene) (3:1, v:v). Aliquots were pipetted into eppendorf tubes and overlayed with nitrogen gas. The tubes were sealed with parafilm and kept at -20°C.

3.7 Animals and diets

All animal experiments were approved by the Austrian Federal Ministry of Science and Research, Division of Genetic Engineering and Animal Experiments, Vienna, Austria (BMWF-66.010/0039-II/10b/2009, BMWF-66.010/0057-II/3b/2011). Mice with a targeted deletion of CGI-58 in myeloid cells (macCGI-58-/- mice) were generated by crossing CGI-58$^{flox/flox}$ mice (42) (provided by Dr. Guenther Haemmerle, University of Graz, Austria) with transgenic mice that express Cre recombinase under the control of the murine M lysozyme promoter (143) (LysMCre, C57BL/6 background; provided by Dr. Thomas Ruelicke, University of Veterinary Medicine Vienna, Austria). CGI-58$^{flox/flox}$ [wild-type (Wt)] mice were used as controls. To investigate atherosclerosis susceptibility, we generated CGI-58$^{flox/flox}$/ApoE-/- (designated as ApoE-/-) and macCGI-58/ApoE-DKO mice by crossing CGI-58$^{flox/flox}$ and macCGI-58-ko mice with ApoE-/- mice (The Jackson Laboratory, Bar Harbor, ME). Mice were either fed a standard chow diet [containing 4% fat and 21% protein (R/M H; Ssniff, Soest, Germany)], challenged with a Western type diet (WTD) [TD88137mod; 21% fat, 0.2% cholesterol (Ssniff, Soest, Germany)] or a high-fat/high cholesterol diet (HF/HCD) [E15126-34 EF R/M, 30% fat, 1% cholesterol] for 10-30 weeks starting at the age of 4-6 weeks. Mice were kept with water ad libitum on a regular light-dark cycle (12 h light, 12 h dark) in a clean environment. Body weights were measured weekly and plasma lipid parameters once a month.

For atherosclerosis studies using ASO-mediated KD of CGI-58, 6 week old male Ldlr-/- mice were fed a diet enriched in 0.2% (w/w) cholesterol and 20% of energy as lard for 16 weeks in conjunction with weekly injections (50 mg/kg) of either a non-targeting control ASO or CGI-58 ASO as previously described. (38) Plasma samples were collected by submandibular vein puncture at baseline (chow-fed animals, 6 weeks of age), and after 4, 8, and 16 weeks of diet and ASO treatment

for subsequent lipid and lipoprotein analyses. The ASO-mediated KD studies of CGI-58 were conducted in an American Association for Accreditation of Laboratory Animal Care-approved animal facility, and all experimental protocols were approved by the Institutional Animal Care and Use Committee at either the Wake Forest University School of Medicine or the Cleveland Clinic Lerner Research Institute.

To generate ATGL-/- HSL-/- (*A0H0)* mice*,* ATGL+/- mice were bred with female HSL-/- (*H0)* mice to create ATGL+/- HSL+/- mice. ATGL-/- (*A0)* (due to their short life span) (24) and male *H0* (infertile) mice (16) cannot be used for breeding. Mice were kept on chow diet (containing 4% fat and 19% protein; Altromin Spezialfutter GmbH, Lage, Germany) and water ad libitum on a regular light-dark cycle (12 h/12 h).

3.8 Genotyping

To collect DNA for genotyping, ear punches were dissolved in 140 µl DirectPCR-tail lysis reagent (Peqlab, Erlangen, GER) and 10 µl proteinase K (10 mg/ml; Roth, Karlsruhe, Germany) for 2 h at 56°C. Proteinase K was deactivated by incubating the samples at 85°C for 45 min. For genotyping, the following primers were used:

CGI-58$^{flox/flox}$-fwd: 5'-GTCATGGTTGTGGGGAAATC-3'; CGI-58$^{flox/flox}$-rev: 5'-GACTGGAAGGATTTGAGGGG-3'; Cre-mut: 5'-CCCAGAAATGCCAGATTACG-3'; Cre-comm: 5'-CTTGGGCTGCCAGAATTTCTC-3'; Cre-wt: 5'-TTACAGTCGGCCAGGCTGAC-3'; ApoE-fwd: 5'-GCCTAGCCGAGGGAG-AGCCG-3'; ApoE-rev: 5'-TGTGACTTGGGAGCTCTGCAGC-3'; ApoE-neo: 5'-GCCGCCCC-GACTGCATCT-3'; HSL-fwd: 5'-CATGCACCTAGTGCCATCCTTC-3'; HSL-rev: 5'-CTCACTGAGGCCTGTCTCGTTG-3'; ATGL-fwd: 5'-AGAGAGAGAAGCTGAAGCCTG-3'; ATGL-rev: 5'-GCCAGCGAATGAGATGTTCC-3'.

For amplification 1 µl of DNA was used and the corresponding DNA fragment was quantified using Hot FirePol DNA Polymerase according to the manufacturer's protocol (Solis Biodyne, Riia, Estonia). The PCR programs are listed in table 2 and table 3.

Table 2: PCR programs for genotyping of macCGI-58-/- and macCGI-58/ApoE-DKO mice.

	Cre recombinase		**CGI flox**	
Initial denaturation	95°C 15 min		95°C 15 min	
Denaturation	95°C 60 sec	40x	95°C 30 sec	35x
Annealing	60°C 60 sec		55°C 60 sec	
Elongation	72°C 90 sec		72°C 60 sec	
Final elongation	72°C 10 min		72°C 10 min	
Cool down	4°C ∞		4°C ∞	
	ApoE			
Initial denaturation	95°C 15 min			
Denaturation	95°C 30 sec	40x		
Annealing	65°C 60 sec			
Elongation	72°C 60 sec			
Final elongation	72°C 10 min			
Cool down	4°C ∞			

Table 3: PCR programs for genotyping of *A0*, *H0* and *A0H0* mice.

	ATGL		**HSL**	
Initial denaturation	95°C 15 min		95°C 15 min	
Denaturation	95°C 30 sec	35x	95°C 30 sec	35x
Annealing	62°C 60 sec		64°C 60 sec	
Elongation	72°C 60 sec		72°C 60 sec	
Final elongation	72°C 10 min		72°C 1 min	
Cool down	4°C ∞		4°C ∞	

3.9 Macrophage isolation and cultivation

Peritoneal macrophages were collected after an intraperitoneal (i.p.) injection of 2.5 ml 3% thioglycolate. After 3 days, the peritoneum was flushed with 10 ml PBS containing 1 mM EDTA. The cells were cultivated in DMEM (Gibco, Invitrogen, Carlsbad, CA) containing 10% lipoprotein-deficient serum (LPDS) and 1%

penicillin/streptomycin for 2-3 h. Thereafter, the cells were washed 3 times with prewarmed PBS and the adherent cells (macrophages) were cultured in DMEM containing 25 mM glucose, 4 mM glutamine, 1 mM pyruvate, 10% LPDS, and 1% penicillin/streptomycin for 24 h. Bone marrow-derived macrophages were isolated from femur and tibia by flushing bones with sterile PBS. Cells were cultured in DMEM containing 10% LPDS, 1% penicillin/streptomycin, and 10 ng/ml M-CSF for 7 days.

To assess *in vitro* LPS-induced acute-phase response, macrophages were treated with PBS (control) or LPS (100 ng/ml) for 16 h. IL-6 concentrations in supernatants were determined by ELISA (Enzo Life Sciences, Lausen, Switzerland).

For the studies using ASO-mediated KD, elicited peritoneal macrophages were collected 4 days after injection of 1 ml of 10% thioglycolate into the peritoneal cavities of C57BL/6 mice that had been treated with ASOs and fed a chow diet for 6 weeks, as previously described. (144) Following 2 h of culture, non-adherent cells were removed by washing three times with PBS, and remaining adherent macrophages were harvested for Western blotting using methods previously described. (38)

3.10 Plasma lipid parameters

Blood was collected from 12 h-fasted mice or from 12 h-fasted/2 h-refed mice, and plasma was prepared by centrifugation at 5,200 *g* for 7 min at 4°C. Plasma TG, TC, FC, and nonesterified FA concentrations were measured enzymatically by commercially available kits (DiaSys, Holzheim, Germany; Wako Chemicals GmbH, Neuss, Germany). For atherosclerosis studies using ASO-mediated KD of CGI-58, total plasma concentrations of TC and TG were measured enzymatically by commercially available kits (Wako Chemicals, Richmond, VA). In addition, plasma lipoproteins were separated by fast protein liquid chromatography, and cholesterol concentrations in lipoprotein fractions were measured using an enzymatic assay as previously described. (144)

3.11 Lipid parameters in macrophages

Macrophages were plated for 2 h in serum-free DMEM. After washing the cells three times with PBS, lipids were extracted with 2 ml hexane:isopropanol (3:2, v:v) for 1 h at 4°C. One hundred microliters of 1% Triton X-100 in chloroform were added and the lipid extract was dried under a stream of nitrogen. The samples were dissolved in 100 µl ddH_2O for 15 min at 37°C in a water bath. TG, TC, and FC concentrations were measured enzymatically by using 30 µl of the sample and above mentioned kits. The readings were normalized to protein concentrations. Protein was quantitated using a Lowry Assay (Bio-Rad Laboratories, Hercules, CA) after dissolving the cell proteins in 2 ml NaOH (0.3 M) for 2 h at RT. Thirty microliters were used to determine protein concentration.

FA composition was quantitated by GC-flame ionization detection. Lipids were extracted from macrophages by using hexane/isopropanol (3:2, v/v; 1 h, 4°C). Lipid extracts were separated by thin layer chromatography (TLC) (hexane:diethylether:acetic acid, 70:30:1, v:v:v), TLC plates were stained with iodine vapor, bands corresponding to selected lipid species were scraped off, extracted with $CHCl_3$/MeOH (2:1, v:v), dried, and transesterified in BF_3/toluene. (145) For transesterification, 1 ml of BF_3 was added to lipids dissolved in 1 ml of toluene and incubated for 1 h at 110°C. Reactions were stopped by the addition of 2 ml of ice-cold H_2O. FA methyl esters (FAMEs) were extracted twice by the addition of 200 µl of hexane and shaking for 10 min at RT. After centrifugation (1,480 *g*, 10 min, 4°C) the upper phase was collected. The combined phases were evaporated under nitrogen, and FAMEs were dissolved in 10 µl of toluene. The GC conditions were set to split injection (split flow, 15 ml/min; split ratio, 1/5; injection volume, 2 µl) using an injector temperature of 230°C and a wall-coated open tubular fused silica column (25 m, 0.32-mm inner diameter, free fatty acid phase-coated, film thickness 0.3 µm; Agilent Technologies, Santa Clara, CA). The carrier gas consisted of helium. As a temperature gradient, two consecutive ramps from 150 to 230 °C (ramp 1, 2.5 °C/min to 215 °C hold for 10 min; ramp 2, 10 °C/min to 230 °C hold for 12.5 min) were used. Flame ionization detector (Trace-GC Ultra, Thermo- Quest Corp., Atlanta, GA) conditions were as follows: base temperature, 150 °C; gas flow, split ratio 1:7, 350 ml/min air, 35 ml/min hydrogen, and 60kPa helium, constant pressure). Data acquisition and analysis were done

with Chrom-Cad data system software. For quantitative analysis the corresponding peaks of FAMEs were integrated, and peak areas were calculated in relation to the C15:0 peak as the internal standard. FAME concentrations were calculated as percentage of total FAMEs in a given sample and/or as amounts per microgram protein (µg/ml). Pentadecanoic acid was used as internal standard. Separation and quantitation were performed as previously described. (145) This experiment was performed by Helga Reicher.

3.12 Tissue lipid analysis

Lipid parameters were determined from livers of macCGI-58/ApoE-DKO and control mice fed a HF/HC diet for 10 weeks. Liver pieces were homogenized in PBS. Lipids were isolated via folch extraction. A chloroform/methanol (2:1) solution in 20-fold excess was added to tissues lysates, which were then rotated for 2 h. After centrifugation at 2,630 *g* for 15 min, PBS (0.2 parts) was added to the supernatant. Samples were vortexed and centrifuged again for 15 min at 660 *g*. The lower phase (folch extract) was taken and dried under a stream of nitrogen. One hundred µl 1% Triton-X100 in chloroform were added and the samples dried under nitrogen gas. The samples were dissolved in 100 µl ddH_2O, and TG, TC, and FC concentrations were measured enzymatically (DiaSys, Holzheim, Germany; Wako Chemicals GmbH, Neuss, Germany). Values were normalized to protein concentrations.

3.13 Nile Red staining and fluorescence microscopy

Macrophages were plated on chamber slides in DMEM containing 10% LPDS and 1% penicillin/streptomycin for 24 h. Cells were washed three times with PBS and fixed with 4% paraformaldehyde in PBS (Sigma-Aldrich, Vienna, Austria) for 30 min. Lipid droplets were visualized after Nile Red staining (2.5 µg/ml) by confocal laser scanning microscopy using an LSM 510 META microscope system (Carl Zeiss GmbH, Vienna, Austria). Pictures (x63 magnification) were taken at excitation 543 nm and signals were recorded using a 560 nm long pass filter.

3.14 Neutral and acid TG and CE hydrolase activity assays

Macrophages were lysed with 100 µl lysis buffer [100 mM potassium phosphate, 250 mM sucrose, 1 mM EDTA, 0.1 mM dithiothreitol (DTT, pH 7) or 250 mM sucrose, 1 mM EDTA, 1 mM DTT (pH 4)] and protein concentrations were measured using a Lowry assay (BioRad Laboratories, Hercules, CA). The TG substrate contained 17 nmol triolein/assay and 2,000 cpm/nmol of [9,10-^{3}H(N)]-triolein (Perkin Elmer, Waltham, MA). The CE substrate contained 20 nmol cholesteryl oleate/assay and 1,000 cpm/nmol of cholesteryl [1-^{14}C]oleate (Amersham Biosciences, Piscataway, NJ). Fifty micrograms of protein from cell lysates were mixed with 100 µl of substrate and incubated in a water-bath for 1 h at 37°C. The reaction was stopped by the addition of 3.25 ml stop solution (methanol:chloroform:n-heptane, 10:9:7, v:v:v) and 1 ml of 0.1 M potassium carbonate and 0.1 M boric acid (pH 10.5). The tubes were vortexed for 10-15 s and centrifuged at 800 *g* for 20 min at 4°C. The radioactivity in 1 ml of the upper phase was determined by liquid scintillation counting, and the release of FAs was calculated.

3.15 LPAAT activity assay

Macrophages were lysed with 100 µl of lysis buffer [0.25 M sucrose, 1 mM EDTA, 1 mM DTT; pH 7.0] and protein concentrations were measured using a Bradford assay (BioRad Laboratories, Hercules, CA). LPAAT activity was assessed by mixing 100 µl lysates of CGI-58-/- macrophages with 100 µl substrate solution containing 100 µM lysophosphatidic acid (LPA) as acyl group acceptor and 20 µM [1-^{14}C-oleoyl]oleoyl-CoA as acyl group donor in 50 mM Tris-HCl buffer, pH 7.5, followed by incubation of samples for 10 min at 37°C in a waterbath without shaking. Reactions were stopped by the addition of 1.2 ml chloroform:methanol (2:1, v:v) and 400 µl of acidified water (2% ortho-phosphoric acid). Samples were mixed vigorously and centrifuged at 800 *g* for 10 min at RT. After phase separation, the top aqueous phase was discarded and the lower organic phase containing ^{14}C-labeled phosphatidic acid (PA) was dried under a stream of nitrogen. Dried lipids were dissolved in 50 µl chloroform and spotted onto a silica gel 60 plate. Lipids were separated using developing solvent of chloroform:methanol:acetone:glacial acetic acid:water (50:10:20:15:5, v:v:v:v:v),

and radiolabeled lipids were visualized using a PhosphorImager Screen (GE Healthcare) on a phosphor imager (Storm 860, Molecular Dynamics). Bands corresponding to PA were scraped from the TLC plates and radioactivity quantified by liquid scintillation counting.

3.16 LPL activity in macrophages

Macrophages were incubated in 6-well plates with 300 µl medium, 2% FA-free bovine serum albumin (BSA) (Sigma-Aldrich, St. Louis, MO), and 2 units/ml of heparin for 1 h at 37°C under continuous shaking. For substrate preparation per sample, 0.6 µCi [^{3}H]triolein, 920 ng glycerol trioleate, and 0.1% Tritson X-100 in chloroform were evaporated under a stream of nitrogen. Forty microliters of 1 M Tris-HCl (pH 8.6) and 80 µl ddH_2O were added, and the mixture was sonicated six times (1 min on and 1 min off) on ice. Forty µl of heat-inactivated human serum containing ApoC-II as activator (obtained from a pool of donors, heated at 50°C for 1 h and stored at 20°C) and 40 µl of 10% FA-free BSA were added to the substrate. For the analysis, 200 µl of the substrate were incubated with 100 µl of the sample for 1 h at 37°C. The reaction was stopped by the addition of 3.25 ml of a mixture of methanol/chloroform/heptane (1.41:1.25:1, v:v:v) and 1 ml of 100 mM potassium carbonate and 100 mM boric acid (pH 10.5). FAs were extracted by vortex mixing for 10 s, and phases were separated by centrifugation at 800 *g* for 10 min. Radioactivity in 1 ml of the upper phase was measured by liquid scintillation counting. Macrophages were lysed, and protein was quantitated by the method of Lowry.

3.17 Real time PCR including primer sequences

Macrophages were cultivated in DMEM (Gibco, Invitrogen, Carlsbad, CA) containing 10% LPDS and 1% penicillin/streptomycin for 24 h to get rid of the thioglycolate effect. To investigate if ATGL or HSL deficiency or bafilomycin A1 treatment affects cholesterol metabolism, macrophages were cultivated in DMEM/1% P/S containing 2% FA-free BSA in the absence and presence of Atglistatin (Ai; 40 µM), HSL inhibitor 76-0079 (Hi; 25 µM) (146), and bafilomycin A1 (10 nM) for 6h.

Total RNA from macrophages was isolated using PerfectPure RNA Cultured Cell kit (5Prime, Hamburg, Germany). Macrophages were lysed with lysis buffer containing 1% β-mercaptoethanol. Total RNA from tissues was isolated using TriFast (Peqlab, Erlangen, Germany). RNA concentrations were measured at 260 nm on a NanoDrop (Thermo Scientific, Wilmington, DE). Two micrograms of total RNA were reverse-transcribed by using the high capacity cDNA reverse transcription kit (Applied Biosystems, Foster City, CA, protocol see table 4 and 5).

Table 4: Mastermix for reverse transcription.

Reagent	**Volume (µl)/reaction**
10X RT Buffer	2
25X dNTP Mix (100mM)	0.8
10X RT Random Primers	2
Multiscribe Reverse Transcriptase	1
RNase Inhibitor	0.7
Nuclease-free H_2O	3.5
1µg RNA/10µl H_2O	10
Total volume per reaction	**20**

Table 5: PCR program for reverse transcription.

	Step 1	**Step 2**	**Step 3**	**Step 4**
Temperature	25°C	37°C	85 °C	4 °C
Time	10 min	120 min	5 s	∞

Quantitative real time PCR (qPCR) was performed on a LightCycler 480 (Roche Diagnostics) using the Quantifast™ SYBR® Green PCR kit (Qiagen, Hilden, Germany) (qPCR protocol see table 6).

Table 6: PCR program for real time PCR.

Denaturation and Amplification	95°C 60°C	10 s 30 s	40
Melting curve	95°C 60°C 95°C	10 s 20 s continuous	1 1
Cool down	4°C	20 s	1

Amplification of either murine hypoxanthine-guanine phosphoribosyltransferase (HPRT) (for cells) or Cyclophilin A (for tissues) as housekeeping genes was performed on all samples as internal controls for variations in mRNA amounts. Expression profiles and associated statistical parameters were determined using the public domain program Relative Expression Software Tool — REST 2008 (http://www.gene-quantification.com/download.html) (147) or analyzed by the 2^{-ddCt} method. (148) Primer sequences which were used are listed in Table 7.

Table 7: Primer sequences.

Gene	Forward primer (5'-3')	Reverse primer (5'-3')
Hprt	GCCTGTATCCAACACTTCG	GCTGACCTGCTGGATTACA
Cgi-58	GGTTAAGTCTAGTGCAGC	AAGCTGTCTCACCACTTG
Bcl-XL	GACAAGGAGATGCAGGTATTGG	TCCCGTAGAGATCCACAAAAGT
Mcl-1	AAAGGCGGCTGCATAAGTC	CTGGCGGTATAGGTCGTCCTC
Pdi	CAAGATCAAGCCCCACCTGAT	AGTTCGCCCCAACCAGTACTT
Erdj4	CCCCAGTGTCAAACTGTACCAG	AGCGTTTCCAATTTTCCATAAATT
Cpt1α	CTCCGCCTGAGCCATGAAG	CACCAGTGATGATGCCATTCT
Aox	AGATTGGTAGAAATTGCTGCAAAA	ACGCCACTTCCTTGCTCTTC
Vlcad	CTACTGTGCTTCAGGGACAAC	CAAAGGACTTCGATTCTGCCC
Mcad	GCAACTGCCCGCAAGTTT	TACTCCCCGCTTTTGTCATATTC
Gro-1	CTGGGATTCACCTCAAGAACATC	CAGGGTCAAGGCAAGCCTC
Mcp-1	ACTGAAGCCAGCTCTCTCTTCCTC	TTCCTTCTTGGGGTCAGCACAGAC
Mcp-2	TCTACGCAGTGCTTCTTTGCC	AAGGGGGATCTTCAGCTTTAGTA
Ccl5	GCTGCTTTGCCTACCTCTCC	TCGAGTGACAAACACGACTGC

Mrc-1	GCTGAATCCCAGAAATTCCGC	ATCACAGGCATACAGGGTGAC
Atgl	GCCACTCACATCTACGGAGC	GACAGCCACGGATGGTCTTC
Hsl	GCTGGTGACACTCGCAGAAG	TGGCTGGTGTCTCTGTGTCC
Lpl	ACATTCCCGTTACCGTCCATC	GGACCCCTGAAGACACAG
Lal	CGGCTTGCTGGCAGATTCTA	GTGCAGCCTTGAGAATGACC
TNF-α	CCACCACGCTCTTCTGTCTAC	AGGGTCTGGGCCATAGAACT
IL-6	TGATGCACTTGCAGAAAACA	ACCAGAGGAAATTTTCAATAGGC
IL-10	ATCGATTTCTCCCCTGTGAA	TGTCAAATTCATTCATGGCCT
IL-1β	TGTGAAATGCCACCTTTTGA	GGTCAAAGGTTTGGAAGCAG
SAA	ACCAGGAAGCCAACAGACATG	GCAGGCCAGGAGGTCTGTAG
SAP	TCTGGGATTGAGATCTTACAACAAAA	CTGCCGCCTTGACCTCTTAC
Adiponectin	GGAGATGCAGGTCTTCTTGG	CGAATGGGTACATTGGGAAC
Emr1	CTTTGGCTATGGGCTTCCAGTC	GCAAGGAGGACAGAGTTTATCGTG
Arg-1	TGGCTTGCGAGACGTAGAC	GCTCAGGTGAATCGGCCTTTT
Cd68	GTCACTCATAACCCTGCCACC	GGACACATTGTATTCCACCGCC
FcγR1	GAAGTCCCTTTGGTTTCTGAGC	CACTGAGCTTCGAGGTCCATC
FcγR2	ATGGGAATCCTGCCGTTCCTA	CCGTGAGAACACATGGACAGT
FcγR3	TCACTGTCCAAGACCCAGCAA	CGGGGTTTGAAGATTTCTCCGTA
Abca1	CTCTTCATGACTCTAGCCTGGA	ACACAGACAGGAAGACGAACAC
Abcg1	GACGCTGACTATAAGAGAGACC	GGAGTTGCTCAGGACCTTCTTG
SrB1	TTTGGAGTGGTAGTAAAAAGGGC	TGACATCAGGGACTCAGAGTAG
Cd36	GCAGGTCTATCTACGCTGTG	GGTTGTCTGGATTCTGGAGG
Srebp2	GTGCGCTCTCGTTTTACTGAAGT	GTATAGAAGACGGCCTTCACCAA
HMGCoAR	CTATTGCACCGACAAGAAGCCT	GCCATCACAGTGCCACATACAA

3.18 Western blotting

Protein samples of macrophages from the different genotypes (40 or 50 µg protein/lane) lysed in radioimmunoprecipitation assay (RIPA) buffer (50mM Tris-HCl, 150mM NaCl, 1% Triton X-100, 0.5% Deoxychelate) were separated by SDS-PAGE (12.5% or 15%). Proteins were transferred to polyvinylidene difluoride or nitrocellulose membranes. Blots were incubated with monoclonal anti-mouse

antibodies against β-actin (1:20,000) and cyclooxygenase 4 (1:500) (Santa Cruz, Heidelberg, Germany), ABHD5/CGI-58 (1:1,000) (Abnova GmbH, Heidelberg, Germany), and CHOP (1:1,000) (Cell Signaling Technology, Danvers, MA), or a monoclonal anti-mouse antibody cocktail (MitoProfile® Membrane Integrity WB Antibody Cocktail; 1:200; Abcam Cambridge, UK), or anti-rabbit polyclonal antibodies against Bax (1:1,000), cytochrome C (1:1,000), IRE1α (1:1,000), ATGL (1:200), HSL (1:800), LC3B (1:1,000), p62 (1:1,000), cathepsin B (1:1,000), GAPDH (1:1,000) (Cell Signaling Technology), and LAL (1:500; Seven Hills Bioreagents, Cincinnati, OH). HRP-conjugated goat anti-rabbit (1:5,000) or rabbit anti-mouse antibodies (1:1,000) (Dako, Glostrup, Denmark) were visualized by enhanced chemiluminescence detection (Clarity™ Western ECL Substrate; Bio-Rad) using a ChemiDoc™ MP Imaging System (Bio-Rad).

3.19 Mitochondrial respiration measurement

Macrophages were plated in XF96 polystyrene cell culture microplates (Seahorse Bioscience®, North Billerica, MA) at a density of 60,000 cells per well. After 24 h, cells were washed and preincubated for 30 min in XF assay medium supplemented with sodium pyruvate (1 mM) with or without glutamine (2 mM) and glucose (25 mM) at 37°C in a non-CO_2 environment. The oxygen consumption rate (OCR) was subsequently measured every 7 min using an XF96 extracellular flux analyzer (Seahorse Bioscience®). A standard protocol with 15 min basal measurement followed by 10 µM oligomycin, addition of 0.3 µM carbonyl cyanide *p*-trifluoromethoxyphenylhydrazone (FCCP), and 2.5 µM antimycin A was performed. Oxygen consumption was either normalized to protein content (pmol O_2/min × µg protein) or expressed as a percentage of the maximal mitochondrial respiration in the presence of 0.3 µM FCCP. This experiment was performed by Corina Madreiter.

3.20 Confocal analysis of mitochondrial area

To label mitochondria, macrophages were seeded on glass coverslips in 6-well plates. After 24 h, cells were incubated with MitoTracker® Red probes (25 nM) in a loading buffer containing 135 mM NaCl, 5 mM KCl, 2 mM $CaCl_2$, 1 mM $MgCl_2$, 10

mM HEPES, 2.6 mM $NaHCO_3$, 440 µM KH_2PO_4, 340 µM Na_2HPO_4, 10 mM D-glucose, 0.1% vitamins, 0.2% essential amino acids, and 1% penicillin/streptomycin (pH 7.4). Staining solution was replaced after 20 min with fresh loading buffer. Z-scans of stained cells were performed on a Nipkow-disk-based array confocal laser-scanning microscope, equipped with VoxCell Scan® (VisiTech, Visitron Systems, Puchheim, Germany) and controlled by VisiView Premier Acquisition software (Visitron Systems). Stained cells were imaged with a 100X objective (α-Plan-Fluar 100x/1.45 NA Oil, Zeiss Microsystems, Oberkochen, Germany) using the 514 nm diode laser (50 mW, Visitron Systems) for illumination. Emitted light was filtered at 568 nm (Chroma Technology Corp., Bellows Falls, VT, USA) and images were taken with a CCD camera (CoolSNAP-HQ, Roper Scientific Corp., Martinsried, Germany). Mitochondrial area analysis was performed with MetaMorph 7.7.0.0 software (Visitron Systems). This experiment was performed by Corina Madreiter.

3.21 Phagocytosis of fluorescein-labeled *Escherichia coli* particles

Macrophages were plated in black 96-well µClear plates (Greiner Bio-One GmbH, Solingen, Germany). After 24 h of preincubation in DMEM, 10% LPDS, and 25 mM glucose, cells were incubated in DMEM, 10% LPDS, and 0, 6, or 25 mM glucose for 1 h, respectively. Cells were washed and incubated with 100 µl of fluorescein-labeled *Escherichia coli* (*E. coli)* BioParticles [Vybrant™ phagocytosis assay, Molecular Probes, Invitrogen; suspended in Hank's balanced salt solution (HBSS); 2 h]. The suspension was removed and subsequently 100 µl of trypan blue was added (1 min) to quench the extracellular probe. After aspiration of trypan blue, the fluorescence was measured at 484 (excitation) and 535 nm (emission) on a Victor 1420 multilabel counter (PerkinElmer Life Sciences, Turku, Finland). Fluorescence was normalized to the protein content of each well.

To analyze phagocytosis *in vivo*, mice were injected i.p. with 200 µl of fluorescein-labeled *E. coli* BioParticles suspended in HBSS. After 2 h, macrophages were collected by flushing the peritoneal cavity with 10 ml PBS containing 1 mM EDTA and incubated in DMEM containing 25 mM glucose and 10% LPDS for 90 min. The cells were washed three times with PBS, and fluorescence was measured

before and after adding trypan blue to obtain total and intracellular fluorescence, respectively. Experimental readings were normalized to protein content.

3.22 Apoptosis assay

Apoptosis was assayed by annexin V and propidium iodide (PI) co-staining (Annexin-V-Fluor staining kit; Roche, Vienna, Austria). Two hundred thousand cells were washed twice with 200 µl PBS, 50 µl staining buffer was added, and cells were incubated for 10 min. Macrophages were immediately analyzed on a FACScalibur flow cytometer (BD Biosciences, San José, CA).

3.23 Glucose tolerance test

Animals were fasted for 6 h (6 AM to 12 PM) with free access to drinking water. Blood was taken from the tail vein before and 15, 30, 60, 120, and 180 min after an i.p. injection of glucose (2.0 g/kg body weight). Glucose concentrations from blood were determined using a portable glucometer (AccuCheck).

3.24 Oil Red O staining

Oil red O (0.5 g) was mixed with 100 ml isopropanol under constant stirring for 24 h. Working reagent: 30 ml of filtered stock + 20 ml distilled water mixed for 10 min (use on the same day). Aortic root sections were dipped in 4% paraformaldehyde-PBS for 10 min. Sections were transferred to 60% isopropanol for 5 min and incubated with working oil red O stain for 15 min. Thereafter, sections were dipped in 60% isopropanol for 1 s and counter stained with haematoxylin for 5 min and washed in tap water. Sections were air dried and mounted with glycerine jelly or DPX mountant. Mean lesion area (μm^2) was calculated from at least 10 consecutive oil red O-stained sections per mouse. Quantification of oil red O-stained sections was done by using the Leica image analysis system.

3.25 Preparation of histological sections and lesion analysis

I analyzed atherosclerotic lesions in the aortic root and aorta of ApoE-/- and macCGI-58/ApoE-DKO animals after 10 weeks of HF/HCD feeding. Mice were euthanized and the arterial tree was perfused in situ with PBS (100 mm Hg) for 10 min via a cannula in the left ventricular apex. Mice were perfused with 4% paraformaldehyde in PBS for 15 min. After fixing the hearts in 4% paraformaldehyde in PBS, serial sections (8 µm) were cut (HM 560 Cryo-Star; Microm International GmbH, Walldorf, Germany). Images of the atherosclerotic lesion areas in Oil Red O-stained (Sigma-Aldrich, St. Louis, MO) sections were taken with ScanScope T3 whole slide scanner (Aperio Technologies, Bristol, UK). Plaque areas were quantitated by ImageJ software. Mean lesion area was calculated from 10 consecutive Oil Red O-stained sections, starting at the appearance of the tricuspid valves. For *en face* analysis in macCGI-58/ApoE-DKO mice, aortas were dissected and plaques were stained with Oil Red O. Images were analyzed using ImageJ software.

For studies in ASO-treated mice, hearts and aortas were carefully separated and hearts were immediately slow frozen in OCT for cross-sectional lesion analysis of the aortic sinus. Whole aortas were fixed in 4% neutral buffered paraformaldehyde for subsequent *en face* analysis. For atherosclerosis quantification in the aortic sinus, histological cross sections were stained with Oil Red O. Images were captured using a Leica DMR microscope (W. Nuhsbaum Inc., McHenry, IL) equipped with a Q imaging Retiga EX camera. Images were analyzed using Image-Pro Plus 7.0 (MediaCybernetics, Rockville, MD). Additionally, *en face* lesion area was determined for the whole aorta. Studies in ASO-treated mice were performed by Mark Brown's group.

3.26 Monoclonal antibody to macrophages-2 immunostaining

Sections were fixed for 10 min in 4 % paraformaldehyde in PBS and washed with PBS. Sections were blocked for 10 min with peroxidase blocking and washed with PBS. Thereafter, UV protein block was added on sections for 7 min. Primary monoclonal antibody to macrophages-2 (MoMa-2, 1:600; Acris, Hiddenhausen, Germany) was added for 1h at RT, then at 4°C overnight. Thereafter sections

were washed three times with PBS and incubated for 30 min with goat anti-rat coupled to horse radish peroxidase (1:100; Dako Denmark A/S, Glostrup, Denmark) and washed three times with PBS. AEC substrate was added to the sections for 10 min and then washed 3 times with water. Sections were put into haematoxylin for 5 min and washed with water. The sections were dipped into ammonium water for 1 min, dehydrated, and fixed with DPX mountant.

3.27 Masson's Trichome staining

This staining was performed by using the Masson's Trichrome kit (Sigma). Aortic root sections were washed with water for 5 min and put into haematoxylin for 5 min. Sections were washed with water for 5 min, incubated in 1% panceau-acetic acid fuchsin solution for 5 min, washed with water and dipped in 1 % phosphomolybdic acid for 5 min, aniline blue for 5 min and 1 % acetic acid for 2 min, washed with water, and dehydrated (50, 70, 95 and 99% of ethanol and xylene). Sections were fixed with DPX mountant.

3.28 Cellular cholesterol efflux

Macrophages were incubated with 50 µg acLDL [preloaded with 0.5 µCi/ml [^{3}H]cholesterol (ARC Inc., St. Louis, MO)] and 30 µg/ml nonlabeled cholesterol in DMEM/0.2% FA-free BSA for 32 h at 37°C. After washing the cells twice with PBS, the cells were cultivated for 16 h in equilibration medium (DMEM/0.2% FA-free BSA). We determined cholesterol efflux after incubating the cells in DMEM/0.2% FA-free BSA in the absence or presence of 15 µg/ml ApoA-I (Calbiochem, La Jolla, CA) or 100 µg/ml HDL_3. Radioactivity in 80 µl medium and in the cells was measured by scintillation counting after 1, 3, 6, and 9 h of incubation. Cholesterol efflux is expressed as the percentage of total cell [^{3}H]cholesterol present in the medium after 1, 3, 6, and 9 h. Basal efflux in the absence of ApoA-I and HDL_3 was subtracted from the data shown.

3.29 LPS-induced acute-phase response

Mice were injected i.p. with either PBS or 5 mg/kg LPS (*E. coli* 0111:B4). Following injection, plasma was collected after 1 h by submandibular puncture [for

TNF-α measurements, TNF-α (mouse) ELISA kit, Enzo Life Sciences]. Exactly 6 h after injection mice were anesthetized with pentobarbital (0.9%) and plasma was isolated [for IL-6 measurements, IL-6 (mouse) ELISA kit, Enzo Life Sciences]. Thereafter, a midline laparotomy was performed and a whole-body perfusion was conducted by puncturing the inferior vena cava and slowly delivering PBS for 10 min (1 ml/min) into the left ventricle of the heart to remove residual blood. Multiple tissues were collected and snap-frozen for subsequent analysis. For *in vitro* LPS-induced acute-phase response, macrophages were treated with either PBS (control) or LPS (100 ng/mL) for 16h. Supernatant was used for IL-6 measurements using an IL-6 (mouse) ELISA kit (Enzo Life Sciences).

3.30 Induction of lipolysis via β-adrenergic stimulation

Mice were injected i.p. with 1 mg/kg of CL316,243 (Santa Cruz Biotechnology, Inc.) or PBS twice (4 h between each injection). Mice were sacrificed 14 h after the second injection. Perigonadal adipose tissue was excised, snap-frozen, and analyzed by qPCR.

3.31 Autophagic flux analyses and lysosomal function analysis

Macrophages were incubated with bafilomycin A1 (10 nM) or chloroquine (30 μM) (Sigma-Aldrich, Vienna, Austria) for 0 and 14 h for protein isolation and western blotting experiments using anti-p62 and anti-LC3 antibodies. DQ^{TM} Red BSA (DQ-BSA; Molecular Probes, Eugene, OR), a self-quenched red BODIPY dye conjugated to BSA, was used for measuring lysosomal activity. DQ-BSA requires enzymatic cleavage in acidic intracellular lysosomal compartments to generate a fluorescent product that can be monitored by flow cytometry and fluorescence microscopy. Macrophages were cultured in DMEM/10% LPDS/1% penicillin/streptomycin for 24 h. To induce autophagy, cells were fasted for 1 h in HBSS (PAA Laboratories, Linz, Austria). DQ-BSA was added at a final concentration of 10 μg/ml and incubated for 15 min at 37°C. After washing the cells twice with PBS, macrophages were cultured in DMEM/10% LPDS, and samples were taken after 0, 2, and 6 h, respectively. Red-fluorescent DQ-BSA

was analyzed by flow cytometry using a FACSCalibur flow cytometer (BD Biosciences, Mountain View, CA).

3.32 Oleate uptake

Macrophages were plated in 12-well plates and incubated with 300 µM OA-BSA and 1 µCi of [^{3}H]OA-BSA in DMEM/1% P/S per well for 24 h. Cells were washed twice with PBS and then equilibrated in DMEM/1% P/S for 1 h. Thereafter, macrophages were cultivated in DMEM/1% P/S containing 2% FA-free BSA in the absence and presence of the ATGL inhibitor Atglistatin (146) (Ai; 40 µM), the HSL inhibitor 76-0079 (Hi; 25 µM) (146), and bafilomycin A1 (10 nM). After 2, 6, and 14 h, an aliquot of medium was taken for determination of FA release. After 14 h, lipids were isolated from cells by hexane:isopropanol (3:2) extraction for 1 h. The extract was dried under a stream of nitrogen and dissolved in 50 µl of human serum. Each sample was loaded on a TLC plate and separated using hexane:diethyl ether:acetic acid (70:30:1, v:v:v) as solvent. The incorporated radioactivity was determined by liquid scintillation counting. Cells were lysed in 1 ml of 0.3 M NaOH and protein content was quantitated by Lowry assay.

3.33 Immunofluorescence

Macrophages were plated on coverslips in 12-well plates in DMEM/10% LPDS/1%P/S containing Bodipy ® 500/510 C1, C12 (C12-BODIPY; 0.4 µg/ml, Life Technologies) for 24 h. After incubation, cells were washed twice with PBS and then equilibrated in DMEM/1% P/S for 1 h. Thereafter, cells were washed and incubated in HBSS and bafilomycin A1 (10 ng/ml) for 1 h to chase incorporated C12-BODIPY. After rinsing, cells were fixed with 4% paraformaldehyde for 10 min at RT. Cells were washed three times for 5 min with PBS. Permeabilization was then performed with 0.25% Triton X-100 in PBS for 10 min at RT followed by washing three times for 5 min with PBS. Subsequently, cells were blocked with 1% BSA in glycine/PBS for 30 min at RT and incubated with anti-cathepsin D primary antibody (1:1200; Abcam, Cambridge, UK) in 1% BSA/PBS at 4°C overnight. Macrophages were washed three times with PBS for 5 min and incubated with secondary antibody [1:250, goat anti-mouse IgG (H+L) Alexa Fluor® 594

conjugated, Life Technologies] for 1 h at RT. Afterwards, cells were washed three times for 5 min with PBS and nuclear staining was performed with Hoechst. After washing (three times for 5 min with PBS), slides were mounted in Dako fluorescent mounting medium (Dako Denmark A/S, Glostrup, Denmark). Confocal images were acquired with a Zeiss Observer Z.1 inverted microscope (Carl Zeiss Microimaging GmbH, Goettingen, Germany) equipped with a Yokogawa CSU-X1 Nipkow spinning disk system (via Visitron Systems GmbH, Puchheim, Germany), a piezoelectric z-axis motorized stage (CRWG3-200, Nippon Thompson Co., Ltd, Tokyo, Japan), and a CoolSNAP HQ2 CCD Camera (Photometrics, Tucson, AZ). Fixed cells were excited with 405 nm, 488 nm and 568 nm laser lines (Visitron Systems GmbH) with exposure times of 2000, 500 and 600 ms using an alpha Plan-Fluor 100x/1.45 Oil M27 objective (Carl Zeiss Microimaging). Images were automatically background corrected and blind-deconvolved using Huygens 2.4.1 (Scientific Volume Imaging, SVI, VB Hilversum, The Netherlands). Colocalization analysis was performed with the ImageJ plugin JACOP. (149) Images were taken by Benjamin Gottschalk.

3.34 Electron microscopy

Macrophages were cultured on an Aclar film and fixed in 2.5% (w/v) glutaraldehyde and 2% (w/v) formaldehyde in 0.1 M phosphate buffer (pH 7.4, 2 h), postfixed in 2% (w/v) osmium tetroxide (2 h) at RT, dehydrated in graded series of ethanol, and embedded in a TAAB epoxy resin (Gröpl).

For high-pressure freezing (HPF), macrophages were grown on carbon-coated sapphire discs and frozen under liquid nitrogen conditions using 2000 bar within ms. Freezing was followed by freeze substitution in acetone by adding 2% OsO_4 and 0.2% uranyl acetate at temperatures below -70°C. After water in form of ice within the cells was replaced by substitution media, samples were embedded in epoxy resin. Ultrathin sections (75 nm) were cut with a Leica UC 7 Ultramicrotome and stained with lead citrate (5 min) and uranyl acetate (15 min). Images were taken using a FEI Tecnai G2 20 transmission electron microscope (FEI, Eindhoven, The Netherlands) with a Gatan ultrascan 1000 CCD camera (acceleration voltage 120 kV). Electron microscopy was performed by Dagmar Kolb.

3.35 Statistics

Statistical analyses were performed using GraphPad Prism 5.0 software. Significance was calculated by student's unpaired *t*-test, followed by Welch's correction (in case of unequal variances), or ANOVA, followed by Bonferroni correction. Data are presented as mean values ± SEM or + SD. Significance levels were set at $p < 0.05$ (*), $p \leq 0.01$ (**) and $p \leq 0.001$ (***).

4. Results: Role of CGI-58 in macrophages

4.1 CGI-58 is expressed in tissues, macrophages and foam cells and macrophage CGI-58 deficiency does not influence CGI-58, ATGL or HSL mRNA expression in tissues

CGI-58 is expressed in Wt mouse tissues, with its highest expression in testis, followed by BAT, WAT, and SM. Its lowest expression was found in the brain (Fig. 14A) Importantly, CGI-58 is expressed in murine macrophages as well as in foam cells (Fig. 14A, B). mRNA expression of CGI-58 (Fig. 14C), ATGL (Fig. 14D), and HSL (Fig. 14E) was unaltered in macCGI-58-/- murine tissues.

Figure 14

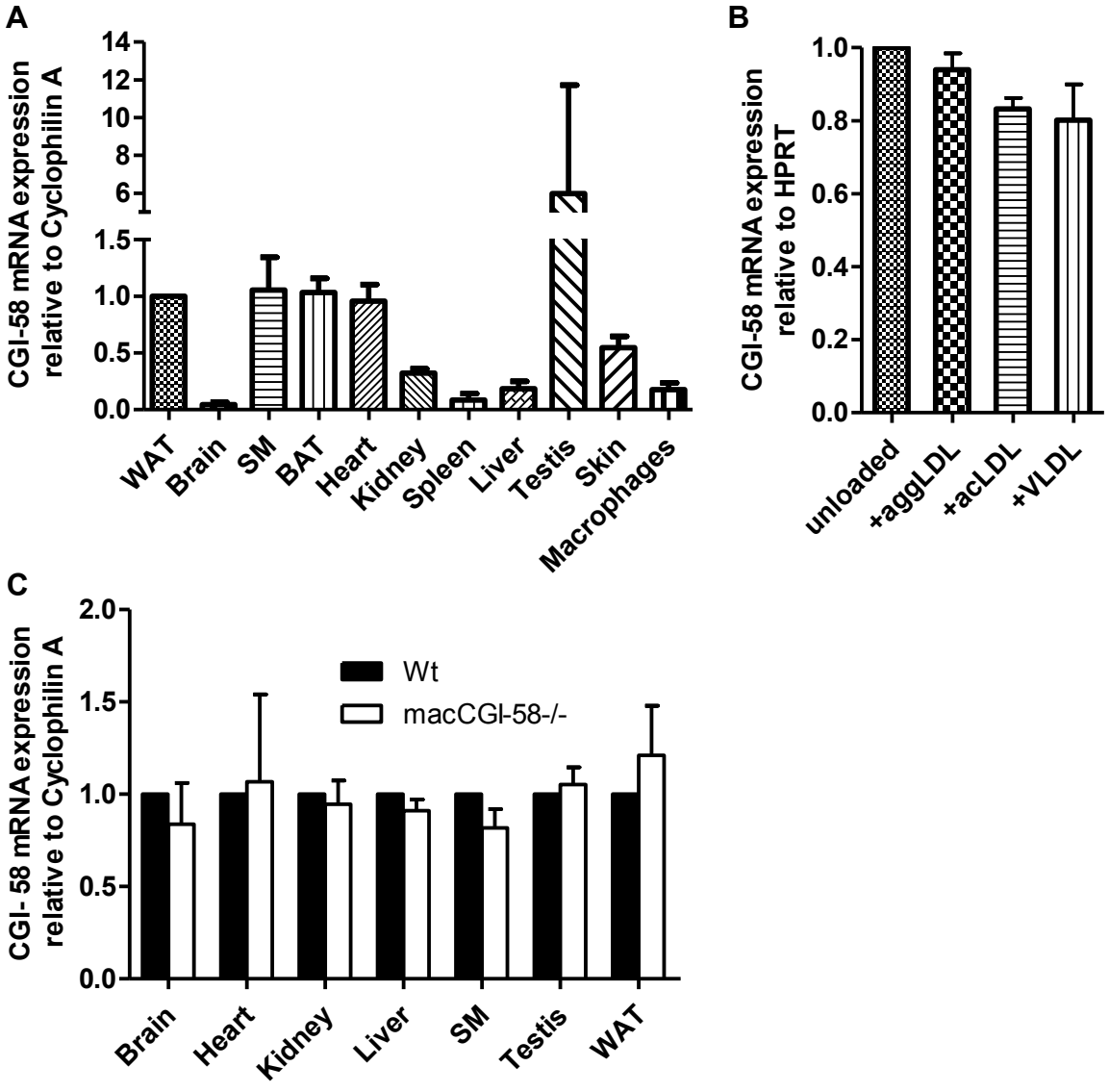

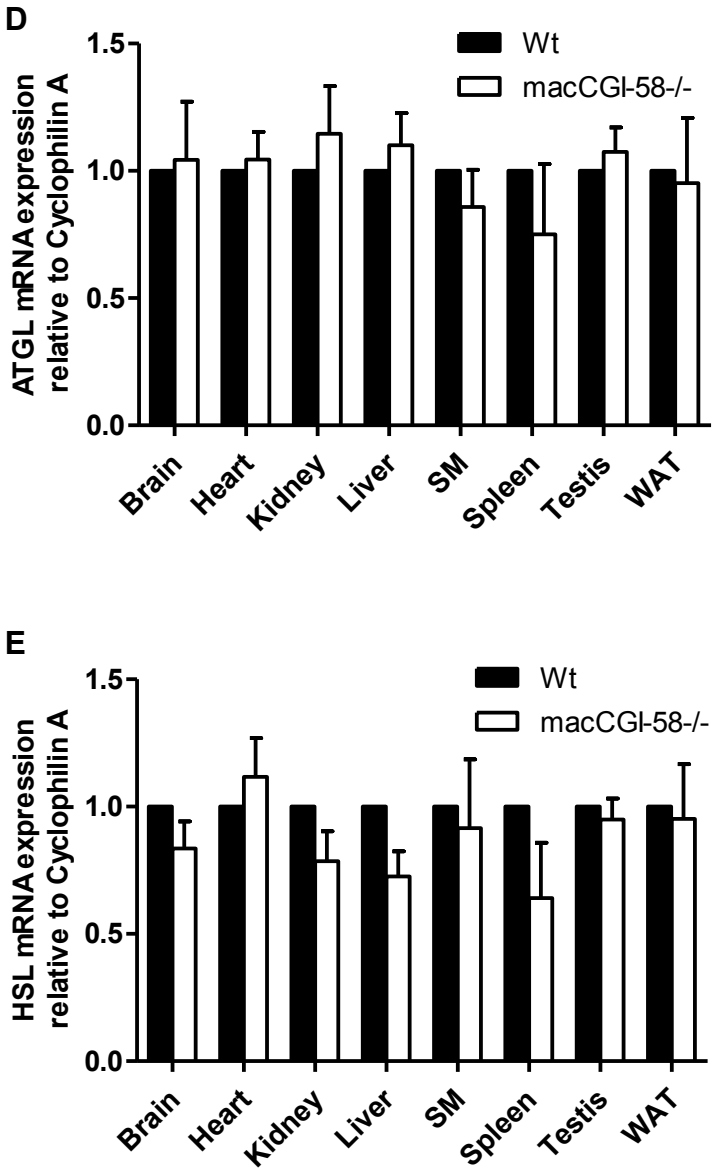

Figure 14: CGI-58 is expressed in murine tissues, macrophages, and foam cells. (A) CGI-58 mRNA expression in murine tissues and macrophages (n=2) and (B) in peritoneal macrophages and foam cells [macrophages either loaded with aggregated LDL (aggLDL), acetylated LDL (acLDL) or VLDL, 100 µg/ml each] (n=2). (C) CGI-58 (D) ATGL, and (E) HSL mRNA expression in Wt and macCGI-58-/- murine tissues. Data are shown as mean values (n=4) + SEM. Expression profiles were determined using the REST program.

4.2 Plasma lipid parameters, body weight, and glucose levels are unaffected in macCGI-58-/- mice

macCGI-58-/- mice are viable with no apparent changes in skin phenotype (not shown). We observed no differences in lipid parameters and body weight between female Wt and macCGI-58-/- mice, neither on chow (Fig. 15A, B) nor on WTD (Fig. 15C, D). Glucose concentrations were decreased at 39 weeks of age but comparable to control levels at all other time points (Fig. 15E). Glucose tolerance in mice fed WTD was unchanged as well (Fig. 15F).

Figure 15

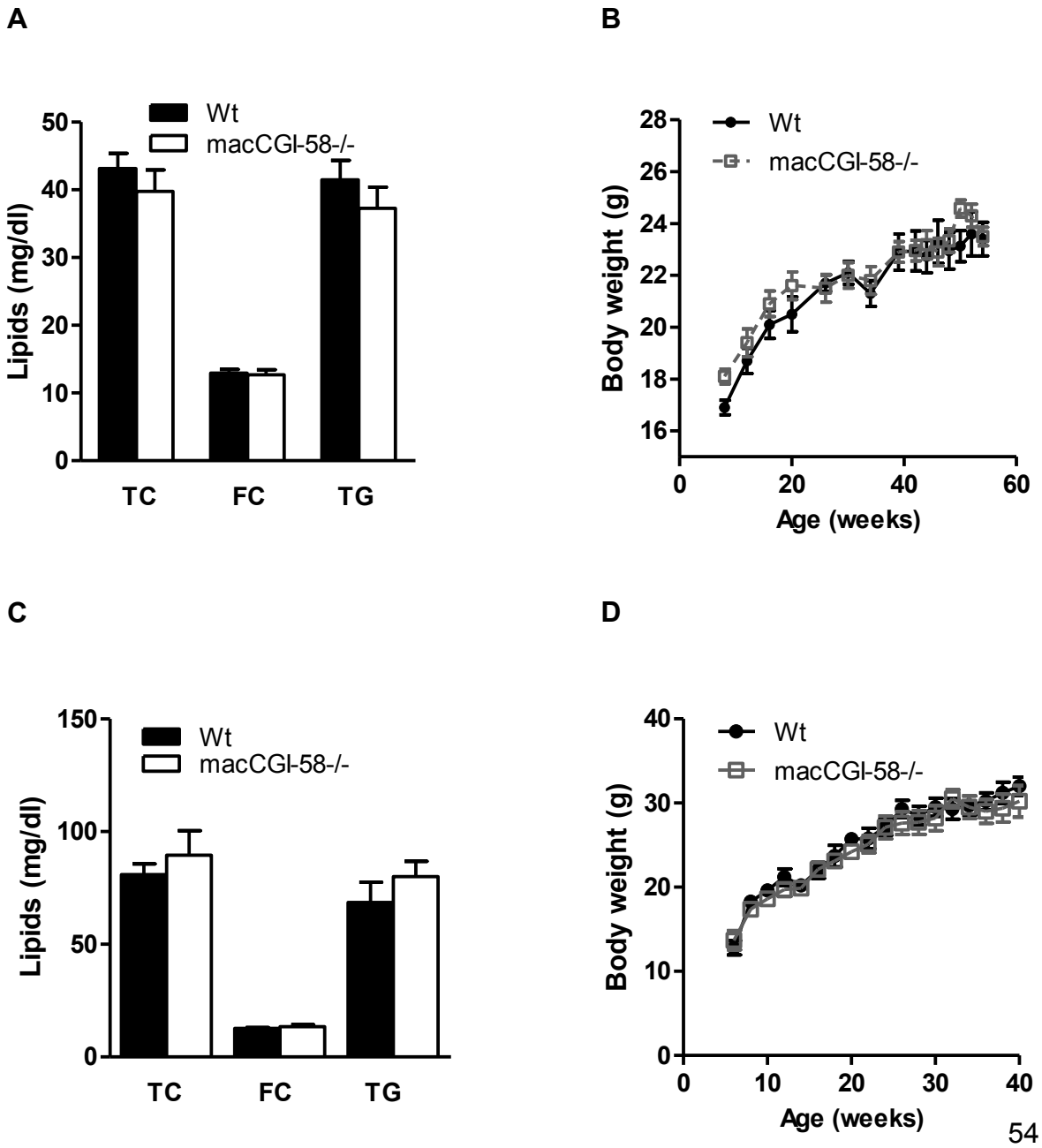

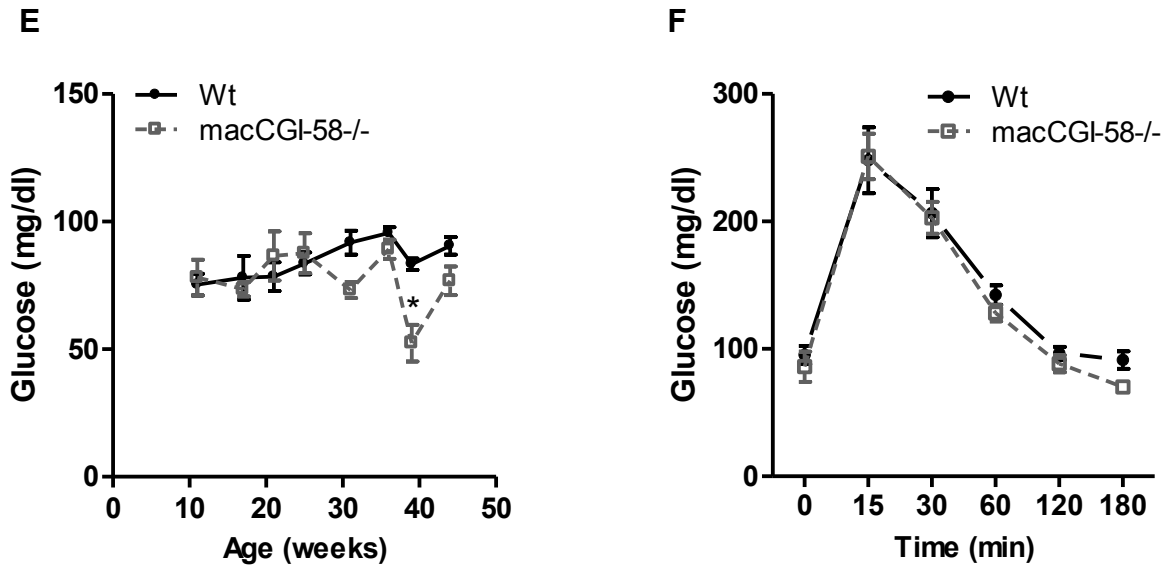

Figure 15: Unchanged plasma lipid parameters, body weight, glucose concentrations, and glucose tolerance in macCGI-58-/- mice. (A) Plasma parameters and (B) body weight of overnight fasted 12-14 weeks old female Wt and macCGI-58-/- mice fed a standard chow diet. (C) Plasma parameters and (D) body weight of overnight fasted 16-18 weeks old female Wt and macCGI-58-/- mice fed a WTD. (E) Glucose concentrations in female mice at 11 to 46 weeks of age on chow diet. (F) Glucose tolerance test of 34-35 weeks old female Wt and macCGI-58-/- mice fed a WTD. Data are shown as mean values (n=4-5) ± SEM. *, $p < 0.05$.

4.3 Significantly decreased TG hydrolase activity and TG-rich LD accumulation in CGI-58-/- macrophages

We confirmed the absence of CGI-58 expression in macrophages by qPCR (Fig. 16A) and Western blotting (Fig. 16B). TG hydrolase activity of lysates was significantly decreased (-29%) in CGI-58-/- compared to Wt macrophages (Fig. 16C). CGI-58-/- macrophages showed an increased number of LDs as evidenced by immunofluorescence and electron microscopy (Fig. 16D). Biochemical measurements revealed a specific accumulation of TG (Fig. 16E). CE hydrolase activities were comparable in macrophages from CGI-58-/- and Wt mice (Fig. 16F), which is in accordance with unaltered TC and FC concentrations (Fig. 16E). Furthermore, acid TG and CE hydrolase activities were unaffected in CGI-58-/- macrophages (Fig. 16G, H).

Figure 16

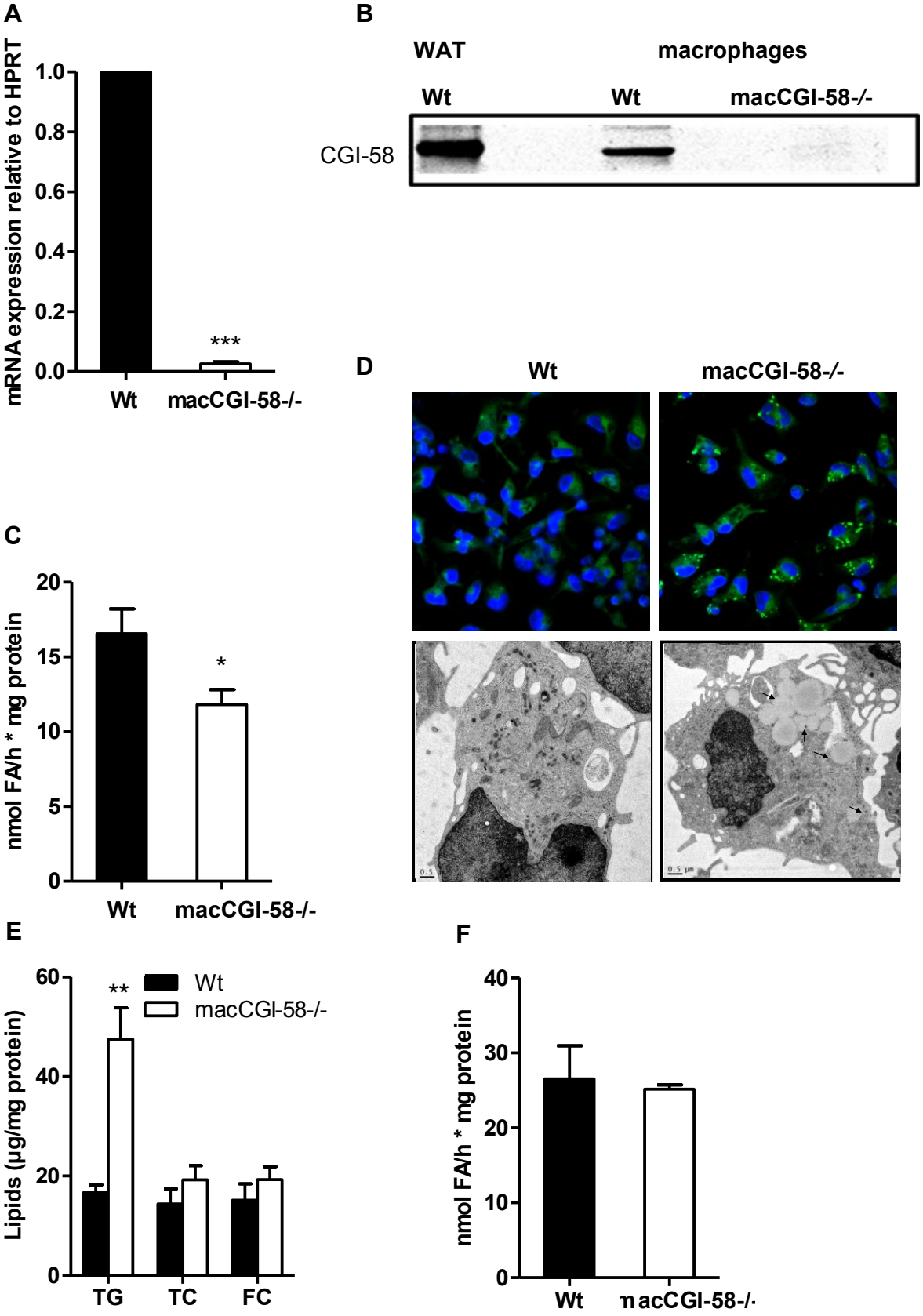
A
mRNA expression relative to HPRT
1.0
0.8
0.6
0.4
0.2
0.0
***
Wt
macCGI-58-/-
B
WAT
macrophages
Wt
Wt
macCGI-58-/-
CGI-58
C
nmol FA/h * mg protein
20
15
10
5
0
*
Wt
macCGI-58-/-
D
Wt
macCGI-58-/-
E
Lipids (µg/mg protein)
60
40
20
0
**
Wt
macCGI-58-/-
TG
TC
FC
F
nmol FA/h * mg protein
40
30
20
10
0
Wt
macCGI-58-/-

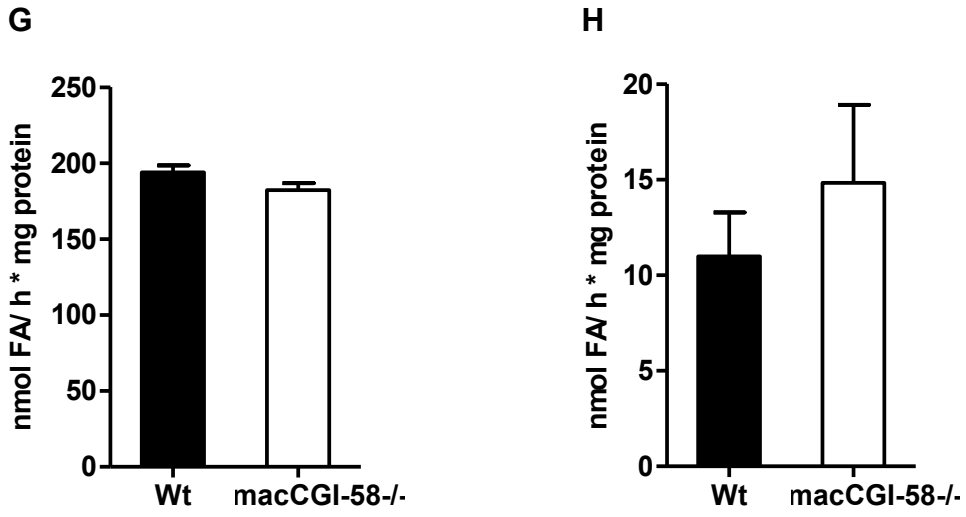

Figure 16: Decreased TG hydrolase activity and TG-rich LD accumulation in CGI-58-/- macrophages. (A) mRNA expression of CGI-58 in Wt and CGI-58-/- macrophages determined by qPCR, including normalization to HPRT, expressed as mean values (n=3-4) performed in duplicate + SEM. Expression profiles were determined using the REST program. (B) Western blot analysis of CGI-58 protein expression in Wt WAT as well as Wt and CGI-58-/- macrophages (50 µg protein per lane). (C) TG hydrolase activities in cell lysates of Wt and CGI-58-/- macrophages are presented as mean values (n=4) performed in duplicate + SEM. (D) Representative fluorescent microscopy images after Nile Red staining and electron micrographs of Wt and CGI-58-/- macrophages. LDs in CGI-58-/- macrophage are indicated by arrows. (E) TG, TC, and FC concentrations in lipid extracts of macrophages presented as mean values (n=4-5) + SEM. (F) CE hydrolase activities were assayed in cell lysates from Wt and CGI-58-/- macrophages (n=5). (G) Acid TG and (H) CE hydrolase activites in cell lysates of Wt and CGI-58-/- macrophages are presented as mean values (n=4-5) performed in duplicate + SEM. *, $p < 0.05$; **, $p \leq 0.01$; ***, $p \leq 0.001$.

4.4 TG hydrolysis preferences are comparable between both macrophage genotypes

Lipid composition analysis revealed that there is a significantly increased TG concentration in CGI-58-/- macrophages (Fig. 17A), as already shown in Fig. 16E. Analysis of FA composition within TG revealed increased concentrations of all FA species analyzed (Fig. 17B). Unchanged relative distribution of FAs within TG indicates that hydrolysis preferences are comparable between macrophages of both genotypes (inset Fig. 17B). Furthermore, we found an increased 16:0 FA level within PLs from CGI-58-/- compared to Wt macrophages (Fig. 17C). Analysis of the relative distribution revealed again an increase of 16:0 FA, whereas the

level of other FA-species was decreased (inset Fig. 17C). 18:0 and 18:1 FA-species levels were elevated in CGI-58-/- macrophages, however, when we determined the relative distribution there were no differences detectable (Fig. 17D and inset Fig. 17D).

Figure 17

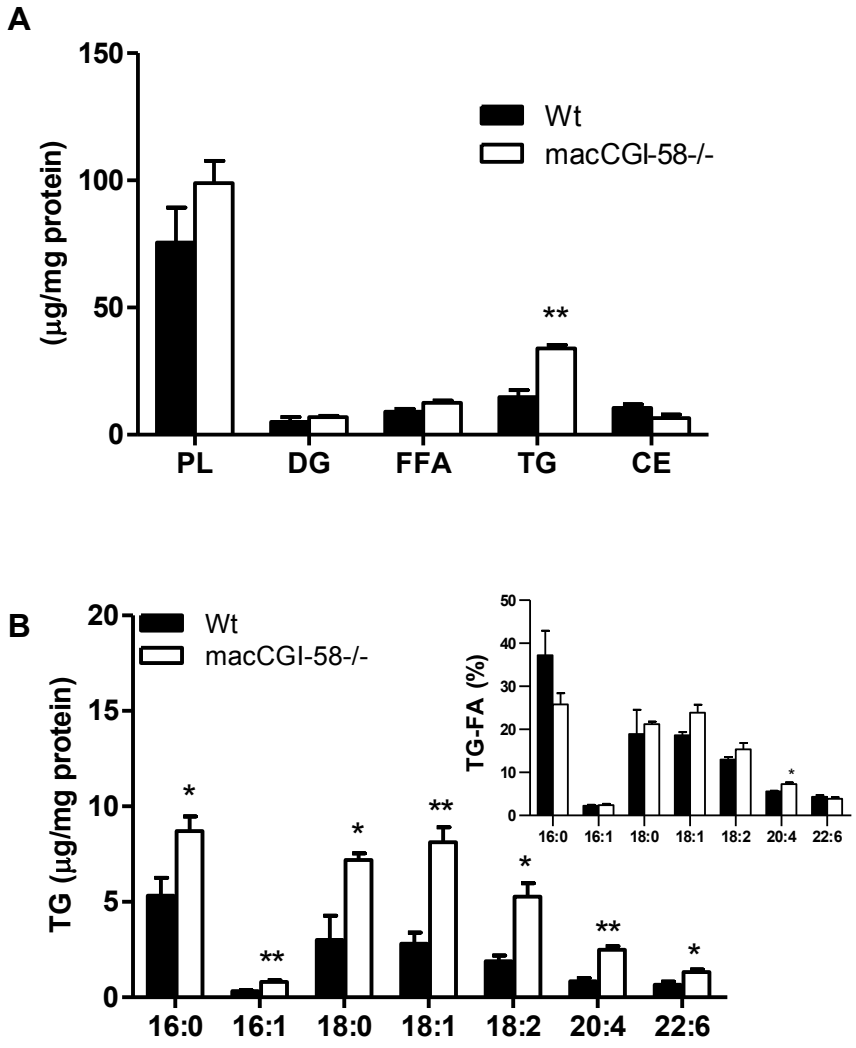

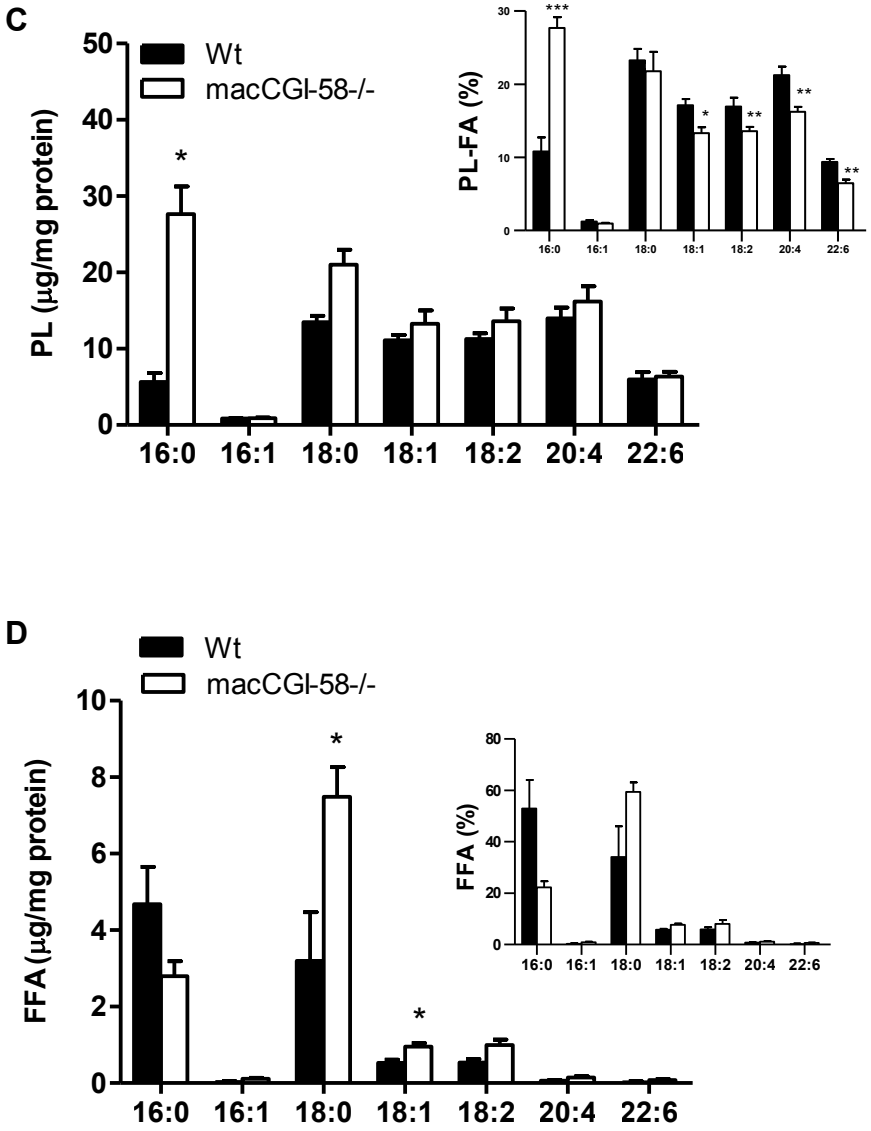

Figure 17: TG hydrolysis preferences are comparable between both Wt and macCGI-58-/- macrophages. (A) Lipid composition of Wt and CGI-58-/- macrophages after separation by TLC determined by GC/FID. (B) FA composition in TG of Wt and CGI-58-/- macrophages. Inset: TG-FA distribution in percentage. (C) FA composition in PL of Wt and CGI-58-/- macrophages. Inset: PL-FA distribution in percentage. (D) FFA composition of Wt and CGI-58-/- macrophages. Inset: FFA distribution in percentage. Data are presented as mean values (n=3-4) + SEM. *, $p < 0.05$; **, $p \leq 0.01$; ***, $p \leq 0.001$.

4.5 Unchanged expression of genes and proteins involved in TG hydrolysis in Wt and CGI-58-/- macrophages

To investigate whether CGI-58 deficiency in macrophages results in a compensatory (up)regulation of genes involved in intra- and extracellular TG hydrolysis, we determined mRNA expression of ATGL, HSL, LAL, and LPL. mRNA expression of these genes was comparable between CGI-58-/- and Wt macrophages (Fig. 18A). ATGL protein expression was unchanged as well (Fig. 18B). To further address whether additional metabolic changes interfere with TG homeostasis in CGI-58-/- macrophages, we examined LPL activity. Like in ATGL-/- macrophages (29), LPL activity was unchanged in CGI-58-/- macrophages (Fig. 18C).

Figure 18

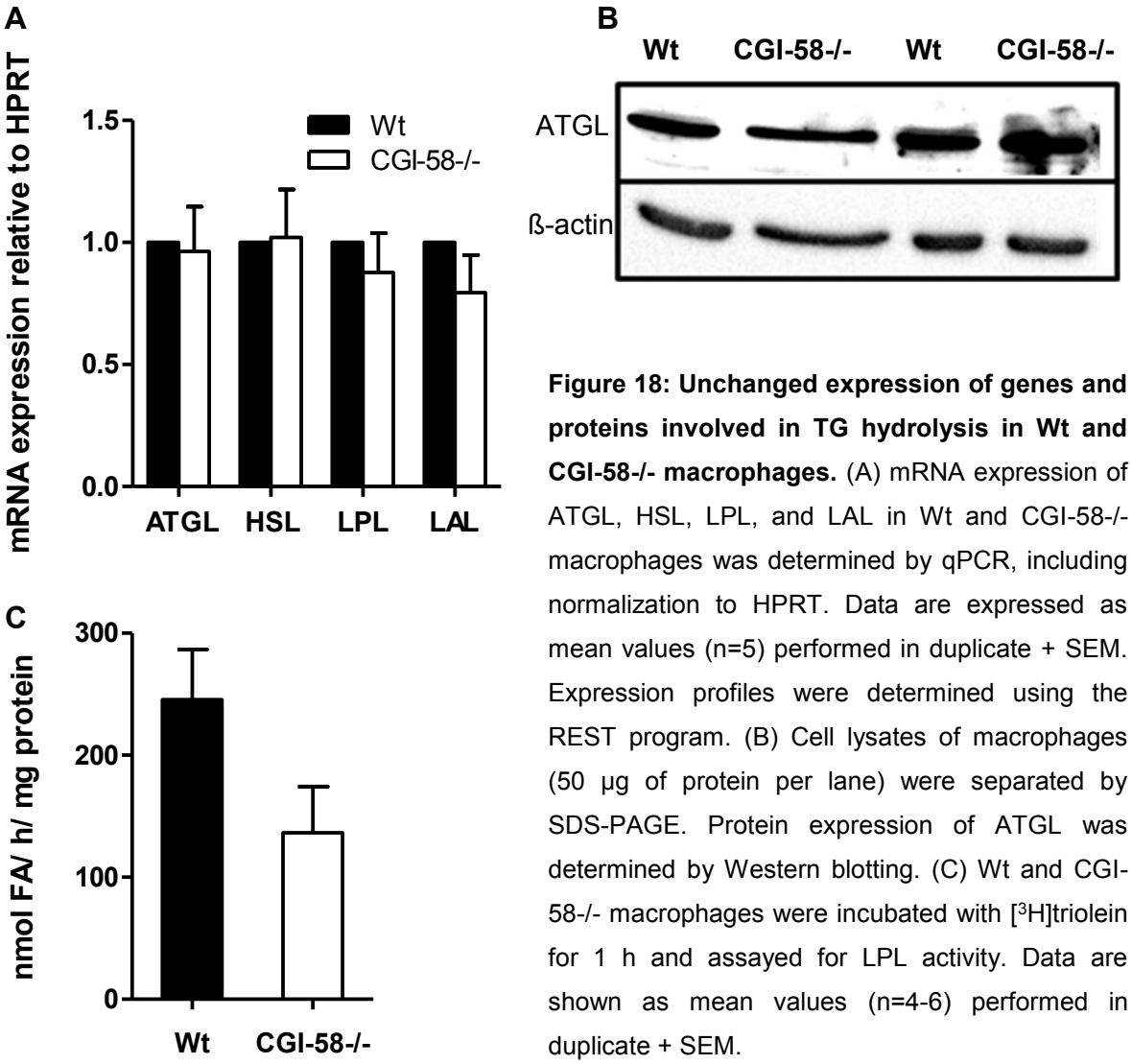

Figure 18: Unchanged expression of genes and proteins involved in TG hydrolysis in Wt and CGI-58-/- macrophages. (A) mRNA expression of ATGL, HSL, LPL, and LAL in Wt and CGI-58-/- macrophages was determined by qPCR, including normalization to HPRT. Data are expressed as mean values (n=5) performed in duplicate + SEM. Expression profiles were determined using the REST program. (B) Cell lysates of macrophages (50 µg of protein per lane) were separated by SDS-PAGE. Protein expression of ATGL was determined by Western blotting. (C) Wt and CGI-58-/- macrophages were incubated with [^{3}H]triolein for 1 h and assayed for LPL activity. Data are shown as mean values (n=4-6) performed in duplicate + SEM.

4.6 Apoptosis and ER stress are not induced in CGI-58-/- macrophages

We have previously shown that the mitochondrial apoptosis pathway is induced in macrophages lacking ATGL. (28) mRNA expression levels of the two anti-apoptotic markers Bcl-XL and Mcl-1, however, were unchanged in macrophages deficient in its co-activator CGI-58 (Fig. 19A). Furthermore, Western blotting analysis revealed no differences in the protein expression of Bax and cytosolic Cytochrome C (Fig. 19B), which are key players in mitochondria-dependent apoptosis. (150) Unlike ATGL-/- macrophages, mitochondria in CGI-58-/- macrophages are electron dense and have intact cristae like in Wt macrophages (Fig. 19C). Finally, AnnexinV/PI staining revealed the same amount of alive, early apoptotic, and necrotic cells. The number of late apoptotic cells was increased by 3.6-fold in CGI-58-/- macrophages but lacked statistical significance (Fig. 19D). Next, we investigated whether ER stress might be activated in CGI-58-/- macrophages due to the TG-rich LD accumulation as observed in ATGL-/- macrophages. (30) qPCR analysis revealed unchanged mRNA levels of the ER-resident chaperones Pdi and Erdj4 (Fig. 19E), unaltered protein expression of IRE1α (Fig. 19F), which is responsible for the Xbp1 splicing during ER stress, and no protein expression of the cell death executor CHOP (Fig. 19G) in CGI-58-/- macrophages. These findings demonstrate that CGI-58-/- macrophages lack any signs of mitochondrial apoptosis, ER stress, and mitochondrial dysfunction as observed in ATGL-/- macrophages.

Figure 19

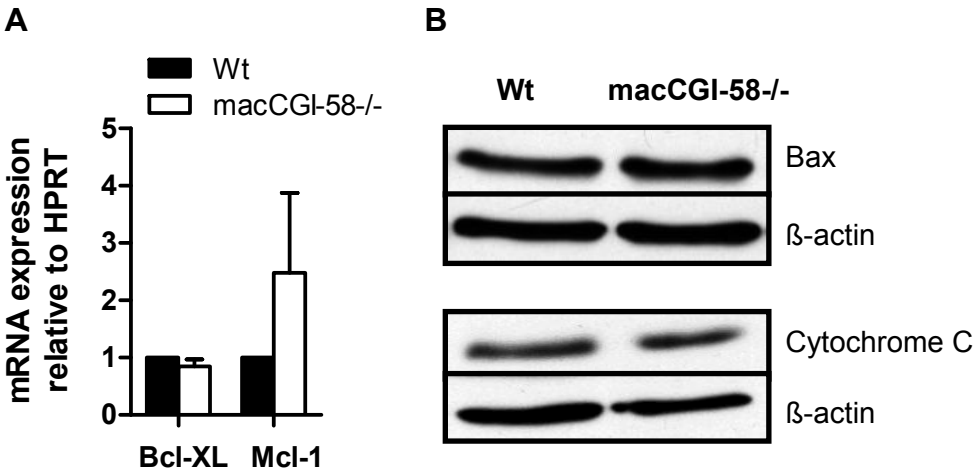

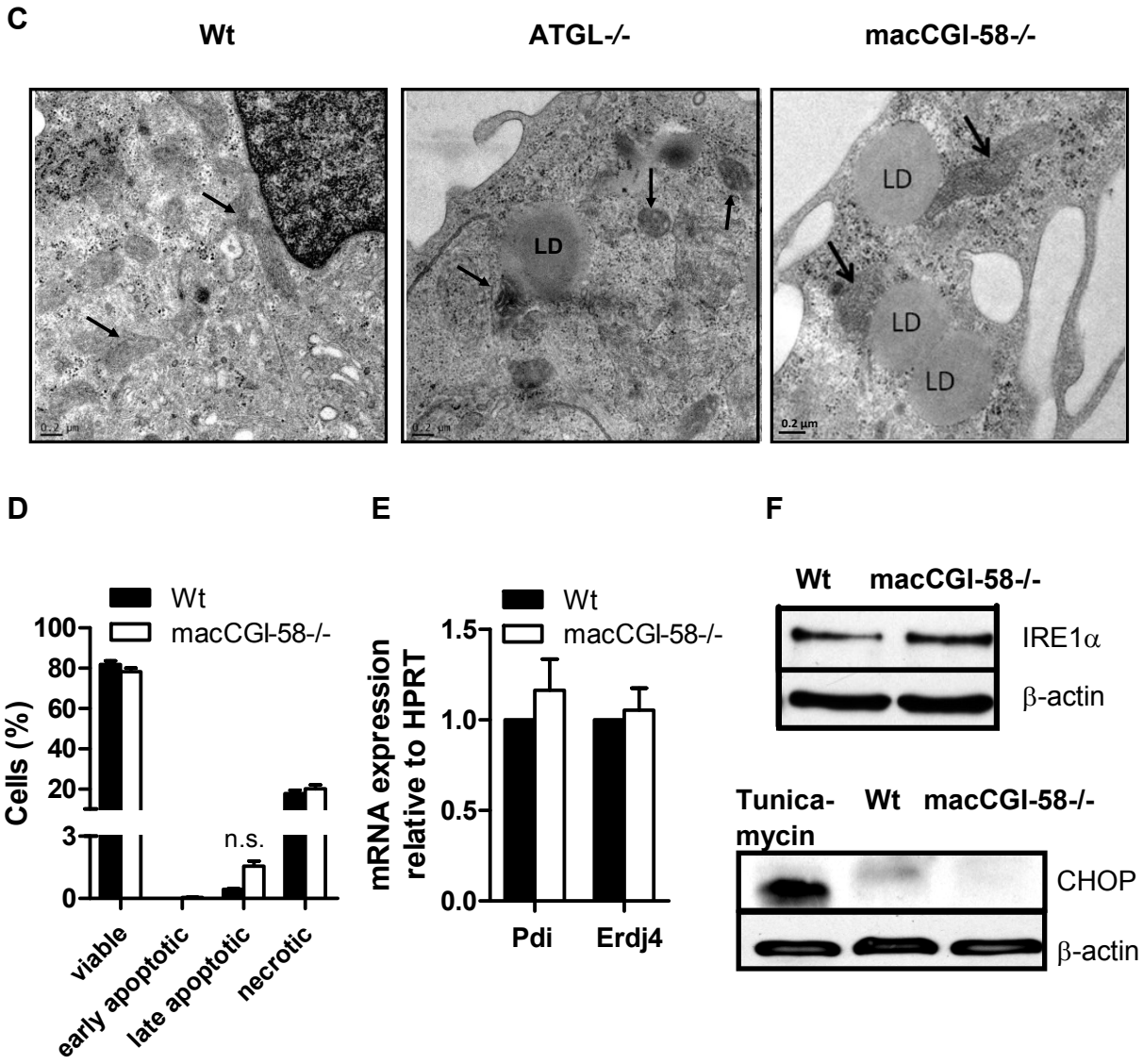

Figure 19: Apoptosis, mitochondrial fragmentation, and ER stress are not induced in CGI-58-/- macrophages. (A) mRNA expression of the anti-apoptotic genes Bcl-XL and Mcl-1 in Wt and CGI-58-/- macrophages determined by qPCR, including normalization to HPRT. Expression in Wt macrophages was arbitrarily set to 1. Data are presented as mean values (n=5) performed in duplicate + SEM. (B) Western blot analysis of Bax protein expression in macrophages (40 µg protein per lane). The cytosolic fraction was blotted for Cytochrome C expression. (C) Representative electron micrographs of mitochondria (indicated by arrows) in Wt, ATGL-/-, and CGI-58-/- macrophages. (D) Quantifications of the total amount of annexin V-positive (early apoptotic), annexin V/PI-double positive (late apoptotic), and PI-positive (necrotic) cells shown as means (n=5) performed in duplicate + SEM. Data represent the percentage of cells stained with annexin V and/or PI. (E) mRNA expression of the ER-resident chaperones Pdi and Erdj4. Data are presented as mean values (n=5) performed in duplicate + SEM. (F) IRE1α and (G) CHOP protein expression determined by Western blotting analyses. As positive control for CHOP expression Wt macrophages were treated with the ER stress inducer tunicamycin. mRNA expression profiles were determined using the REST program. LD, lipid droplet; n.s., not significant.

4.7 Decreased phagocytosis and mitochondrial respiration in CGI-58-/- macrophages

To address whether the absence of CGI-58 in macrophages affects phagocytosis comparable to ATGL deficiency (29), we performed *in vivo* and *in vitro* phagocytosis assays. We observed significantly decreased phagocytic capacity in CGI-58-/- compared to Wt macrophages, independent of glucose availability (Fig. 20A).

To elucidate whether decreased β-oxidation might contribute to the reduced phagocytic capacity of CGI-58-/- macrophages, we analyzed the expression of PPARα target genes. mRNA expression levels of carnitine palmitoyl-transferase 1α (Cpt1α), fatty acyl-CoA oxidase (Aox), very long-chain acyl-CoA dehydrogenase (Vlcad), and medium-chain acyl-CoA dehydrogenase (Mcad), however, were comparable between CGI-58-/- and Wt macrophages (Fig. 20B).

Figure 20

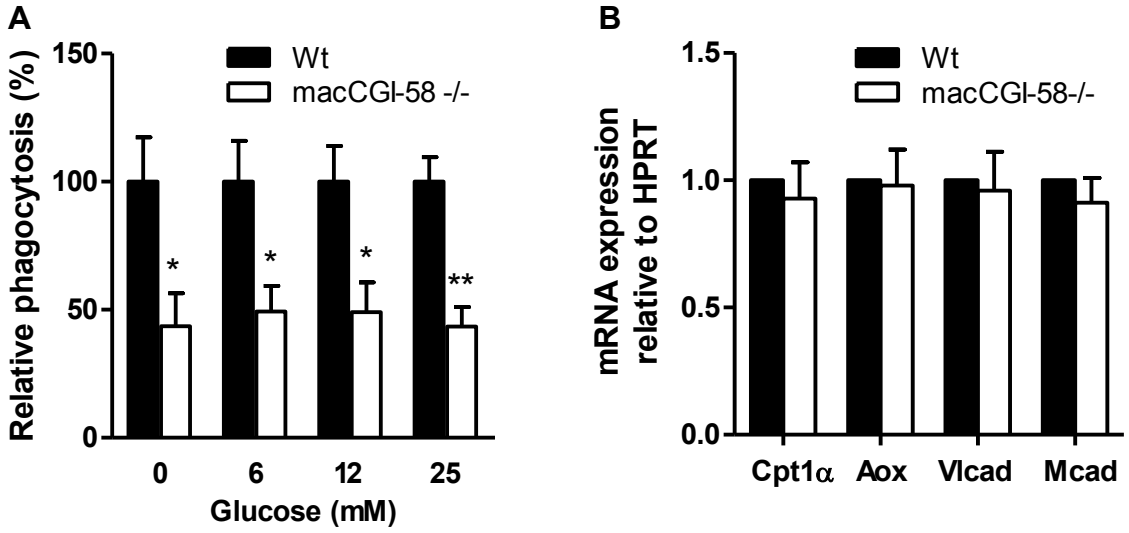

Figure 20: Reduced phagocytic capacity and unchanged mRNA expression of PPARα target genes of CGI-58-/- macrophages. (A) Macrophages from Wt and macCGI-58-/- mice were cultivated in DMEM/10% LPDS containing 0, 6, and 25 mM glucose for 1 h. Phagocytosis of fluorescein-labeled *E. coli* particles is presented as mean values (n=8-9) of two independent experiments performed in triplicate + SEM. Phagocytosis of Wt cells was arbitrarily set to 100%. (B) mRNA expression of PPARα target genes Ctp1α, Aox, Vlcad, and Mcad, including normalization to HPRT was determined by qPCR. Data are expressed as means (n=5) performed in duplicate + SEM. *, $p < 0.05$; **, $p \leq 0.01$. Expression profiles were determined using the REST program.

Next, we analyzed whether basal and maximal respiration rates are changed in mitochondria of CGI-58-/- macrophages in the presence or absence of glucose and glutamine. Measurement of the absolute OCR revealed that mitochondria of CGI-58-/- macrophages respire less compared to mitochondria from Wt mice in both conditions (Fig. 21A). Relative OCR (presented as percent of maximal respiration) demonstrates that mitochondria from CGI-58-/- macrophages are still responsive to oligomycin treatment and chemical uncoupling by FCCP (Fig. 21B, C).

Figure 21

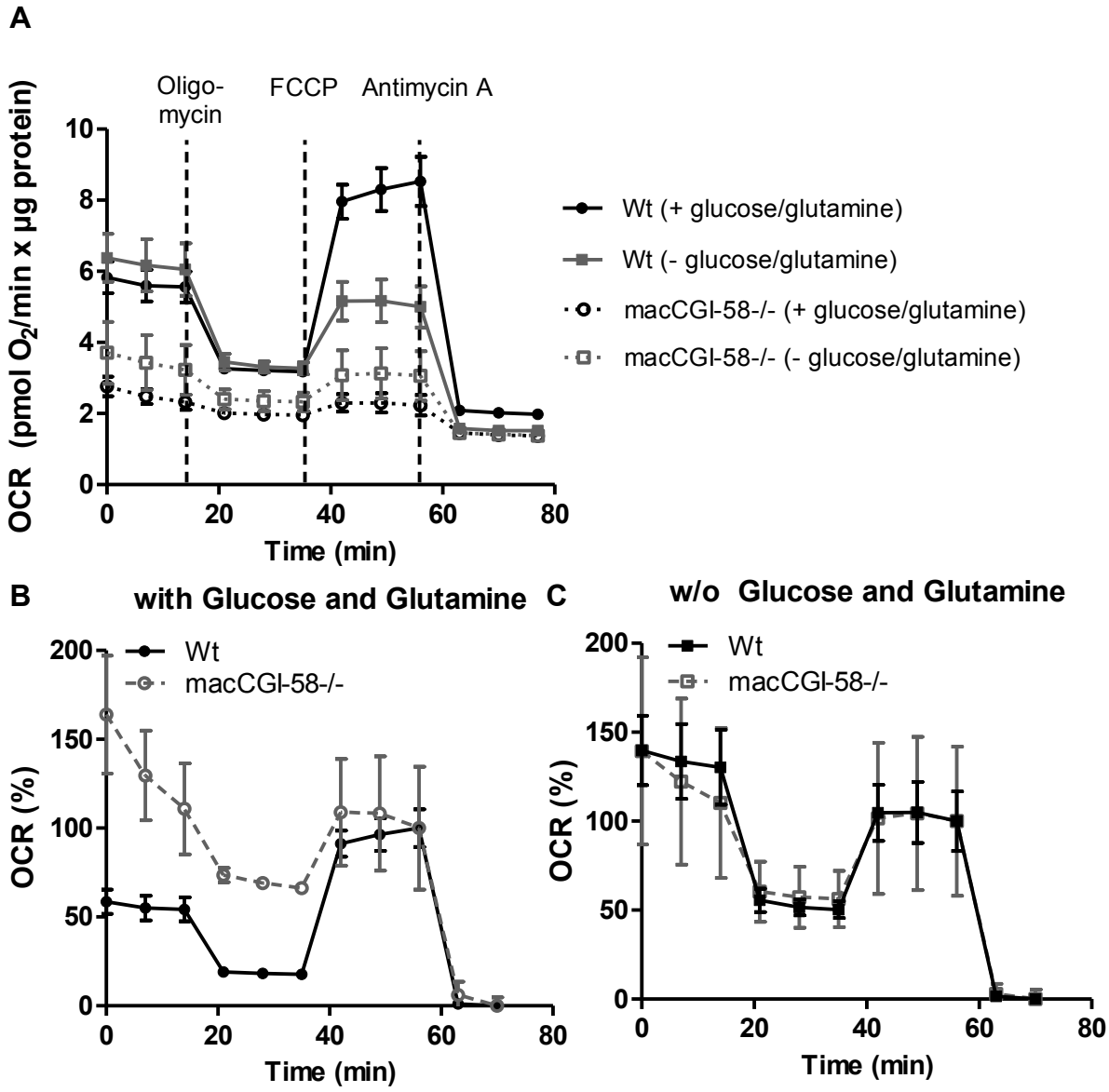

Figure 21: Decreased mitochondrial respiration in macCGI-58-/- macrophages. (A) OCR of Wt (continuous lines) and CGI-58-/- macrophages (dotted lines) in the presence (black) or absence (gray) of 25 mM glucose and 2 mM L-glutamine normalized to protein content. As indicated, cells were treated with 10 µM oligomycin, 0.3 µM FCCP, and 2.5 µM antimycin A. Data are presented as mean values (n=3-4) of triplicate repeats ± SEM. (B,C) OCR calculated as percentage of maximal mitochondrial respiration of Wt and CGI-58-/-macrophages in the (B) presence or (C) absence of 25 mM glucose and 2 mM L-glutamine. Data are presented as mean values (n=3-4) of triplicate repeats ± SEM.

In addition, we observed unchanged mitochondrial surface area (Fig. 22A) and protein expression of cyclooxygenase 4 (COX4), complex Va, and complex III (Fig. 22B) in CGI-58-/- macrophages. *In vivo*, phagocytosis ability tended to be decreased in macCGI-58-/- mice (25%) (Fig. 22C). This effect, however, reached no statistical significance. mRNA expression of Fcγ receptors 1, 2, and 3, which are important for inducing phagocytosis of microbes or microbe infected cells via binding to their antibodies, was unchanged in Wt compared to CGI-58-/- macrophages (Fig. 22D).

Figure 22

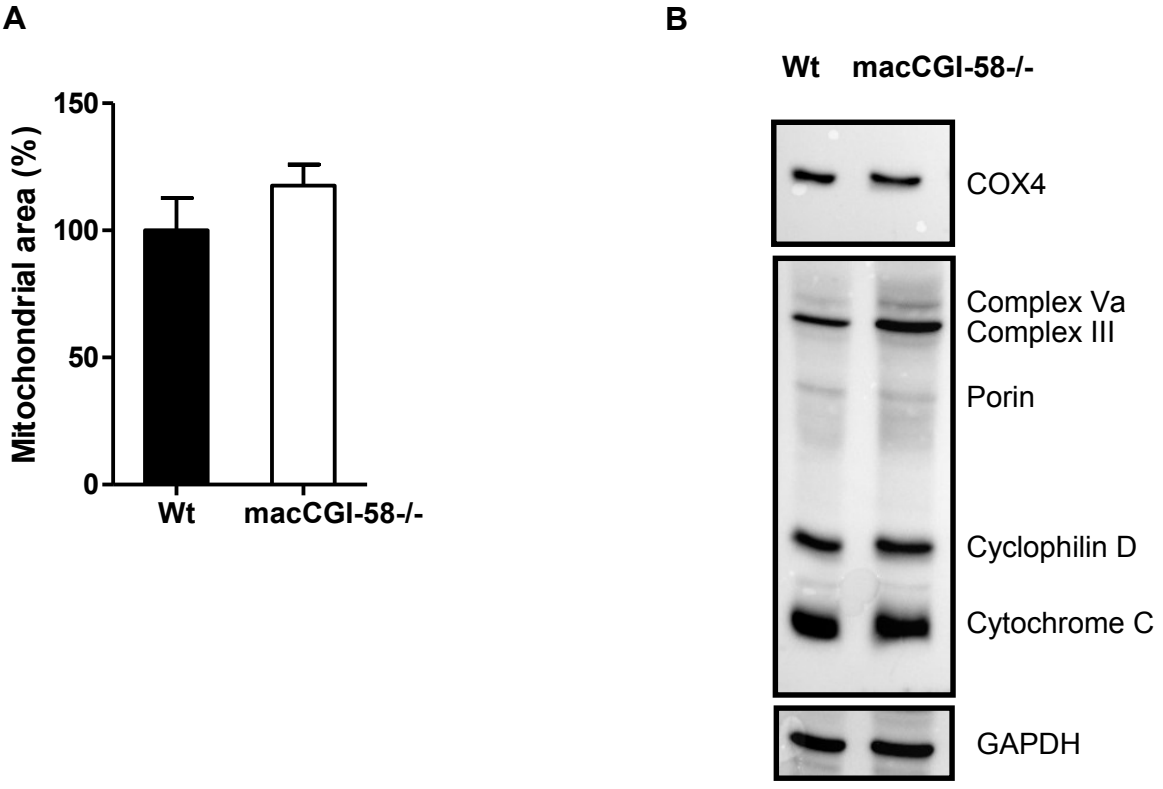

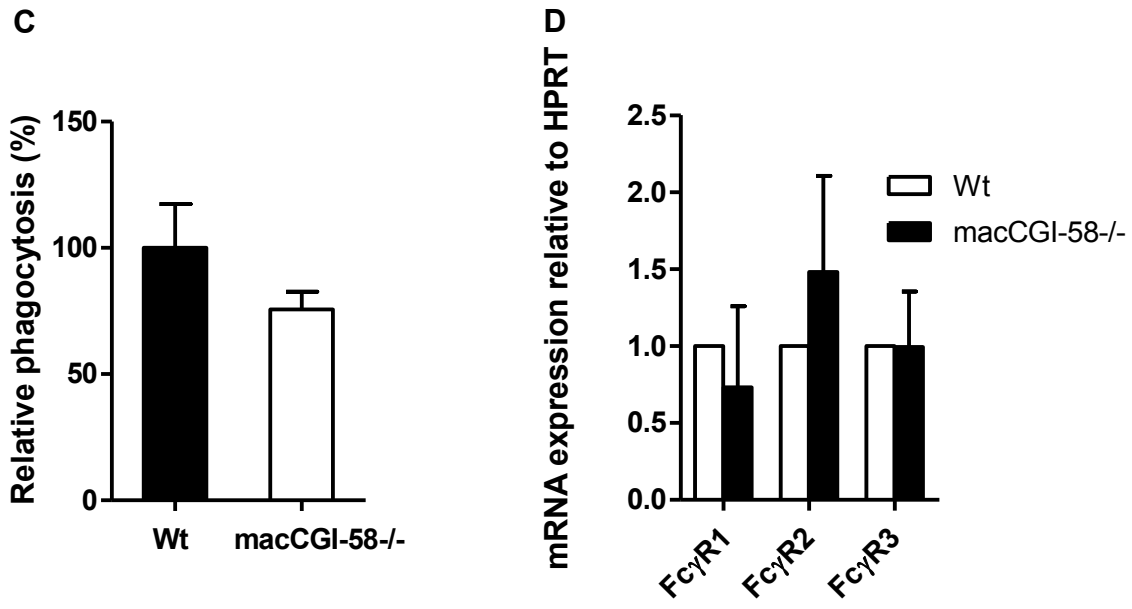

Figure 22: Unchanged mitochondrial area and *in vivo* phagocytosis in macCGI-58-/- macrophages. (A) Mitochondrial area in MitoTracker® Red-stained CGI-58-/- macrophages is expressed as percentage of mitochondrial area relative to Wt cells. Data are shown as means (n=8) + SEM. (B) Cell lysates of macrophages (40 µg of protein per lane) were separated by SDS-PAGE. Western blotting analysis of COX4, Complex Va (ATP5A), and Complex III Core I (ubiquinol-cytochrome C reductase). Antibodies against porin, cyclophilin D, and cytochrome C were present in the antibody mixture (MitoProfile) and expression of these proteins are shown as control. Expression of GAPDH was determined as loading control. (C) Fluorescein-labeled *E. coli* particles (200 µl) were injected into Wt and macCGI-58-/- mice. After 2 h, macrophages were isolated and assayed for internalized fluorescence after quenching of extracellular fluorescence by trypan blue. Phagocytosis of Wt macrophages was arbitrarily set to 100%. Relative phagocytosis is presented as mean values (n=5) + SEM. (D) mRNA expression of Fcγ receptors 1, 2, and 3 in Wt and CGI-58-/- macrophages. Data are shown as mean values (n=4-5) + SEM. mRNA expression profiles were determined using the REST program.

4.8 Increased lysosomal activity in CGI-58-/- macrophages

To investigate lysosomal activity in CGI-58-/- macrophages, we treated cells with DQ^{TM} Red BSA (DQ-BSA) and performed flow cytometry. DQ-BSA is a derivative of BSA that is labeled with a self-quenched red fluorescent dye and dequenched in acidic intracellular lysosomal compartments by lysosomal proteases, releasing red fluorescence. (151) After starving the cells for 1 h and DQ-BSA incubation for 15 min, CGI-58-/- macrophages showed increased red fluorescence immediately after loading (0 h). After chasing the cells for 2 h and 6 h, the fluorescent signal was significantly higher in CGI-58-/- compared to Wt macrophages which suggests an increased lysosomal activity in the KO cells (Fig. 23).

Figure 23

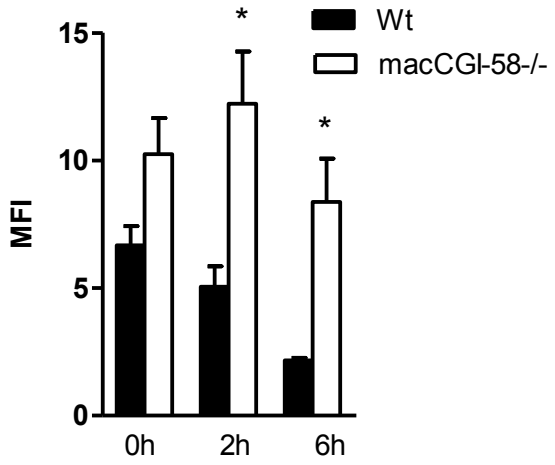

Figure 23: Increased lysosomal activity in CGI-58-/- macrophages. Macrophages were cultured in DMEM/10% LPDS for 24 h and then fasted for 1 h in HBSS to induce autophagy. DQ-BSA was added at a final concentration of 10 µg/ml and incubated for 15 min at 37°C. Red-fluorescent DQ-BSA was analyzed by flow cytometry using a FACSCalibur flow cytometer after 0, 2, and 6 h, respectively. Data are presented as mean (n=5-8) + SEM. *, $p \leq 0.05$.

4.9 CGI-58-/- macrophages polarize toward M1

Macrophages are a heterogeneous and phenotypically polarized cell population consisting of classically activated (pro-inflammatory) M1 macrophages and alternatively activated M2 macrophages with anti-inflammatory properties. (152) We have previously shown that ATGL-/- macrophages adopt an anti-inflammatory M2-like phenotype. (27) To investigate the polarization phenotype of CGI-58-/- macrophages, we determined mRNA levels of pro- and anti-inflammatory cytokines, respectively. These analyses revealed an upregulation of the pro-inflammatory cytokine Gro-1 (4.9-fold), downregulation of Mcp-1 (by 36%), and unchanged mRNA expression of Mcp-2, Ccl5, and Mrc-1 in CGI-58-/- compared to Wt macrophages (Fig. 24A). mRNA expression of the M2 marker Arg-1 was markedly downregulated (by 81%). Furthermore, increased IL-6 concentrations in the supernatant of LPS-treated CGI-58-/- compared to Wt cells (Fig. 24B) support a pro-inflammatory M1-like polarized pattern of CGI-58-/- macrophages.

Figure 24

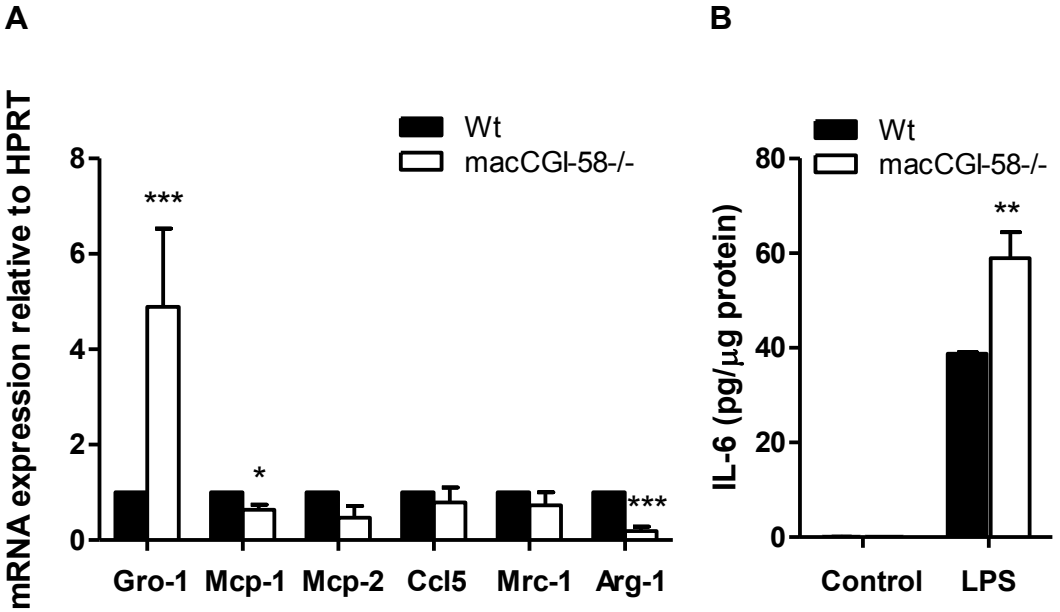

Figure 24: CGI-58-/- macrophages polarize toward a pro-inflammatory M1-like phenotype. (A) mRNA expression of Gro-1, Mcp-1, Mcp-2, Ccl5, Mrc-1, and Arg-1 in Wt and CGI-58-/- macrophages determined by qPCR, including normalization to HPRT. Data are presented as mean values (n=5) performed in duplicate + SEM. Expression profiles were determined using the REST program. (B) Macrophages were treated with PBS (control) or LPS (100 ng/ml) for 16 h. IL-6 secretion in the supernatant was determined by ELISA. Data represent mean values (n=3-5) + SEM. *, $p < 0.05$; **, $p \leq 0.01$; ***, $p \leq 0.001$.

4.10 CGI-58 deficiency in macrophages does not affect the inflammatory response to endotoxin *in vivo*

LPS-induced toll like receptor 4 signaling leads to the production of several cytokines, like TNFα, IL-6, and IL-10. Lord *et al.* (48) have already shown that CGI-58 KD leads to an alteration in the inflammatory response to endotoxin. To address if the lack of CGI-58 in macrophages is sufficient to affect inflammation *in vivo*, we injected mice with LPS and determined TNFα and IL-6 plasma levels as well as mRNA expression of different cytokines in WAT and liver. Plasma levels of TNFα and IL-6 were higher in LPS-treated than in untreated mice, however, comparable between Wt and macCGI-58-/- mice (Fig. 25A). Moreover, mRNA levels of TNFα, IL-6, IL-1ß, IL-10, and adiponectin were higher in WAT of LPS-treated mice compared to control mice (Fig. 25B). Anyway, there was no difference in the mRNA expression of these genes between the two genotypes. In addition, we determined mRNA expression of several cytokines in the livers of these mice. We found increased mRNA levels of TNFα, IL-10, IL-1ß, SAA, and SAP in livers of LPS-treated mice (Fig. 25C), but no differences between macCGI-58-/- and Wt mice. To summarize, LPS injection did not lead to alterations in the inflammatory response to endotoxin in macCGI-58-/- mice. In other words, the lack of CGI-58 only in myeloid cells is not sufficient to affect whole body inflammation.

Figure 25

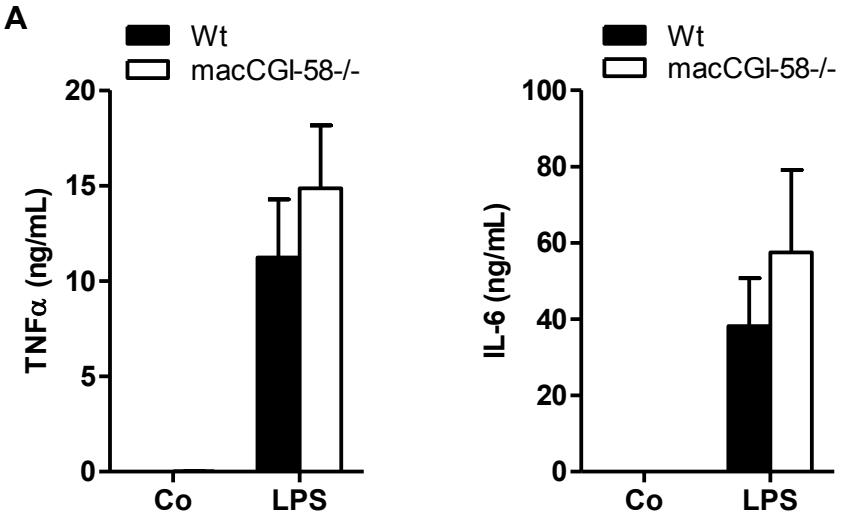

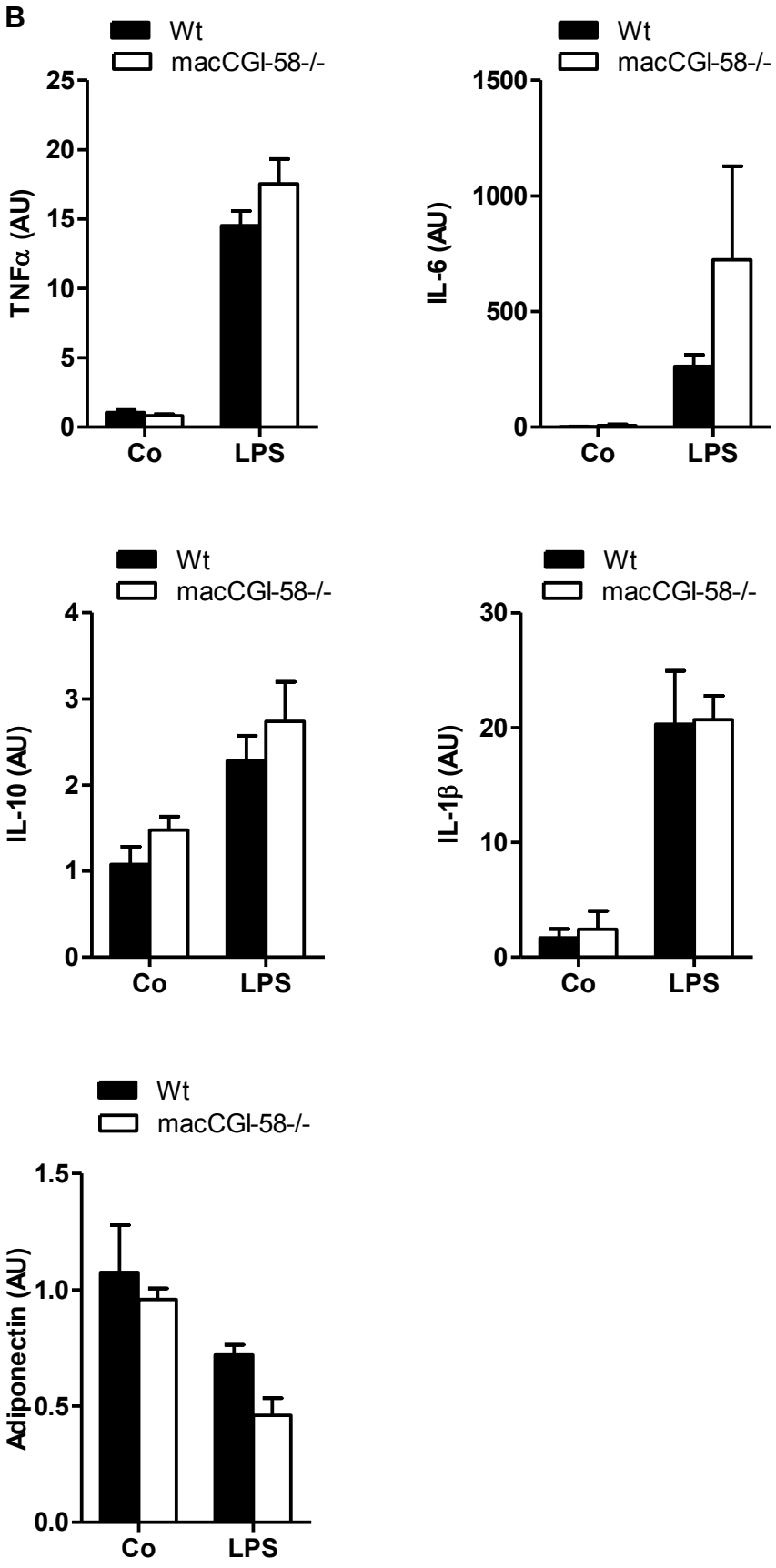
B
Wt
macCGI-58-/-
TNFα (AU)
25
20
15
10
5
0
Co
LPS
Wt
macCGI-58-/-
IL-6 (AU)
1500
1000
500
0
Co
LPS
Wt
macCGI-58-/-
IL-10 (AU)
4
3
2
1
0
Co
LPS
Wt
macCGI-58-/-
IL-1β (AU)
30
20
10
0
Co
LPS
Wt
macCGI-58-/-
Adiponectin (AU)
1.5
1.0
0.5
0.0
Co
LPS

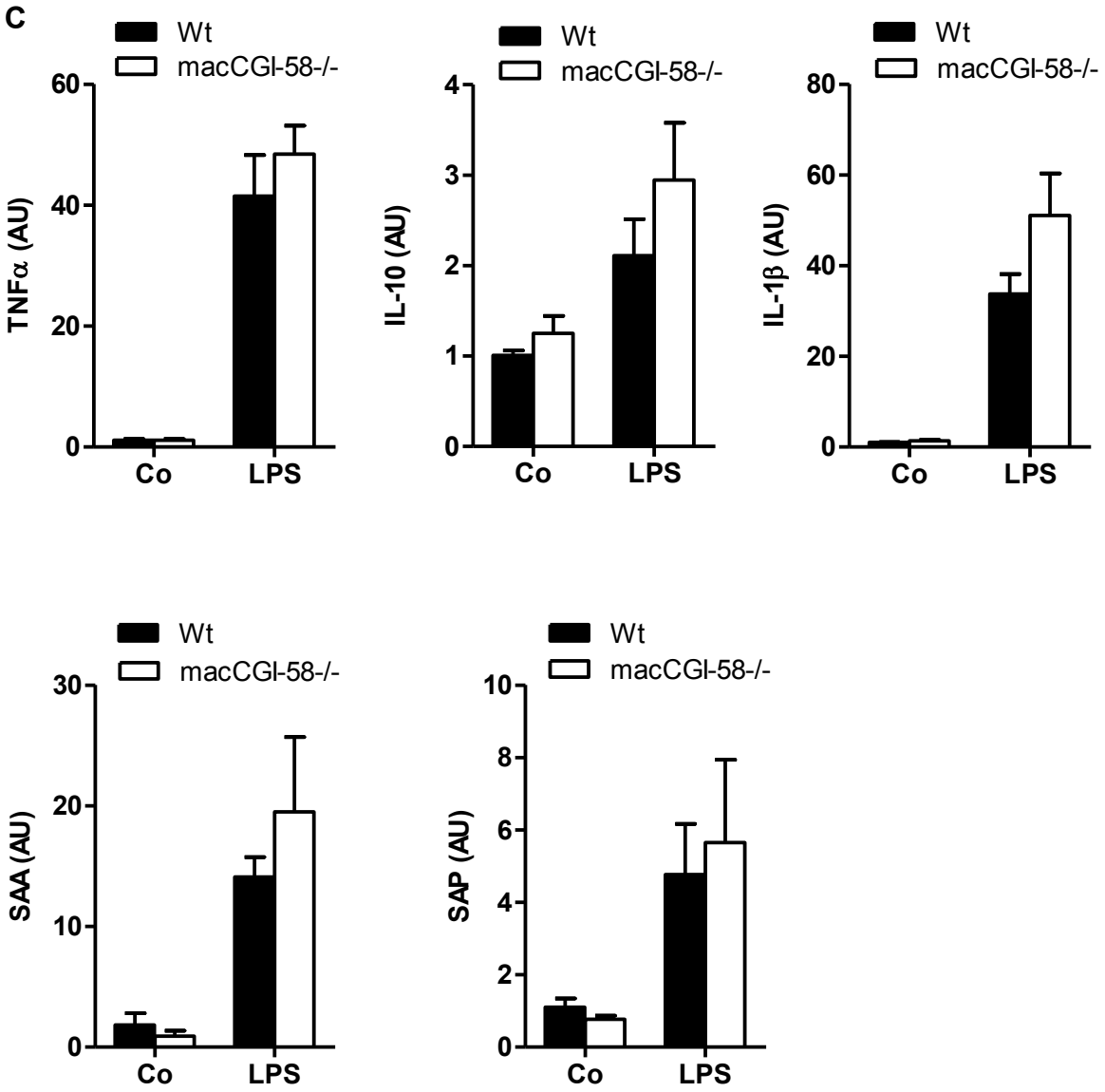

Figure 25: Lack of CGI-58 in macrophages does not affect the inflammatory response to endotoxin *in vivo.* Mice received a single i.p. injection of either PBS or LPS (5 mg/kg/mouse) and were necropsied 6 h after injection. (A) Plasma cytokine and acute-phase response protein levels were measured 1 h (TNFα) and 6 h after injection (IL-6). (B) qPCR analyses of TNFα, IL-6, IL-10, IL-1β, and adiponectin gene expression in epididymal adipose tissue. (C) TNFα, IL-10, IL-1β, SAA, and SAP gene expression in hepatic tissue. AU, arbitrary unit. (n=5) Data are shown as mean + SEM. Expression profiles were determined using the 2^{-ddCt} method.

4.11 Macrophage infiltration and inflammation are unchanged in epididymal WAT of chow- and WTD-fed macCGI-58-/- mice

To investigate if macrophage infiltration and inflammation are altered in epididymal WAT of macCGI-58-/- mice, we determined mRNA expression of the macrophage marker Emr1, CGI-58 and of several cytokines in WAT of Wt and macCGI-58-/- mice either fed chow or WTD. We could not find any differences in the Emr1, CGI-58, and TNFα mRNA expression between Wt and macCGI-58-/- WAT on chow diet (Fig. 26A). Moreover, mRNA expression of Emr1, Cd68, CGI-58, TNFα, and Mcp-1 was unchanged in WAT of macCGI-58-/- compared to Wt mice fed WTD (Fig. 26B).

Figure 26

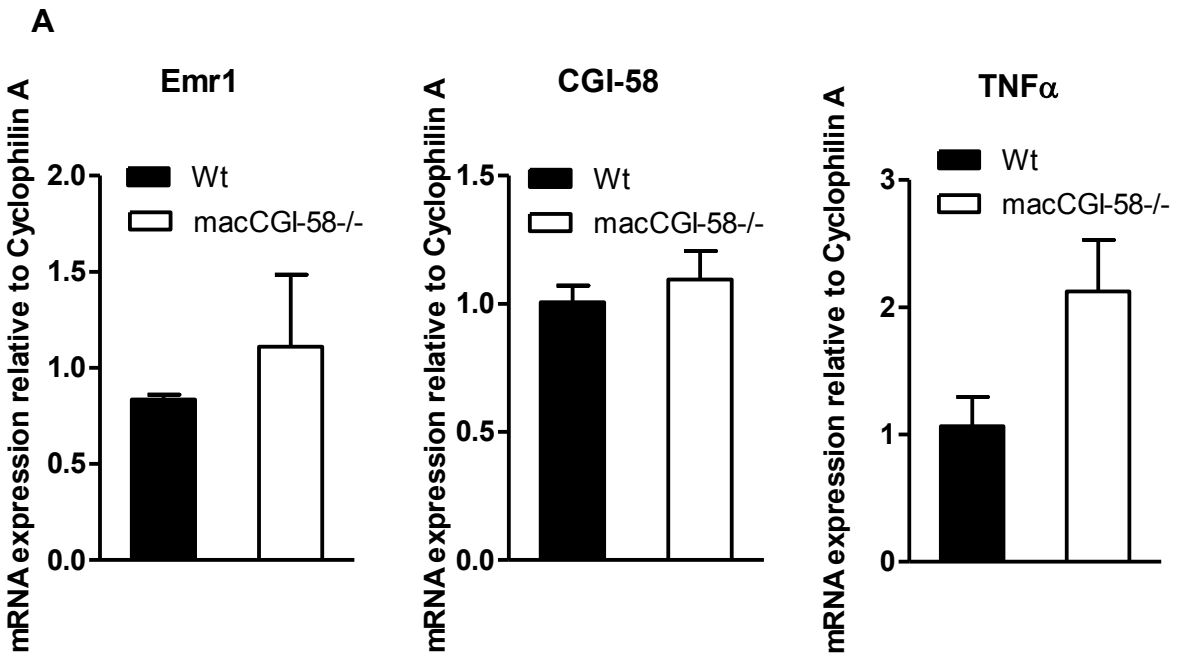

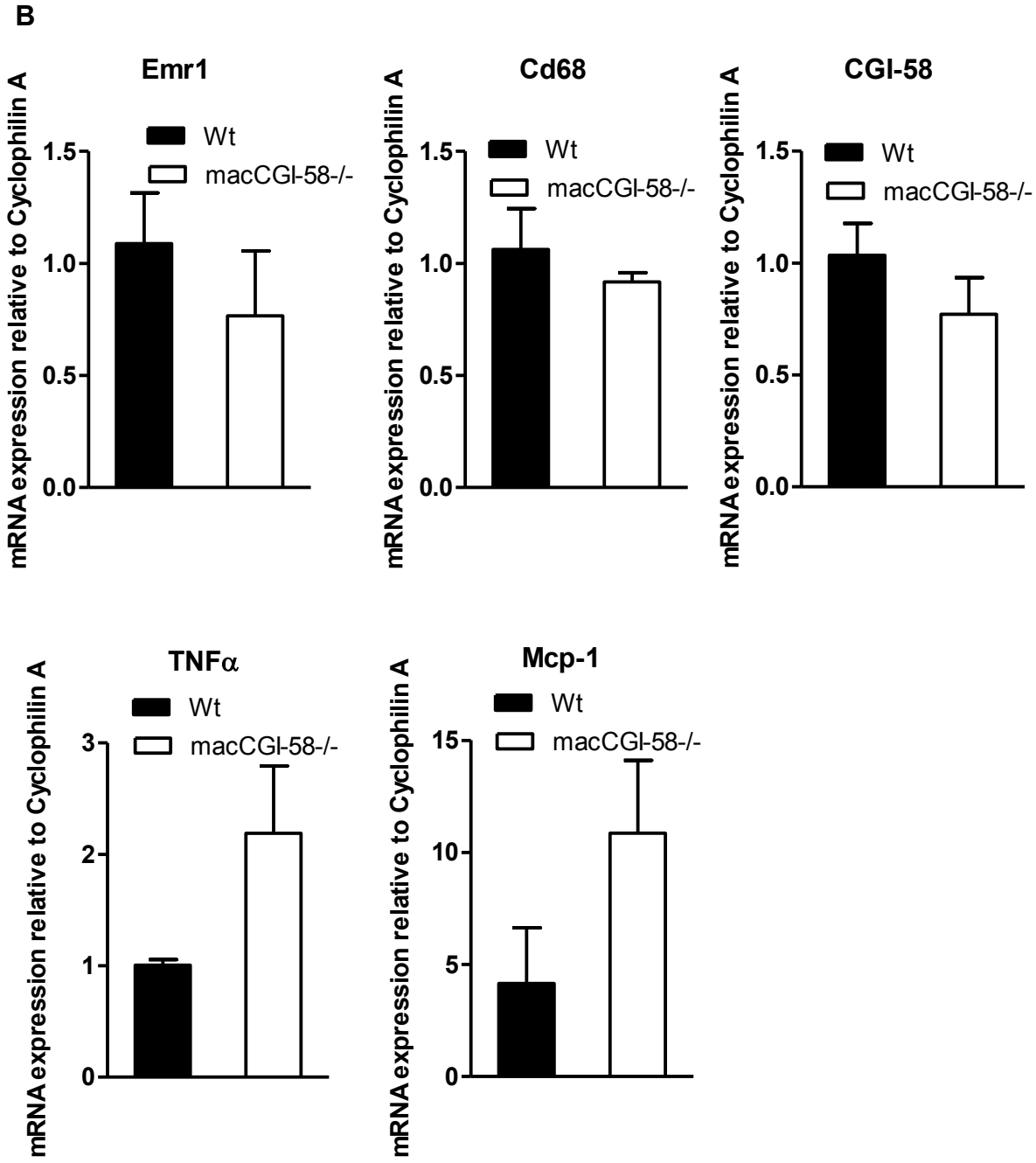

Figure 26: Macrophage infiltration and inflammation are unchanged in WAT of chow- and WTD fed macCGI-58-/- mice. (A) qPCR analyses of Emr1, CGI-58, and TNFα gene expression in epididymal WAT of Wt and macCGI-58-/- mice on chow diet (n=4). (B) Emr1, Cd68, CGI-58, TNFα, and Mcp-1 gene expression in WAT of Wt and macCGI-58-/- mice on WTD (n=5). Data are shown as mean + SEM. Expression profiles were determined using the 2^{-ddCt} method.

4.12 Macrophage infiltration into WAT during lipolysis induction is unchanged in macCGI-58-/- mice

Kosteli *et al.* (153) showed that lipolysis induction via ß-adrenergic stimulation leads to macrophage recruitment into epididymal WAT. The trigger for this macrophage infiltration is an excess of FFAs produced during lipolysis. The authors suggest that adipose tissue macrophages may serve an adaptive function by taking up excess FFA at least over short periods of time. They observed decreased macrophage recruitment in ATGL-/- mice due to insufficient lipolysis. To investigate if loss of CGI-58 in macrophages affects macrophage recruitment into WAT, we injected mice either with PBS (control) or the ß-adrenergic agonist CL316,243, excised epididymal WAT, and determined the Emr1 (F4/80) mRNA expression. We did not find any changes in the Emr1 mRNA expression between macCGI-58-/- and Wt mice (Fig. 27).

Figure 27

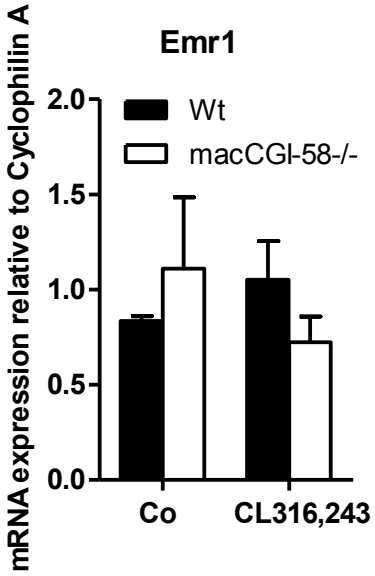

Figure 27: Macrophage infiltration is unchanged in WAT during lipolysis induction in macCGI-58-/- mice. qPCR analysis of Emr1 gene expression in epididymal WAT from Wt and macCGI-58-/- mice of PBS and CL316,243 injected mice. (n=4) Data are presented as mean + SEM. Expression profiles were determined using the 2^{-ddCt} method.

4.13 LPAAT activity is unchanged in CGI-58-/- macrophages

Ghosh *et al.* (34) and Montero-Moran *et al.* (35) reported in 2008 and 2010 that CGI-58 mediates the acylation of LPA. In order to investigate if CGI-58-/- exhibits LPAAT activity in macrophages, we performed an LPAAT activity assay. LPAAT activity was unchanged in CGI-58-/- compared to Wt macrophages (Fig. 28). However, McMahon *et al.* (36) reported in 2015 that CGI-58 lacks LPAAT activity since the LPAAT activity they measured in above mentioned publications was due to impurities of *E. coli*.

Figure 28

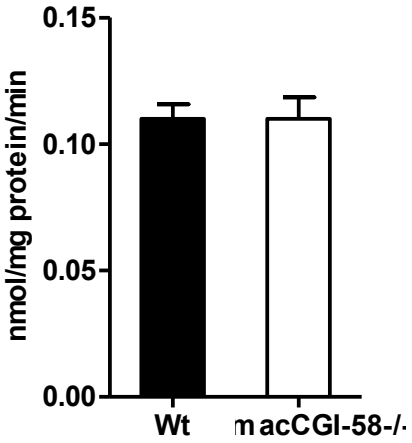

Figure 28: LPAAT activity is unchanged in CGI-58-/- macrophages. LPAAT activities in cell lysates of Wt and CGI-58-/- macrophages are presented as mean values (n=7) performed in duplicate + SEM.

4.14 Unchanged atherosclerotic lesion formation in macCGI-58/ApoE-DKO mice

To examine the consequences of CGI-58-/- deficiency and the concomitant TG accumulation in myeloid cells on atherogenesis, we generated CGI-58$^{flox/flox}$/ApoE-/- (designated ApoE-/-) and macCGI-58/ApoE-DKO mice and challenged them with a HF/HCD to induce lesion formation. We observed no differences in body weight (Fig. 29A), plasma lipid parameters (Table 8), and IL-6 concentrations (Fig. 29B).

Table 8: Plasma lipid parameters of overnight fasted ApoE-/- and macCGI-58/ApoE-DKO mice fed chow diet or challenged with HF/HCD for 10 weeks.

	chow diet		HF/HCD	
	ApoE-/-	DKO	ApoE-/-	DKO
TC (mg/dl)	247 ± 35.0	271 ± 37.6	1059 ± 379	1053 ± 261
FC (mg/dl)	69.9 ± 11.4	75.9 ± 12.5	324 ± 98.9	335 ± 74.5
TG (mg/dl)	108 ± 29.7	117 ± 27.3	73.7 ± 36.0	79.2 ± 37.3
FA (mmol/l)	1.3 ± 0.3	1.5 ± 0.3	0.9 ± 0.1	0.8 ± 0.2

Data represent mean values (n=10-11) ± SEM.

Figure 29

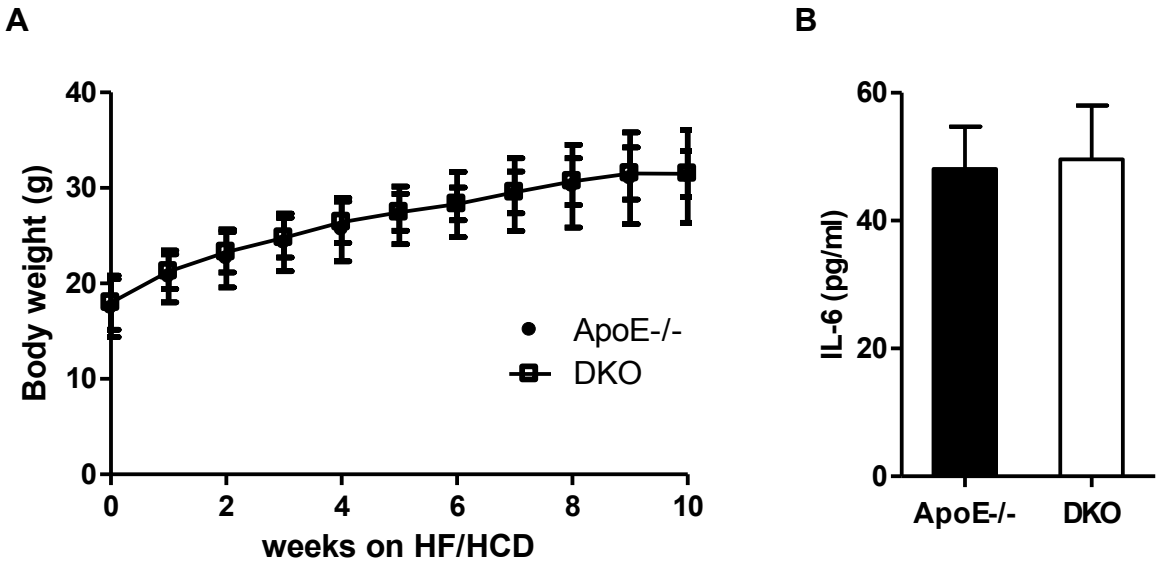

Figure 29: Comparable body weight and plasma IL-6 levels in macCGI-58/ApoE-DKO and ApoE-/- mice. ApoE-/- and macCGI-58/ApoE-DKO mice were challenged with a HF/HCD for 10 weeks. (A) Body weight of macCGI-58/ApoE-DKO and ApoE-/- mice. Data represent mean values (n=10-11) ± SEM. (B) Plasma IL-6 levels were determined by ELISA. Data represent mean values (n=8) + SEM.

Hepatic TC (Fig. 30A) and TG (Fig. 30B) concentrations were comparable between DKO and ApoE-/- mice.

Figure 30

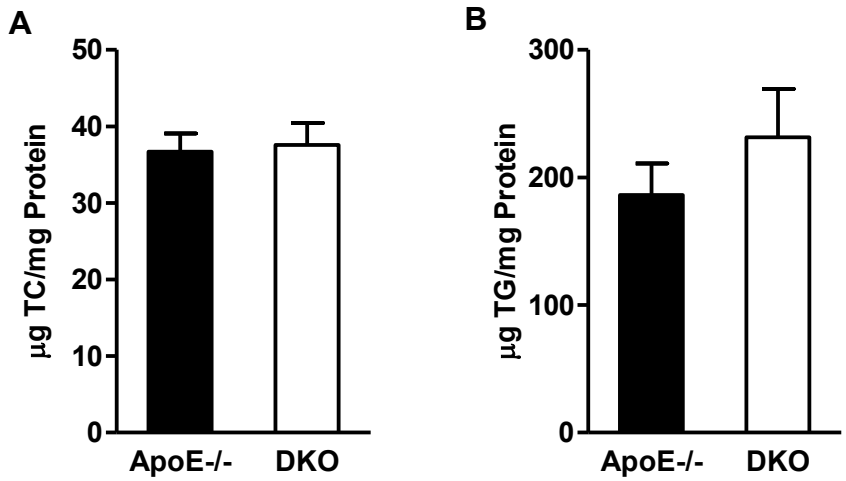

Figure 30: Unchanged hepatic lipid parameters in macCGI-58/ApoE-DKO and ApoE-/- mice. (A) TC and (B) TG levels in livers of macCGI-58/ApoE-DKO and ApoE-/- mice. Data represent mean values (n=10-11) + SEM.

Macrophages from both genotypes showed the same polarization phenotype (Fig. 31), which is in contrast to what we observed in CGI-58-/- compared to Wt macrophages (Fig. 24A).

Figure 31

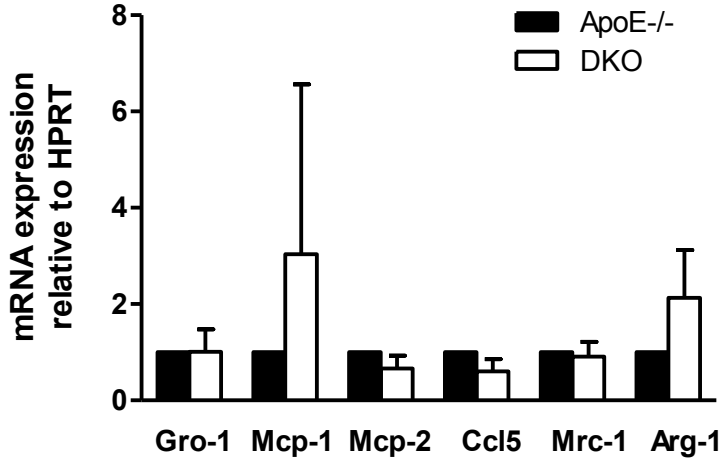

Figure 31: Comparable macrophage polarization in macCGI-58/ApoE-DKO and ApoE-/- mice. mRNA expression of Gro-1, Mcp-1, Mcp-2, Ccl5, Mrc-1, and Arg-1 in ApoE-/- and macCGI-58/ApoE-DKO macrophages was determined by qPCR, including normalization to HPRT. Data are presented as mean values (n=4-5) performed in duplicate ± SEM. Expression profiles were determined using the REST program.

Visual inspection of Oil Red O-stained aortic root sections revealed no differences in lesion formation (Fig. 32). MoMa-2 and Masson's Trichrome staining, which were used to identify macrophages and collagen, were comparable in sections from ApoE-/- and DKO mice (Fig. 32).

Figure 32

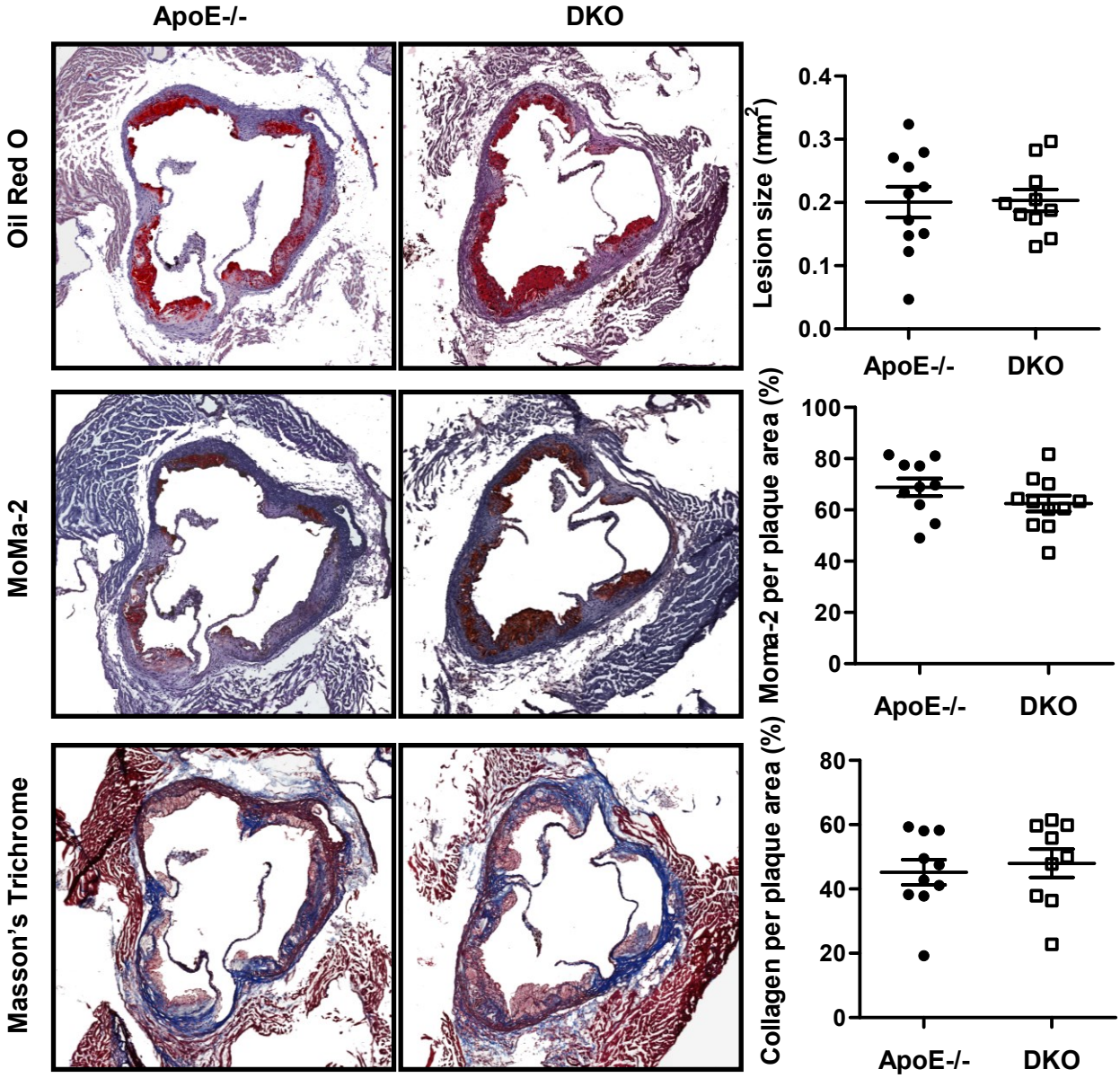

Figure 32: Unchanged atherosclerosis susceptibility by CGI-58 deficiency. Representative images of aortic valve sections stained with Oil Red O, MoMa-2, and Masson's Trichrome for the detection of lipids, macrophages, and collagen, respectively. Magnification, x40. Data represent mean values of 10 aortic valve sections per mouse. Bars represent the mean values of 9-11 mice per group. Data represent mean values (n=10-11) ± SEM.

Quantitative analysis of plaque development in aortic arches (*en face* analysis) revealed a 1.3-fold increase in lesion size in thoracic aortic arches of macCGI-58/ApoE-DKO mice (Fig. 33).

Figure 33

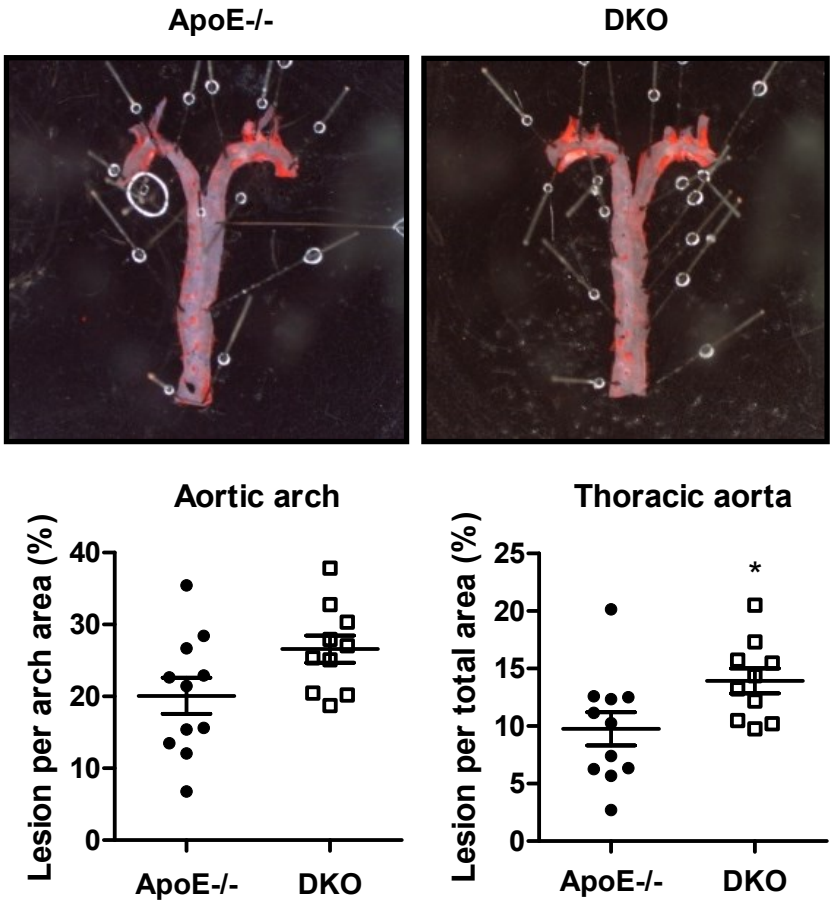

Figure 33: Slightly increased plaque formation by loss of CGI-58. Representative images and quantification of Oil Red O-stained *en face* aorta. Data represent mean values (n=10-11) ± SEM. *, $p < 0.05$.

To investigate the effect of CGI-58 deficiency on cholesterol transport from macrophages to exogenous lipid acceptors, we measured cholesterol efflux to ApoA-I and HDL. As shown in Fig. 34A, cholesterol efflux from DKO macrophages to ApoA-I was increased after 6 h compared to ApoE-/- macrophages but unchanged to both acceptors at all other time points. This result is in line with unaltered mRNA levels of genes involved in cholesterol uptake (Cd36, SrB1) and efflux (Abca1, Abcg1) in CGI-58-/- compared to Wt macrophages (Fig. 34B).

Figure 34

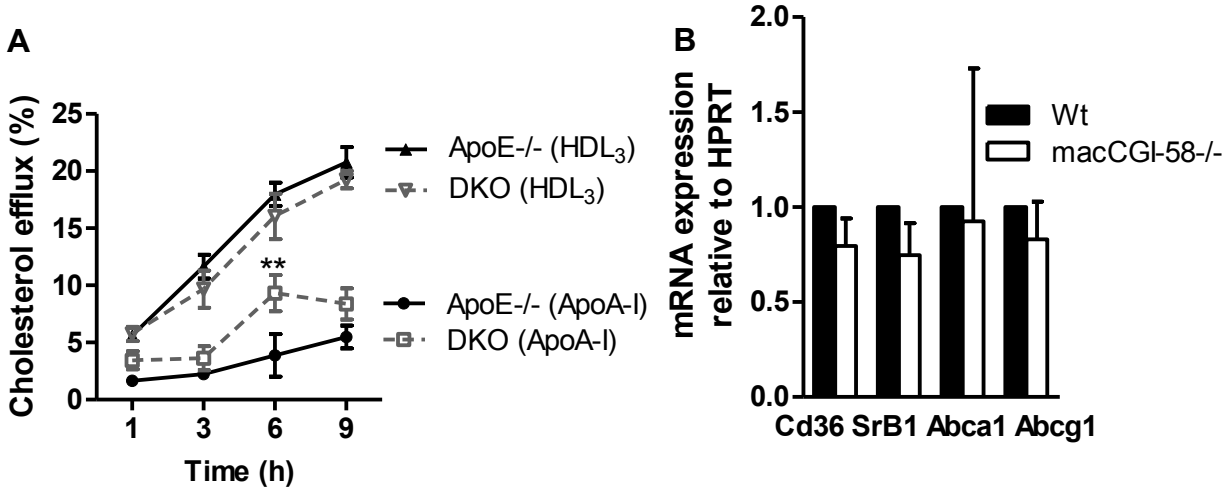

Figure 34: Comparable cholesterol efflux in macCGI-58/ApoE-DKO and ApoE-/- mice. (A) Cholesterol efflux to the extracellular acceptors ApoA-I and HDL_3 expressed as the percentage of [^{3}H]cholesterol transferred from macrophages to the medium. Data show the mean values (n=7) ± SEM. (B) mRNA expression of Cd36, SrB1, Abca1 and Abcg1 in Wt and CGI-58-/- macrophages was determined by qPCR, including normalization to HPRT. Data are presented as mean values (n=4-5) performed in duplicate ± SEM. Expression profiles were determined using the REST program.

To further interrogate the role of CGI-58 in atherosclerosis progression, we utilized ASO-mediated KD of CGI-58 in hyperlipidemic Ldlr-/- mice (in collaboration with Mark Brown, Department of Cellular and Molecular Medicine, Cleveland Clinic Lerner Research Institute, Cleveland, OH). ASO-mediated KD has previously been shown to reduce expression levels of CGI-58 in liver, WAT, and kidney. (38) Here we show that thioglycolate-elicited macrophages from ASO-treated mice have a marked reduction in macrophage CGI-58 expression as well (Fig. 35A). Using this system, we found that CGI-58 KD in macrophages and other organs has no significant effect on plasma TC or TG concentrations in Ldlr-/- mice (Fig. 35B). Likewise, CGI-58 KD did not alter circulating VLDL, LDL, or HDL cholesterol levels (Fig. 35C, 35D, 35E).

Figure 35

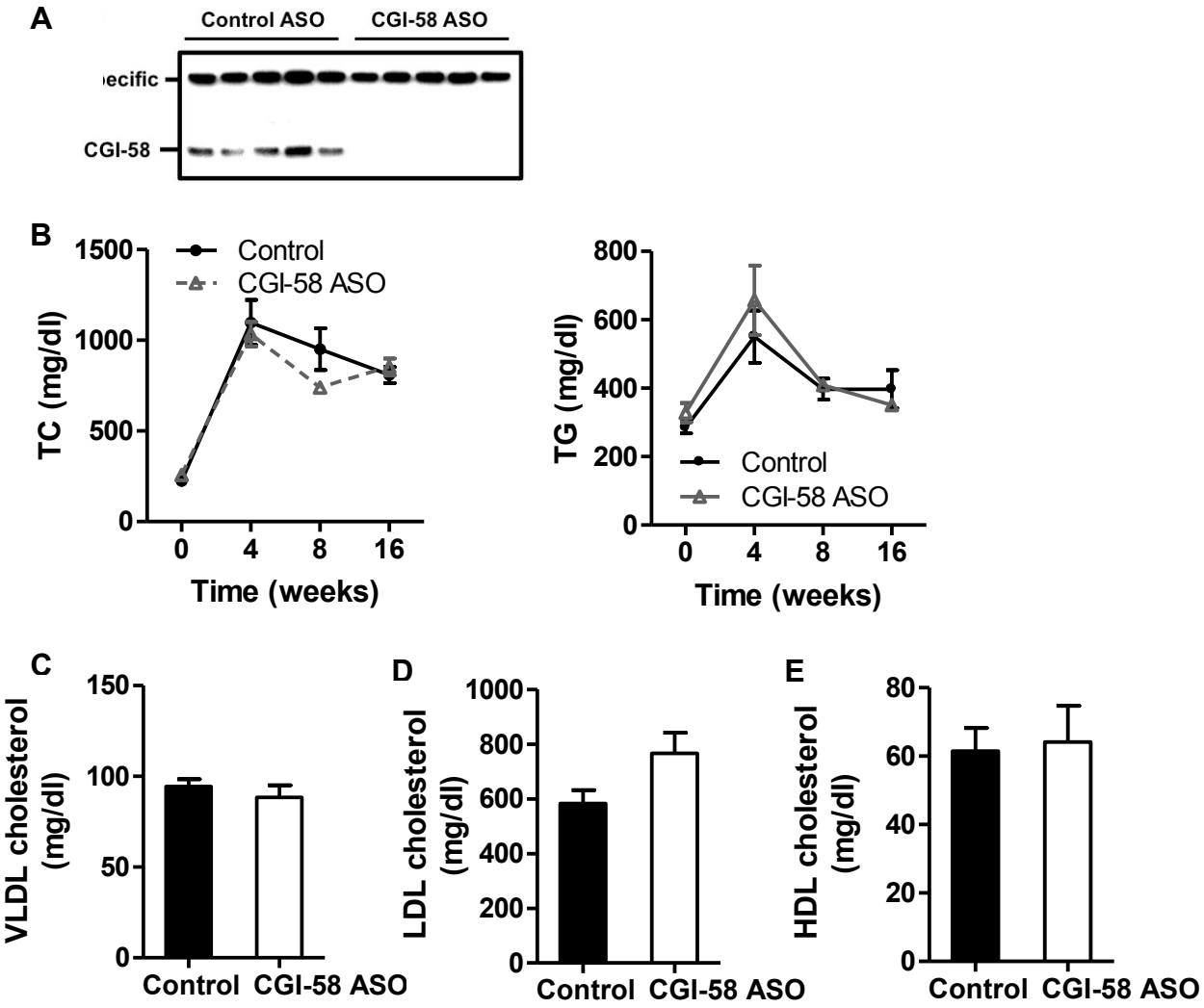

Figure 35: ASO-mediated KD of CGI-58 does not affect plasma lipid parameters. (A) ASO treatment effectively reduces macrophage expression of CGI-58. C57BL/6 mice maintained on a chow diet in conjunction with weekly injections (50 mg/kg) of either a non-targeting control ASO or CGI-58 for 6 weeks. Thereafter, thioglycolate-elicited peritoneal macrophages were isolated from control and CGI-58 ASO-treated mice (n=5 per group), plated for 2 h, and Western blotting was conducted to examine CGI-58 protein expression in isolated macrophages. (B-E) For atherosclerosis studies, 6 weeks old male Ldlr-/- mice were fed a diet enriched in 0.2% (w/w) cholesterol and 20% of energy as lard for 16 weeks in conjunction with biweekly injections (25 mg/kg) of either a non-targeting control ASO or CGI-58 ASO. (B) Plasma TC and TG concentrations during atherosclerosis progression. (C) VLDL, (D) LDL, and (E) HDL cholesterol levels following 16 weeks of diet induction. Data represent the mean ± SEM from 4-10 mice per group.

Comparable to macCGI-58/ApoE-DKO mice (Fig. 32), ASO-mediated KD of CGI-58 did not alter atherosclerosis burden in the aortic sinus (Fig. 36A) or thoracic aorta of Ldlr-/- mice as measured by *en face* morphometry (Fig. 36B).

Figure 36

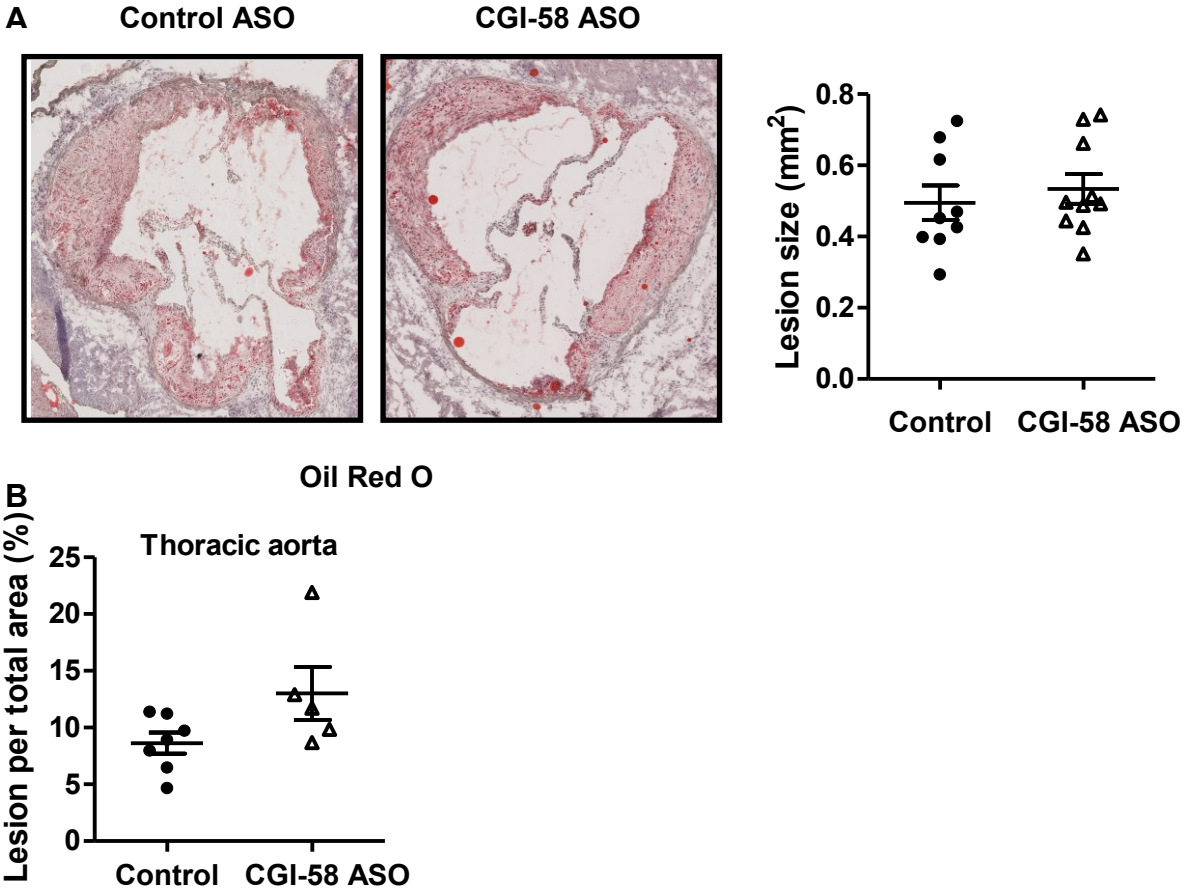

Figure 36: Unchanged atherosclerosis susceptibility by ASO-mediated KD of CGI-58. (A) Representative images of Oil Red O-stained aortic valve sections (magnification, 40x), and quantification of cross sectional aortic valve lesion area. (B) *En face* morphometric analysis of total aortic lesion area. Experiments were performed by Mark J. Brown's group. Data represent the mean ± SEM from 4-10 mice per group.

Collectively, these results indicate that diminished CGI-58 expression in macrophages, liver, and adipose tissue driven by CGI-58 ASO treatment or deficiency of CGI-58 in myeloid cells has minimal effects on atherosclerosis progression.

5. Discussion: Role of CGI-58 in macrophages

Intracellular TG stores are efficiently hydrolyzed by ATGL. Several studies have already shown that lack of ATGL leads to severe alterations in morphology and function of macrophages. (26-31) Therefore, we proposed that the absence of its co-activator CGI-58 results in similar alterations of macrophage function. Since whole body CGI-58-/- mice die soon after birth due to a severe skin barrier defect (37) and to investigate the consequences of CGI-58 deficiency in macrophages, we generated a mouse model lacking CGI-58 exclusively in myeloid cells including monocytes, mature macrophages, and granulocytes (macCGI-58-/-). These mice are viable with no apparent changes in skin phenotype. Compared to Wt mice, the lack of CGI-58 in myeloid cells does not affect body weight, lipid parameters, glucose levels, and glucose tolerance even when mice are challenged with WTD. Unchanged glucose tolerance in WTD-fed mice is contradictory to the results shown recently by Miao *et al.* (55), who reported impaired glucose tolerance in HFD-fed male macCGI-58-/- mice. This discrepancy is difficult to explain as both diets (WTD and HFD) can be used to affect glucose tolerance. Since we have repeated the experiments in male mice that also lacked significant differences between the phenotypes (data not shown), a sex difference leading to the contradictory results can be excluded.

CGI-58 deficiency leads to decreased TG hydrolyse activity and a TG-rich LD accumulation in macrophages, identical to ATGL-/- macrophages. (28, 29) These results suggest that ATGL activity can be increased by CGI-58 as activator protein (18) also in macrophages. Unchanged Cd36 and LPL mRNA as well as LPL activity argue against differences in FA uptake between CGI-58-/- and Wt macrophages. Since LPL is responsible for the extracellular hydrolysis of lipoprotein-associated TG and the subsequent uptake of FAs in underlying cells and tissues, these results indicate that FAs generated by the action of LPL are taken up similarly by CGI-58-/- and Wt macrophages. Unchanged TC and FC concentrations were associated with comparable CE hydrolase activities between Wt and CGI-58-/- macrophages, as observed in ATGL-/- macrophages. (29) In contrast to our results, Miao *et al.* (55) found increased TC and FC concentrations and reduced Cd36 mRNA expression in macrophages of male macCGI-58-/- mice. Whether the differences in the two studies are due to sex-specific differences or

cultivation conditions of the macrophages (LPDS versus FCS) remains to be elucidated. Moreover, in their studies macrophages from mice fed HFD were used, whereas in our studies TC and FC levels of macrophages were isolated from mice fed chow diet.

Measurement of FA composition within TGs of CGI-58-/- macrophages revealed increased concentrations of all saturated, unsaturated, and polyunsaturated FAs analyzed with most pronounced changes in arachidonic acid, oleic acid, and palmitoleic acid, respectively. FA composition has not been determined in ATGL-/- macrophages but in WAT of ATGL-/- mice. Our findings fit to these results, where the authors showed that ATGL hydrolyzes long-chain FA esters *in vivo* with a modest substrate preference for palmitoleic acid. (19)

Fragmented mitochondria in ATGL-/- macrophages are indicative of the mitochondrial apoptosis pathway being triggered as a consequence of defective lipolysis. (28) We expected the same phenotype in CGI-58-/- macrophages. Typical markers of programmed cell death, such as externalization of phosphatidylserine on the plasma membrane measured by flow cytometry after annexin V/PI co-staining, mRNA and protein expression of pro- and anti-apoptotic markers, and lack of fragmented mitochondria prior to cell death, however, revealed that mitochondrial apoptosis is not induced in CGI-58-/- macrophages. Absent CHOP protein expression and unaltered mRNA expression of the ER-resident chaperones Erdj4 and Pdi indicate that CGI-58 deficiency in macrophages does not cause ER stress. These results are different from findings in ATGL-/- macrophages, where we observed induction of apoptosis and ER stress. (28, 30) Interestingly, incubation of Wt macrophages with VLDL resulted in the same apoptotic phenotype and fragmentation of mitochondria as observed in ATGL-/- macrophages. (28) From these results we had initially concluded that intracellular TG accumulation is linked to mitochondrial dysfunction and programmed cell death in macrophages. The results from the present work are therefore counterintuitive. Why TG accumulation leads to mitochondrial dysfunction in ATGL-/- and VLDL-loaded Wt macrophages (28), but fails to affect CGI-58-/- macrophages, is elusive. Since ATGL is present in CGI-58-/- macrophages it might be claimed that there is still basal ATGL-mediated TG hydrolase activity, which is sufficient to rescue the cell from mitochondrial apoptosis. However, macrophage TG concentrations are comparable between

ATGL-/- and CGI-58-/- macrophages, suggesting other factors to be responsible for programmed cell death, mitochondrial dysfunction, and ER stress in ATGL-/- macrophages.

The *in vitro* phagocytic capacity was affected by the lack of ATGL (29) and CGI-58 in a similar manner with reduced phagocytosis in glucose-containing and glucose-free medium compared to Wt macrophages. It has been demonstrated that hydrolysis of cellular TG by ATGL is necessary to produce FAs as ligands for PPAR activation and that ATGL deficiency leads to severely disrupted mitochondrial substrate oxidation and respiration. (25) Although mRNA levels of PPARα target genes in macrophages were unchanged, decreased mitochondrial respiration might contribute to the reduced phagocytic capacity of CGI-58-/- macrophages. Since the surface area of mitochondria was unaffected by CGI-58 deficiency, the reduced respiration is likely due to the decrease in FAs as energy substrate. A decreased OCR was also described in CGI-58-silenced RAW264.7 macrophages. (55) Our *in vitro* finding of reduced phagocytosis could not be confirmed *in vivo* in macCGI-58-/- mice, where we observed a trend to reduced phagocytosis, which, however, lacked statistical significance. We hypothesize that the reason for this discrepancy is the difference in the mouse models: in macCGI-58-/- mice, CGI-58 is absent exclusively in myeloid cells including macrophages, in which phagocytosis is affected *in vitro*. In contrast, the decreased *in vivo* phagocytosis ability was demonstrated in whole-body ATGL-/- mice. (29) Phagocytosis is a highly energy demanding process; reduced FA concentrations in ATGL-/- mice (24) versus unaltered FA levels in macCGI-58-/- mice might explain the observed *in vivo* changes in phagocytic capacity.

Due to the pronounced differences observed between ATGL-/- and CGI-58-/- macrophages, we were particularly interested in the impact of macCGI-58 deficiency on atherosclerosis susceptibility. Unexpectedly, plaque formation, number of macrophages, and collagen content was identical in aortic root sections of macCGI-58/ApoE-DKO and ApoE-/- mice. In line with these results, *en face* analyses of the aortic arch area revealed comparable lesion sizes in both genotypes. When we analyzed lesion per total area of the thoracic aorta, we found slightly increased plaque formation in DKO mice. In agreement, ASO-mediated KD of CGI-58 in Ldlr-/- mice did not alter atherosclerosis burden in the aortic root, but very modestly increased atherosclerosis in the aorta. Collectively, these findings

are again contrary to what we observed in the absence of ATGL, where transfer of ATGL-/- bone marrow into Ldlr-/- mice resulted in markedly reduced plaque formation. (26) Interestingly and contradictory to that, CGI-58 overexpression in macrophages even alleviated atherosclerotic lesion development in ApoE-/- mice (57) although CGI-58 overexpression should in fact increase ATGL activity in macrophages. These findings argue for an ATGL-independent function of CGI-58 in macrophages.

Although different mouse models were used in our studies (Ldlr-/- for ATGL bone marrow transplantation, ApoE-/- for atherosclerosis studies for this project), our results indicate that the absence of ATGL or CGI-58 in myeloid cells results in different phenotypes: reduced lesion development by ATGL deficiency and unaltered or even slightly increased plaque formation by loss of CGI-58. This difference in plaque formation is unlikely due to differences in cholesterol efflux capacities of the cells, since macrophages lacking either ATGL or CGI-58 show comparable cholesterol efflux as control cells. The M2-like polarization of ATGL-/- macrophages and the M1-like phenotype of CGI-58-/- might contribute (at least in part) to the differences in plaque formation. In accordance with our results, Miao *et al.* (55, 56) have recently shown that macrophage CGI-58 deficiency activates the ROS-NLRP3 inflammatory pathway to induce IL-1β secretion and promote insulin resistance in mice. We found increased IL-6 secretion from LPS-treated CGI-58-/- macrophages, suggesting that the lack of CGI-58 in macrophages affects the inflammatory response to LPS. This finding is in line with results from ASO-mediated CGI-58 KD experiments, in which lipid second messengers generated by CGI-58 were shown to be critically involved in maintaining the balance between inflammation and insulin action, thereby predicting a role of CGI-58 in cytokine signalling. (48) On an ApoE-/- background, however, plasma IL-6 concentrations and macrophage polarization markers were no longer different between mice that express or lack CGI-58 in macrophages. Since ApoE promotes macrophage conversion from M1 to the M2 phenotype (154), it might be speculated that the absence of ApoE directs macrophages into an M1-like phenotype, which cannot be further boosted by CGI-58 deficiency. In contrast, reduced plaque formation in aortic roots of Ldlr-/- mice transplanted with ATGL-/- bone marrow was associated with decreased macrophage IL-6 concentrations. (26)

In 2012, Lord *et al.* (48) observed a role of CGI-58 in cytokine signalling showing that the lack of CGI-58 affects the inflammatory response to endotoxin. To investigate if inflammation is affected in macCGI-58-/- mice we injected mice with LPS and determined plasma cytokine concentrations and cytokine mRNA levels in WAT and liver. Cytokine levels were unchanged in both plasma and tissue samples. Apparently, lacking CGI-58 only in myeloid cells is insufficient to affect whole body inflammation in mice. Hence, we decided to examine the inflammatory response by treating cells with LPS. We found markedly increased IL-6 levels in the supernatant of CGI-58-/- compared to Wt macrophages suggesting that the lack of CGI-58 affects the inflammatory response to endotoxin also in macrophages. Furthermore, it fits to our findings that CGI-58-/- macrophages display a pro-inflammatory M1-like phenotype.

The data presented in this study provide evidence that the TG-rich LD accumulation within ATGL-/- macrophages is likely not the reason for attenuated atherosclerosis development as initially hypothesized. Although loss of CGI-58 in macrophages results in comparable TG accumulation, several results were different between CGI-58-/- and ATGL-/- macrophages. Absence of ER stress, mitochondrial apoptosis, and mitochondrial dysfunction, as well as pro-inflammatory M1-like polarization of CGI-58-/- macrophages, and differences in atherosclerosis susceptibility argue for different and/or additional function(s) of CGI-58 in macrophages beside activation of ATGL. We conclude that lack of the enzyme (ATGL) induces a more severe phenotype than loss of the activator (CGI-58).

6. Results: Autophagy in lipase-deficient macrophages

6.1 Neutral TG hydrolase activity is abolished in *A0H0* macrophages

To elucidate the consequences of ATGL and HSL deficiency in macrophages *in vivo*, we generated *A0H0* mice. Genotyping results are shown in Fig. 37A; lack of HSL and ATGL in macrophages was confirmed by Western blot analysis (Fig. 37B). First we determined TG and CE hydrolase activities in macrophage lysates from Wt, *H0*, *A0,* and *A0H0* mice. Neutral TG hydrolase activity was significantly decreased in *A0* and *A0H0* compared with Wt macrophages (51% and 73%, respectively) (Fig. 37C). Neutral CE hydrolase activity was strongly decreased in *H0* (88%) and *A0H0* (90%) compared with Wt and *A0* macrophages (Fig. 37D). These data indicate that the absence of HSL alone markedly contributes to the reduction in neutral CE hydrolase activity, whereas ATGL together with HSL account for the main neutral TG hydrolase activities in macrophages.

Figure 37

A

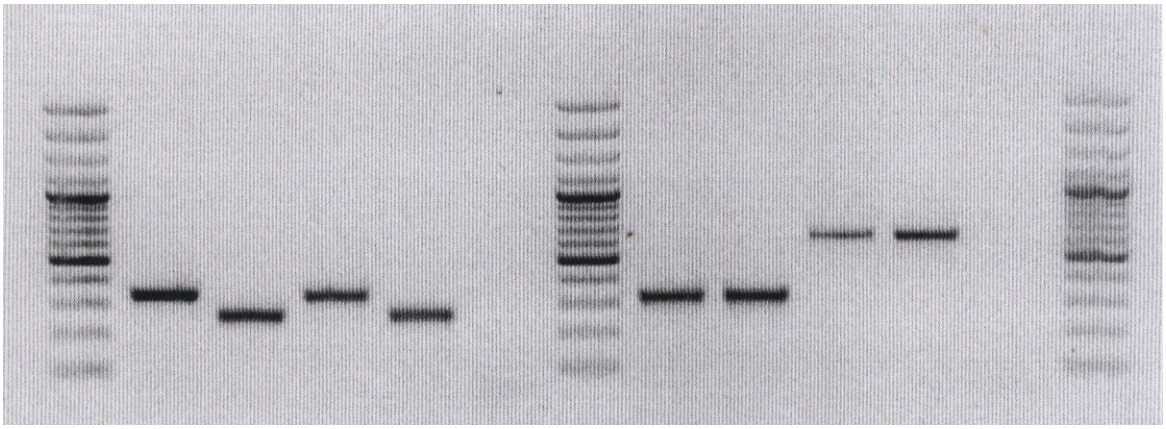

B

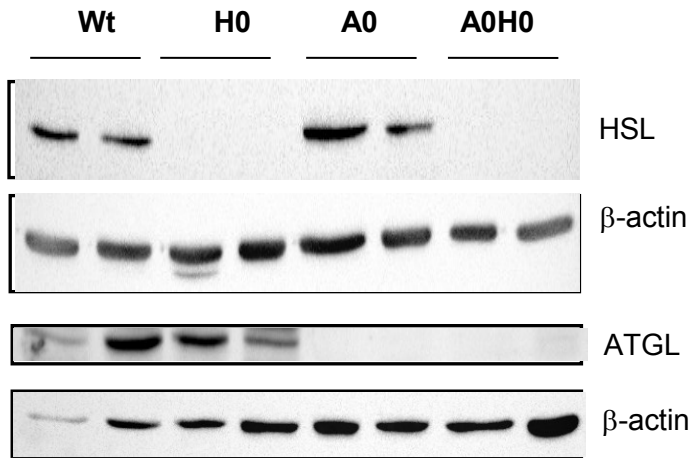

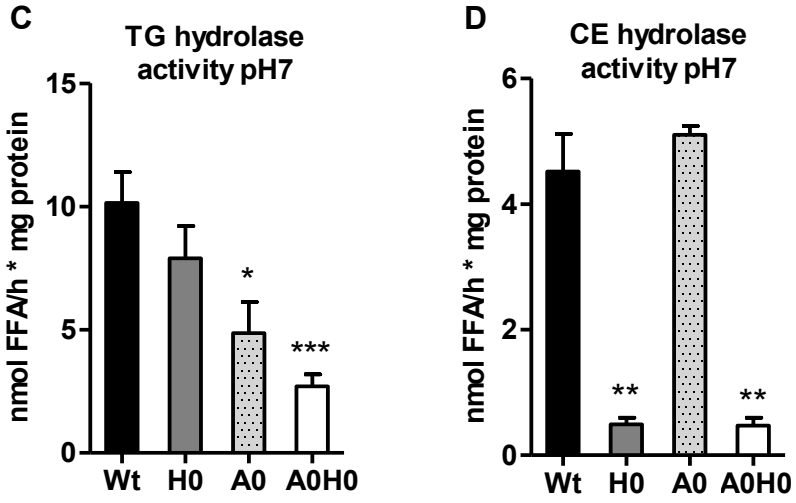

Figure 37: Ábolished neutral TG hydrolase activity in *A0H0* macrophages. (A) Genotyping of *H0* and *A0* mice. The bands represent PCR products of Wt (lane 1), *H0* (lane 2), *A0* (lane 3), and *A0H0* (lane 4) mice. (B) Western blotting of macrophages using anti-ATGL and anti-HSL-specific antibodies. The expression of β-actin was determined as loading control. Neutral (C) TG and (D) CE hydrolase activities were measured in Wt, *H0*, *A0*, and *A0H0* macrophages. Data are presented as mean (n=4-6) + SEM. *, $p < 0.05$; **, $p \leq 0.01$; ***, $p \leq 0.001$.

6.2 TG-rich LD accumulation in *A0H0* macrophages

To investigate the rate of LD accumulation in *A0H0* macrophages, we analyzed intracellular TG and cholesterol concentrations. We observed ~3-fold increased TG concentrations in *A0* and *A0H0* macrophages compared to Wt and *H0* macrophages (Fig. 38A). TG content in *H0* and Wt macrophages were comparable, indicating that the absence of HSL failed to affect intracellular TG stores in *A0H0* macrophages (Fig. 38A). In accordance with our previous findings in *H0* (14) and *A0* macrophages (29), TC concentrations were unchanged in *A0H0* compared to Wt macrophages (Fig. 38B). To determine the LD content, we analyzed the cells after Nile red staining by fluorescence microscopy. Macrophages from *A0* and *A0H0* mice had substantially more LDs compared with macrophages from Wt and *H0* mice (Fig. 38C, D). HSL deficiency did not lead to noticeable alterations in the amount of LDs, neither in *A0H0* compared with *A0* nor in *H0* compared with Wt macrophages.

Figure 38

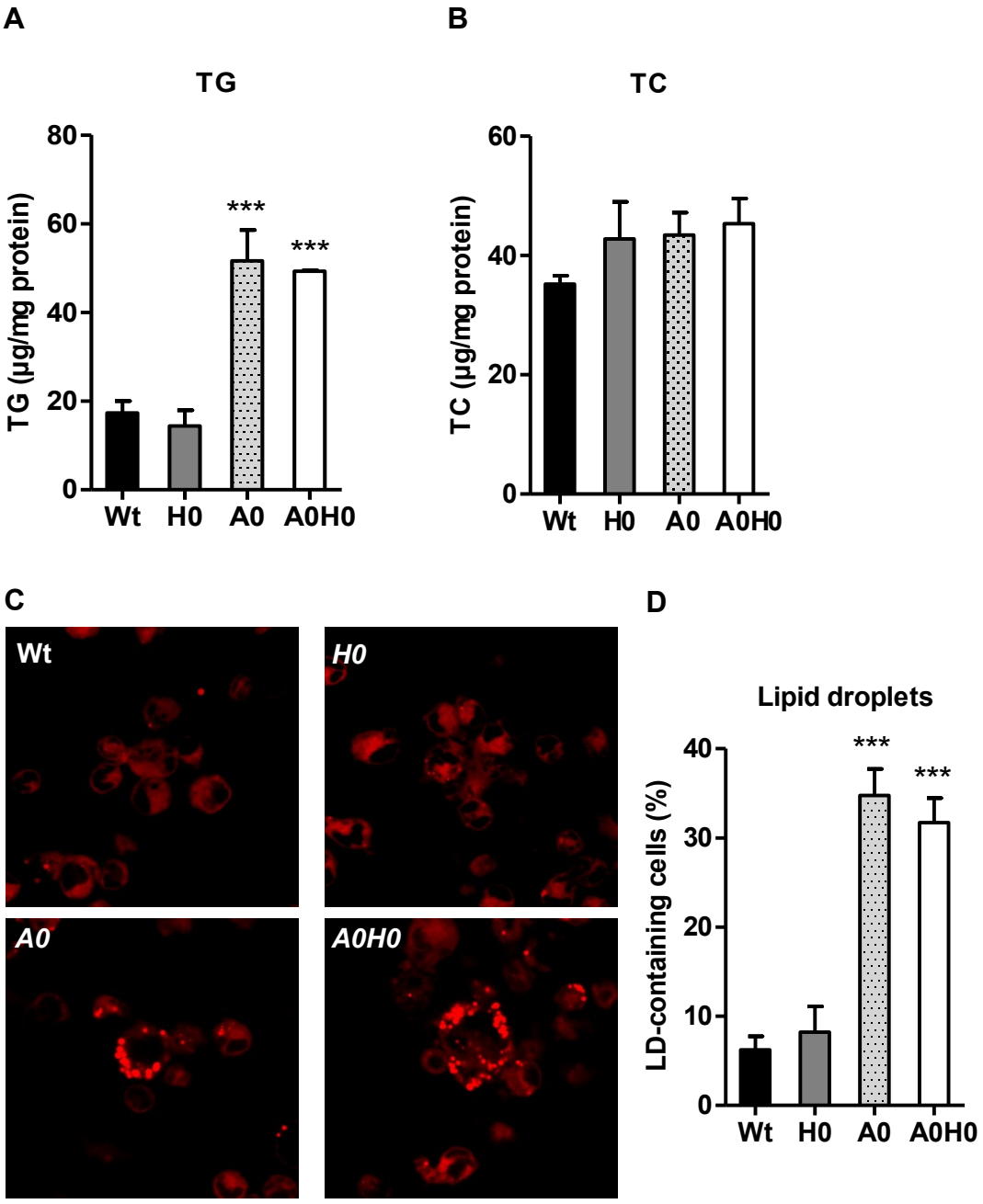

Figure 38: Increased TG concentrations and number of LDs in *A0H0* macrophages. (A) TG and (B) TC concentrations in Wt, *H0*, *A0*, *and A0H0* macrophages after lipid extraction were measured enzymatically. Data are presented as mean values (n=3-6) + SEM. (C) LDs in macrophages were visualized by Nile red staining. Image magnification, X63. (D) Quantification of LD-containing macrophages cultivated in DMEM/10% LPDS. Data are presented as the mean percentage of LD-containing cells + SEM from at least 300 cells per group. ***, $p \leq 0.001$.

6.3 Autophagy is a general recycling mechanism in macrophages

It has been recently shown that autophagy is involved in the regulation of intracellular lipid content. (96) Utilizing electron microscopy we found a substantial amount of structures resembling degradative autophagic vacuoles (AVd) in macrophages from all genotypes (Fig. 39A). In *A0* macrophages, we observed LDs in very close proximity to autophagic vesicle-like structures. Closer inspection revealed that LDs are not enclosed within these membrane structures, which are morphologically not comparable to AVd presented in other images.

To investigate whether autophagy might regulate intracellular TG levels in *A0H0* macrophages, we determined LC3 degradation. During autophagy, cytosolic LC3 (LC3-I) is modified to its membrane-bound form (LC3-II) located on pre-autophagosomes and autophagosomes, which makes it a commonly used autophagosome marker. (94) As shown in Fig. 39B, macrophages from all genotypes showed a substantial amount of LC3-II, indicating that autophagy is a general recycling mechanism in macrophages. The ratio of LC3-II to β-actin trended to be increased in *A0* and *A0H0* macrophages compared to controls (Fig. 39C).

In addition, we analyzed protein expression of p62, a chaperone that shuttles intracellular protein aggregates into autolysosomes for degradation. Since the entire p62-protein aggregate is degraded after engulfment by the autolysosome, expression levels of p62 are inversely correlated with autophagic flux. Protein expression of p62 trended to be reduced in macrophages from *H0* and *A0* mice, however, this reduction was statistical significant in *A0H0* macrophages (Fig. 39C). Reduced expression of p62 and increased abundance of the mature form of the lysosomal protease cathepsin B (Fig. 39D) in *A0H0* macrophages suggest that autophagy is highly active in macrophages deficient in both ATGL and HSL.

Figure 39

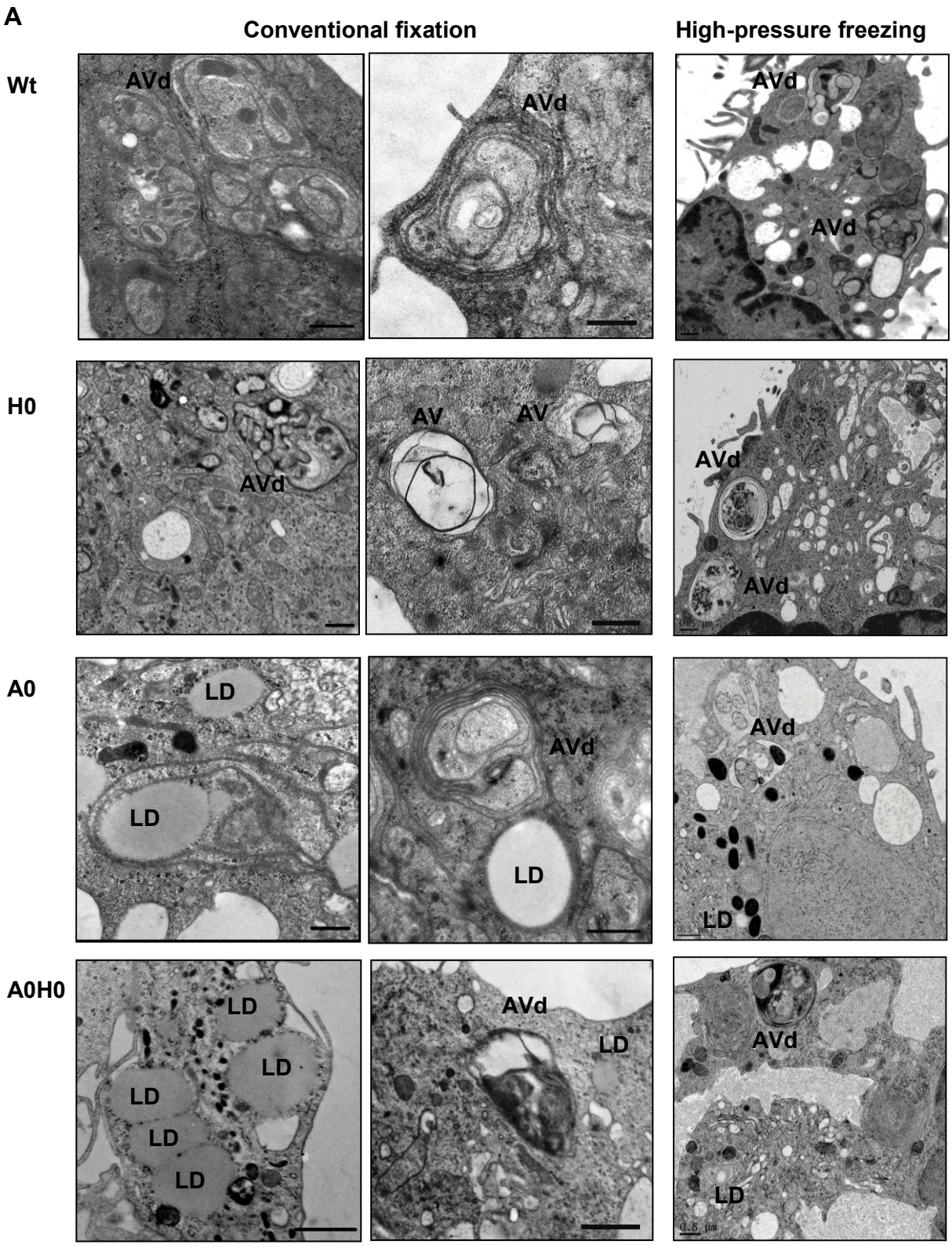
A
Conventional fixation
High-pressure freezing
Wt
H0
A0
A0H0
AVd
AV
LD

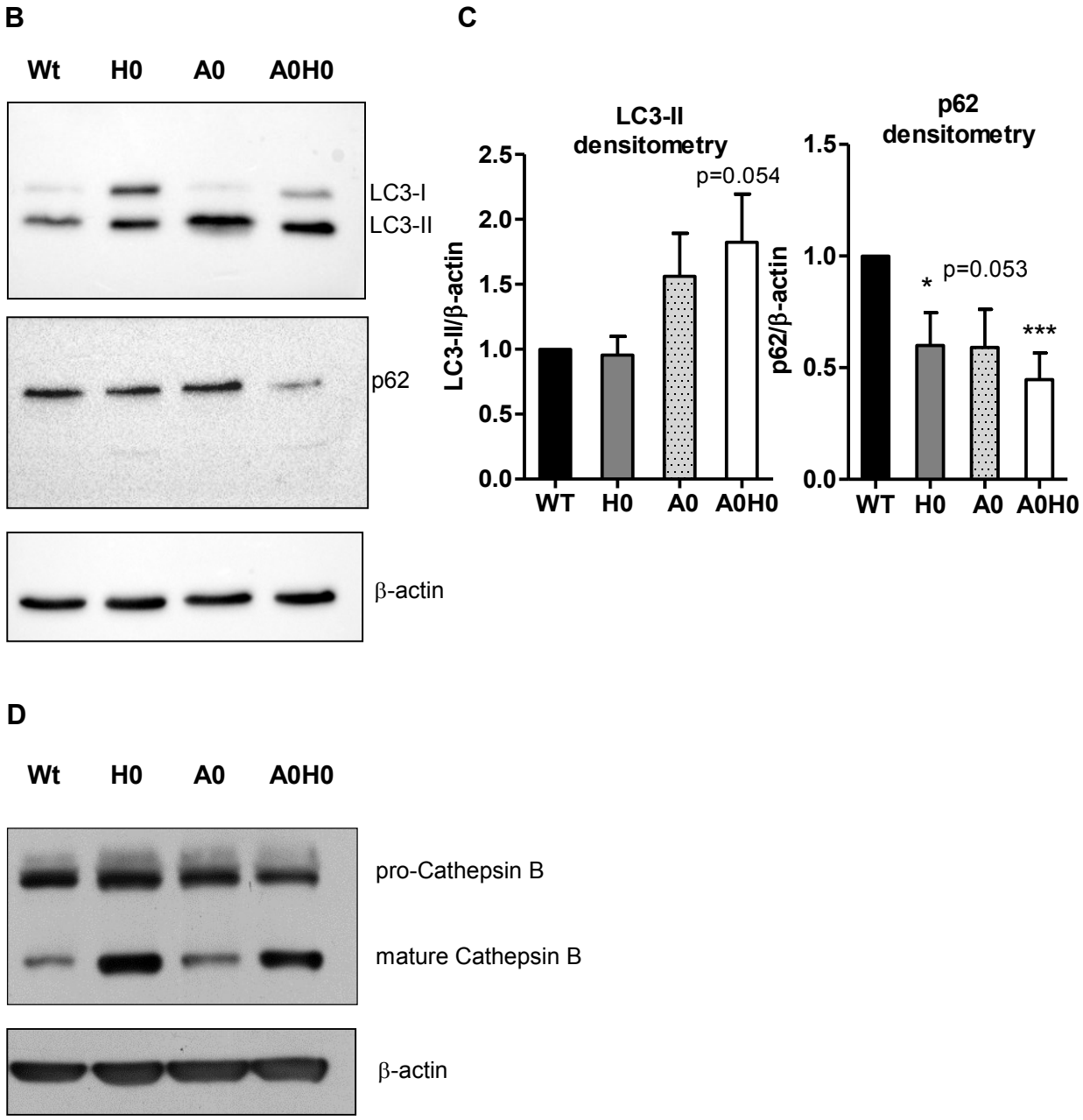

Figure 39: Increased autophagosome formation in *A0H0* macrophages. (A) Representative electron micrographs of Wt, *H0, A0,* and *A0H0* macrophages, showing degradative autophagic vacuoles (AVd) in cells from all phenotypes and LDs in *A0* and *A0H0* macrophages. Right panel: Electron micrographs after high-pressure freezing (HPF). Scale bars: 0.5 µm. (B,D) Western blotting of macrophage lysates using (B) anti-LC3B, anti-p62, and (D) anti-Cathepsin B specific antibodies. Protein expression of β-actin was determined as loading control. (C) Densitometric quantification of LC3-II/β-actin (n=7-11) and p62/β-actin (n=6-7) of independent experiments + SEM, relative to the expression in Wt macrophages. *, $p < 0.05$; ***, $p \leq 0.001$.

6.4 Intact autophagic flux and lysosomal activity in *A0H0* macrophages

To analyze the autophagic flux we next incubated macrophages with bafilomycin A1 or choloroquine, which inhibit the fusion between autophagosomes and lysosomes, thereby preventing maturation of autophagic vacuoles and degradation of LC3-II and p62.

Bafilomycin A1 treatment resulted in comparable increase in LC3-II (Fig. 40A, C) and p62 (Fig. 40B, D) expression in macrophages from Wt*, A0, H0,* and *A0H0* mice with a trend to decreased p62 expression in *H0* (Fig. 40B) and *A0H0* (Fig. 40D) macrophages.

Chloroquine treatment resulted in similarly increased protein expression of LC3-II and p62 in Wt and *A0H0* macrophages (Fig. 40E, F).

In addition, we measured lysosomal activity with another method by treating macrophages with DQ-BSA and analyzing the fluorescence by flow cytometry. DQ-BSA is a derivative of BSA that is labeled with a self-quenched red fluorescent dye and dequenched in acidic intracellular lysosomal compartments by lysosomal proteases, releasing red fluorescence. (151) After starving the cells for 1 h and DQ-BSA incubation for 15 min, Wt, *H0,* and *A0* macrophages showed comparable red fluorescence immediately after loading (0 h) and after chasing the cells for 2 h and 6 h (Fig. 40G). In *A0H0* macrophages, we observed significantly increased amounts of dequenched DQ-BSA at all time points (Fig. 40G), suggesting that *A0H0* macrophages have elevated lysosomal proteolytic activity.

Figure 40

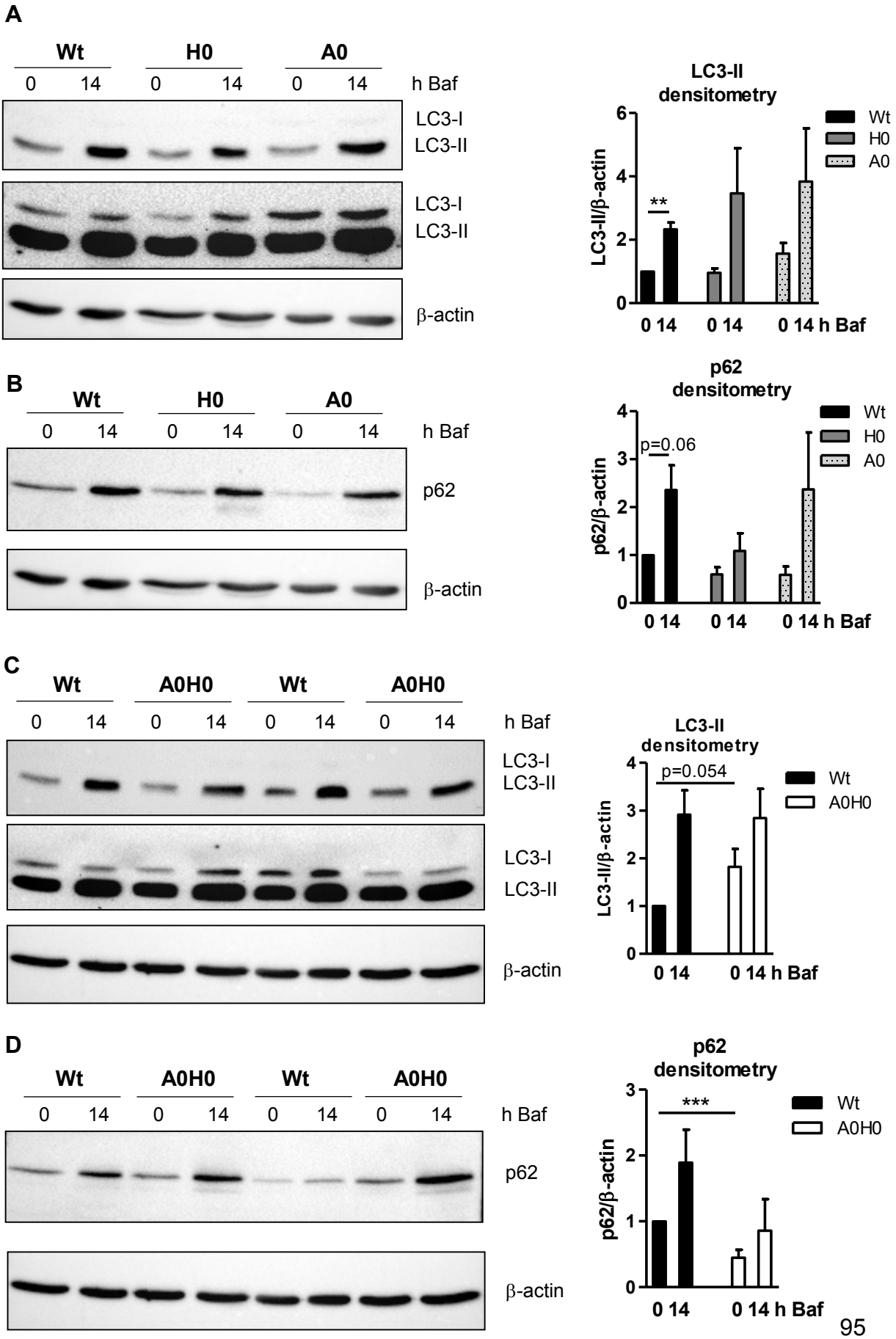
A
Wt
H0
A0
0
14
0
14
0
14
h Baf
LC3-I
LC3-II
LC3-I
LC3-II
β-actin
LC3-II densitometry
LC3-II/β-actin
**
Wt
H0
A0
0 14
0 14
0 14 h Baf
B
Wt
H0
A0
h Baf
p62
β-actin
p62 densitometry
p62/β-actin
p=0.06
C
Wt
A0H0
Wt
A0H0
h Baf
LC3-I
LC3-II
β-actin
p=0.054
D
p62
***

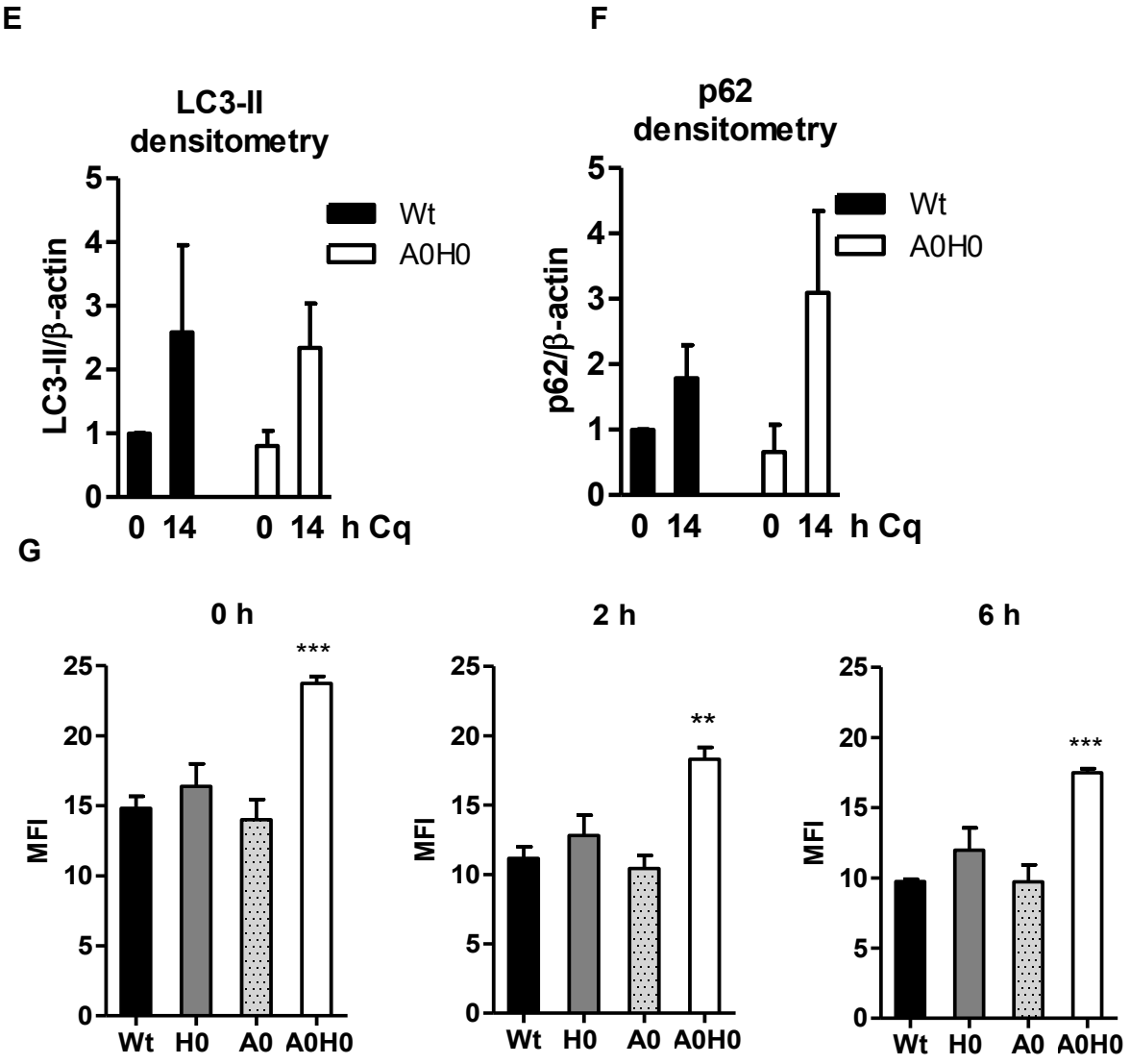

Figure 40: Intact autophagic flux in *A0H0* macrophages. Macrophages were cultured in DMEM/10% LPDS for 24 h. (A-D) Macrophages were incubated with 10 nM bafilomycin A1 (Baf) for 0 and 14 h and assayed for (A,C) LC3 (upper blot: short exposure time to quantify LC3-II; lower blot: longer exposure time to visualize LC3-I) and (B,D) p62 protein expression. Protein expression of β-actin was determined as loading control. Representative Western blot analysis of at least 4 independent experiments is shown. Densitometric quantification of LC3-II/β-actin and p62/β-actin of (A) n=4-7, (B) n=4-8, (C) n=6-10, and (D) n=5-11+ SEM. (E, F) Macrophages were incubated with 30 µM chloroquine (Cq) for 0 and 14 h and assayed for (E) LC3 and (F) p62 protein expression. Protein expression of β-actin was determined as loading control. Data are presented as densitometric quantification of LC3-II/β-actin and p62/β-actin as mean (n=3) + SEM. (G) Cells were starved for 1 h in HBSS and then incubated with DQ-BSA (final concentration 10 µg/ml) for 15 min at 37 °C. Red-fluorescent DQ-BSA was analyzed by flow cytometry using a FACSCalibur flow cytometer after 0, 2, and 6 h, respectively. Data are presented as mean (n=3-9) + SEM. **, $p \leq 0.01$; ***, $p \leq 0.001$.

6.5 Acid TG hydrolase activity is markedly diminished in *A0H0* macrophages

Finally, we investigated whether the terminal step in autophagic lipid degradation is induced in lipase-deficient macrophages. To this extent, we first determined the protein expression of LAL, the major TG and CE hydrolase in lysosomes. As shown in Fig. 41A, LAL protein expression was comparable between macrophages from all genotypes. Lal-deficient (*L0*) macrophages were used as a control.

Acid TG hydrolase activity, which reveals the activity of the lysosomal TG hydrolase LAL, was slightly decreased in *H0* and ~80% reduced in *A0* and *A0H0* compared to Wt macrophages (Fig. 41B). Acid CE hydrolase activity was comparable in macrophages from all genotypes (Fig. 41C). As a control, *L0* macrophages showed drastically reduced acid TG and CE hydrolase activities (Fig. 41B, C).

Comparable with *A0H0* macrophages, *L0* macrophages showed increased dequenched DQ-BSA (Fig. 41D), suggesting an elevated lysosomal proteolysis even in cells lacking the major acid hydrolase.

Starvation, a known inducer of autophagy, failed to decrease intracellular TG concentrations in macrophages of all genotypes (Fig. 41E). We starved the cells for 1.5 h since a longer starvation period drives lipase-deficient cells into cell death (unpublished observation).

In summary, our data suggest that although autophagy is active in macrophages lacking both ATGL and HSL, degradation of LDs by LAL is less effective.

Figure 41

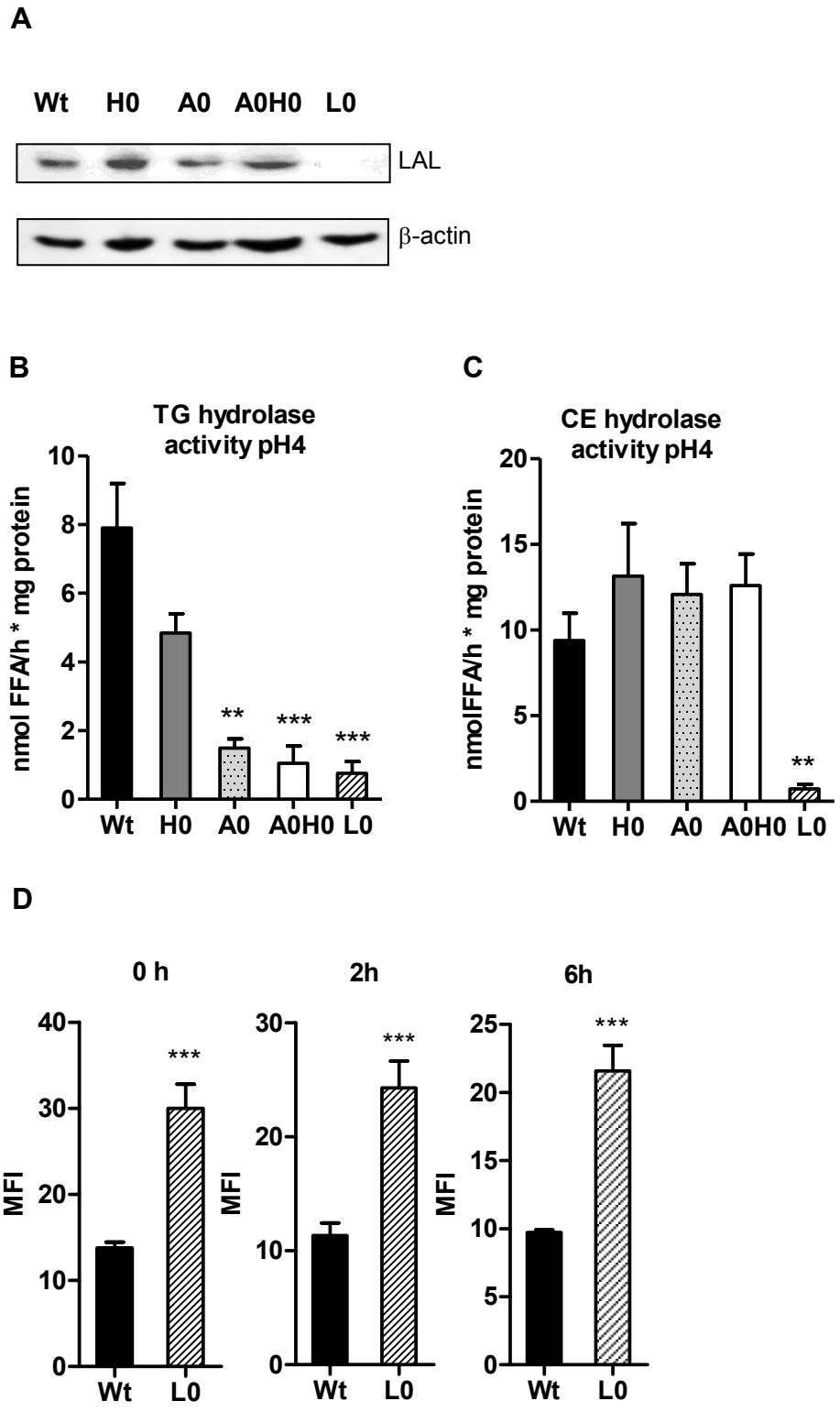
A
Wt H0 A0 A0H0 L0
LAL
β-actin
B
TG hydrolase activity pH4
nmol FFA/h * mg protein
10
8
6
4
2
0
**
***
***
Wt H0 A0 A0H0 L0
C
CE hydrolase activity pH4
nmolFFA/h * mg protein
20
15
10
5
0
**
Wt H0 A0 A0H0 L0
D
0 h
2h
6h
MFI
40
30
20
10
0
25
15
5
***
Wt L0

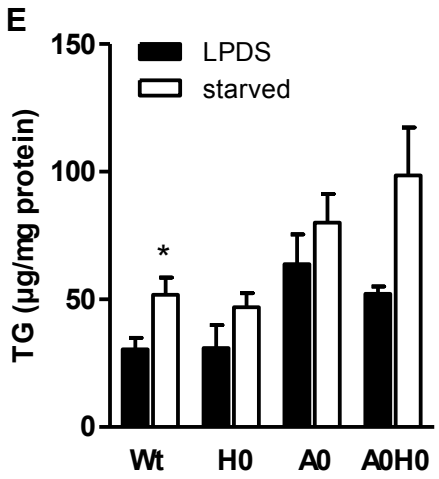

Figure 41: **Reduced acid TG hydrolase activity in *A0H0* macrophages.** (A) Western blot analysis of LAL protein expression in macrophage lysates. Macrophages from Lal-deficient (*L0)* mice were used as control. Protein expression of β-actin was determined as loading control. Acid (B) TG and (C) CE hydrolase activities were measured in Wt, *H0, A0, and A0H0* macrophages. Macrophages from *L0* mice were used as control. Data are presented as mean (n=3-8) + SEM. (D) *L0* macrophages were starved for 1 h in HBSS and incubated with 10 µg/ml DQ-BSA for 15 min at 37°C. Red-fluorescent DQ-BSA was analyzed by flow cytometry after 0, 2, and 6 h, respectively. Data are presented as mean (n=4-7) + SEM. (E) Macrophages were incubated in HBSS for 90 min and intracellular TG concentrations were determined. Data are presented as mean + SEM. *, $p < 0.05$; **, $p \leq 0.01$; ***, $p \leq 0.001$.

6.6 Bafilomycin A1 treatment does not affect lipid turnover in macrophages

To investigate the role of autophagy in LD turnover in macrophages, we loaded macrophages with [^{3}H]OA-BSA and analyzed the flux in the absence and presence of bafilomycin A1.

In *A0* and *A0H0* macrophages, there was a trend toward decreased FA release into the medium after 14 h of bafilomycin A1 treatment. However, we failed to observe any differences in untreated compared to bafilomycin A1-treated cells (Fig. 42A). Furthermore, we found increased FA incorporation into TGs in *A0* and *A0H0* macrophages, which was unaffected by bafilomycin A1 treatment (Fig. 42B). We observed no differences in incorporation of [^{3}H]OA-BSA into other lipid classes between the different genotypes or after bafilomycin A1 incubation.

Next, we treated Wt cells with inhibitors against ATGL and HSL, resulting in significantly decreased FA release (Fig. 42C). This finding suggests that the inhibitors efficiently blocked lipolysis. Comparable to the results from *A0* and *A0H0* macrophages, we observed increased FA incorporation into TGs of inhibitor-treated Wt cells, which was unaffected by bafilomycin A1 treatment (Fig. 42D). In summary, results from these pulse – chase experiments revealed that incorporation of FAs into lipid classes was independent of bafilomycin A1 in macrophages from all genotypes.

Figure 42

A

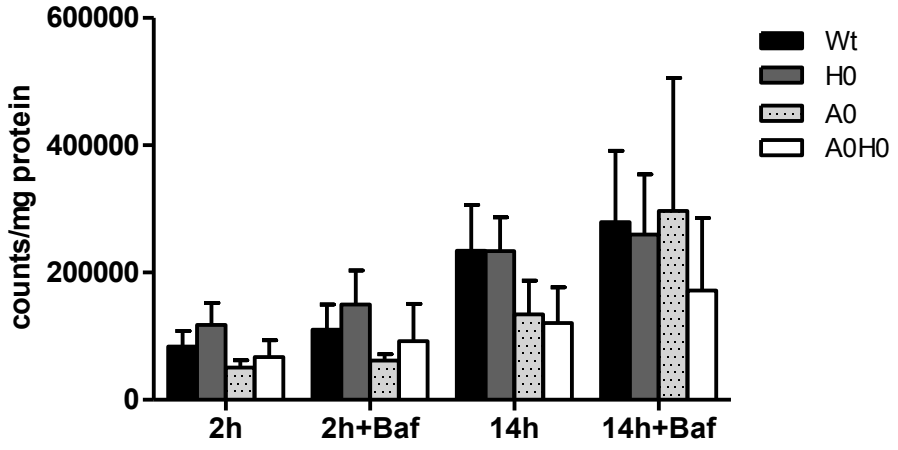

B

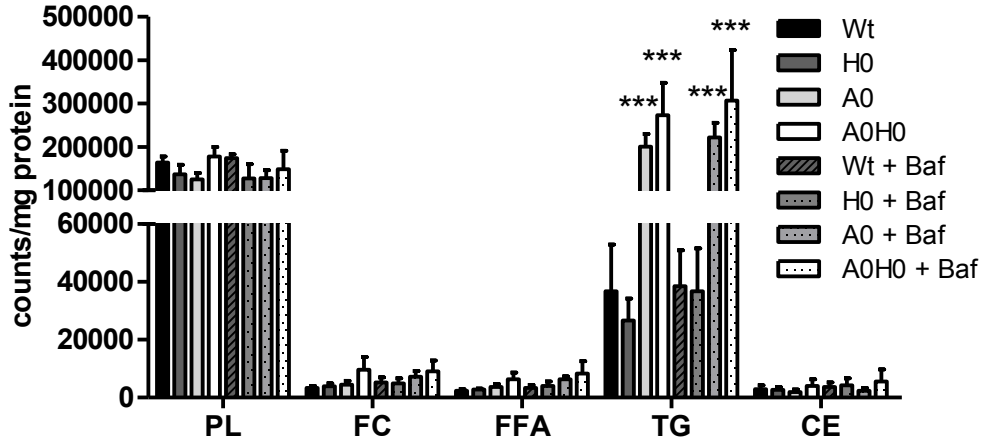

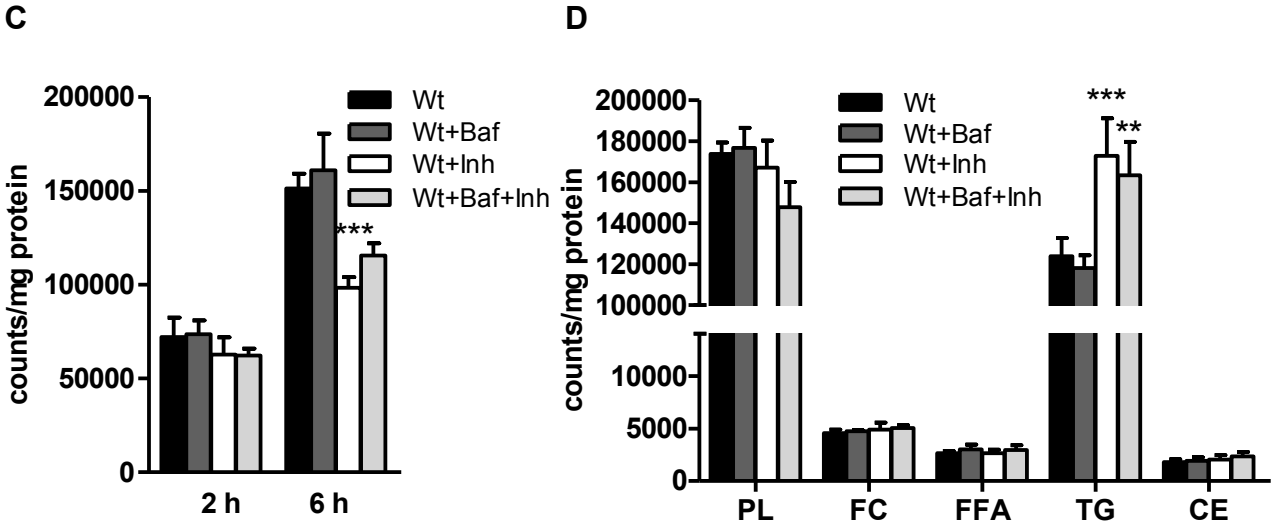

Figure 42: Bafilomycin A1 treatment does not affect lipid turnover in macrophages. Macrophages were cultured in DMEM/1% P/S containing 300 µM OA-BSA and 1 µCi [^{3}H]OA-BSA per ml for 24 h. Thereafter, macrophages were incubated with 10 nM bafilomycin A1 (Baf) +/- ATGL- and HSL-inhibitors (Inh) for 6 or 14 h. (A, C) FA release into the medium and (B, D) intracellular FA incorporation were determined by liquid scintillation counting and normalized to protein content. Data are presented as mean (A, B) (n=3-5) and (C,D) (n=5) + SEM compared to Wt +/- Baf. **, $p \leq 0.01$; ***, $p \leq 0.001$.

In analogy, we incubated macrophages with C12-BODIPY and chased the fluorescently labeled FA analogue under starvation conditions in the absence and presence of bafilomycin A1, respectively. To address whether lipophagy is active, we studied the co-localization of C12-BODIPY with lysosomes by immunohistochemistry using cathepsin D as a lysosomal marker. In macrophages from *A0* and *A0H0* mice, we observed a pronounced number of large LDs, which were absent in Wt and *H0* macrophages (Fig. 43A). In macrophages from all genotypes, we found C12-BODIPY to be present in cytosolic LDs without any overlap with lysosomes, independent of bafilomycin A1 treatment (Fig. 43A and B).

Figure 43

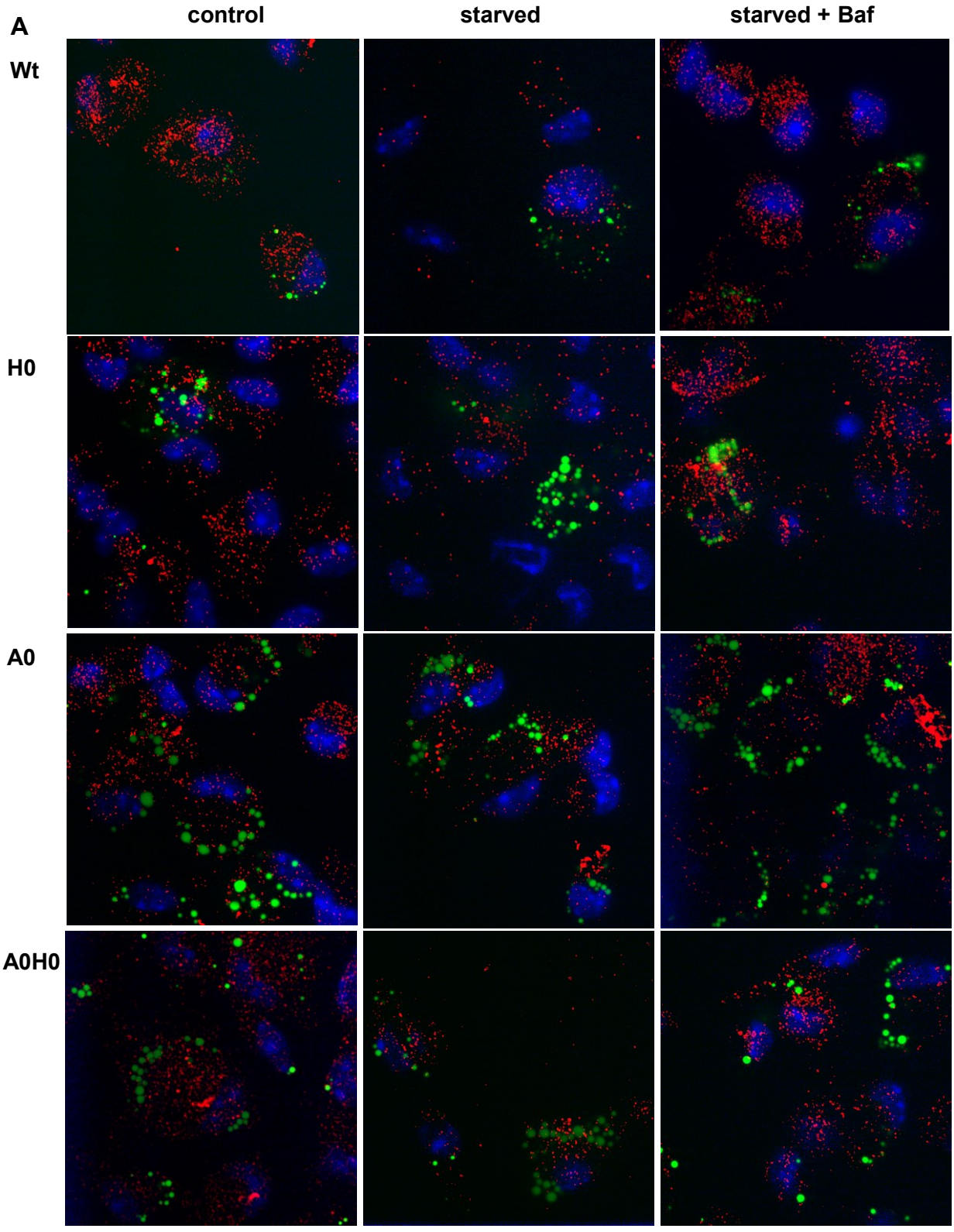

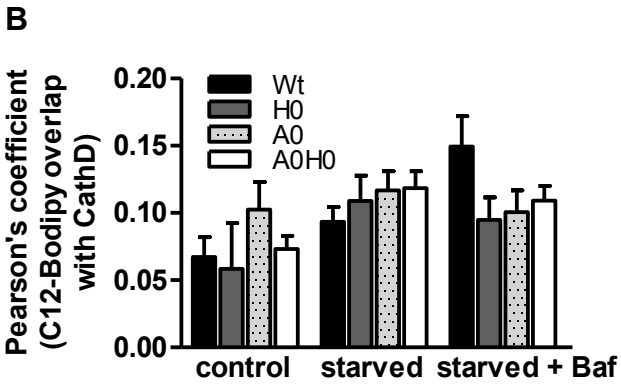

Figure 43: Bafilomycin A1 treatment does not affect lipid turnover in macrophages. (A) Macrophages were pulsed with C12-BODIPY for 24 h, washed (control), and chased with HBSS (starved) and Baf for 1 h. Lysosomes were labeled using cathepsin D antibody. (B) Relative cellular colocalization of C12-BODIPY with cathepsin D in pools of cells from 2 mice per genotype was quantified by Pearson's coefficient analysis. Data are expressed as means (n=7-10 fields/genotype) + SEM.

6.7 Bafilomycin A1 treatment and/or inhibition of ATGL and HSL does not affect cholesterol metabolism in macrophages

To investigate if bafilomycin A1 treatment or inhibition of ATGL and HSL influences cholesterol metabolism, we determined mRNA expression of several genes involved in cholesterol uptake and synthesis. We did not find any differences in the mRNA expression of Abca1, SrB1, Srebp2, Cd36, and HMGCoAR in macrophages treated with bafilomycin A1 and/or lipase inhibitors compared to untreated macrophages. However, the mRNA expression of Abcg1 was slightly increased in Wt cells treated with inhibitors compared to untreated macrophages (Fig. 44).

Figure 44

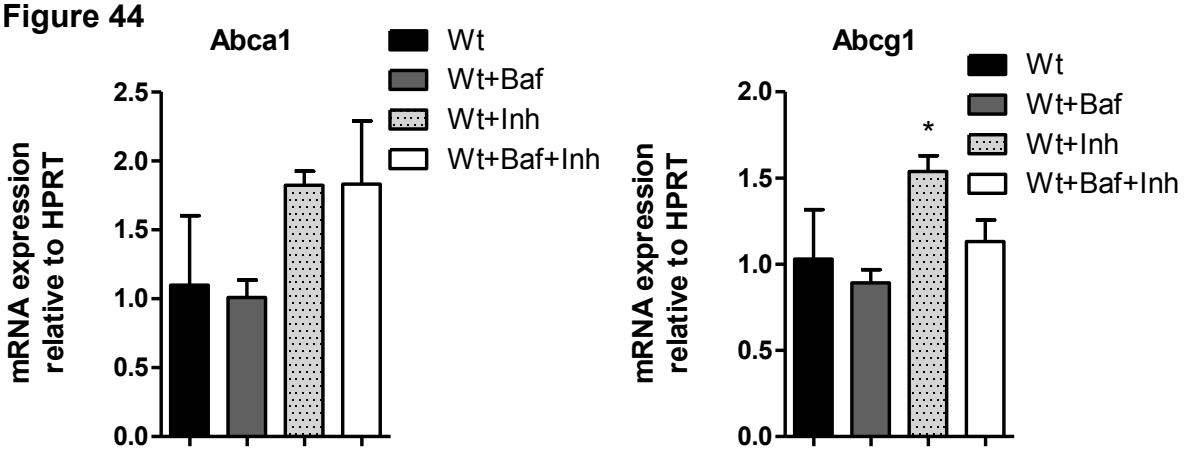

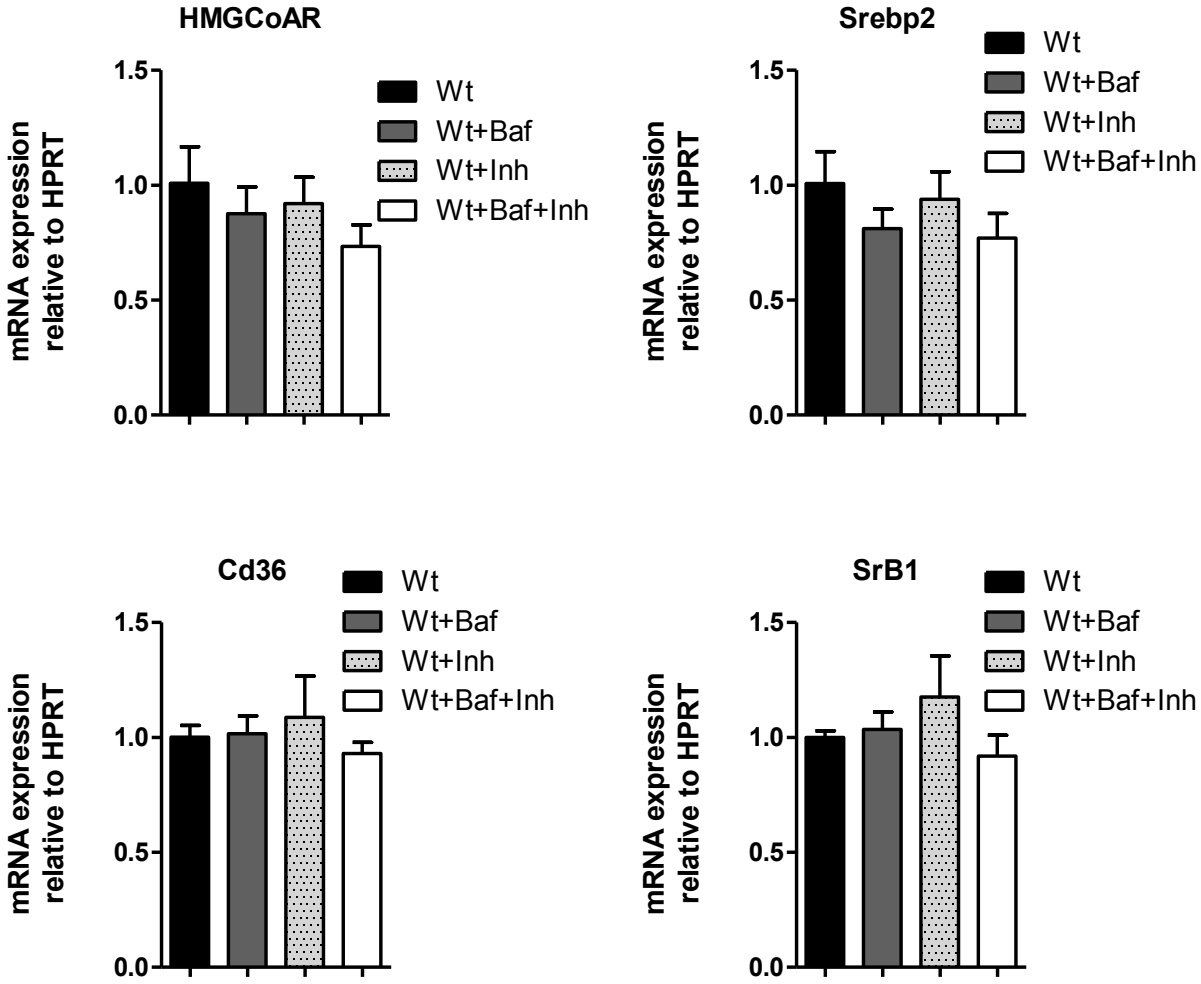

Figure 44: Bafilomycin A1 treatment and/or inhibition of ATGL and HSL does not affect cholesterol metabolism in macrophages. mRNA expression of genes involved in cholesterol metabolism. Macrophages were cultured in DMEM/10%LPDS/1% P/S for 24 h. Thereafter, macrophages were incubated with 10 nM bafilomycin A1 (Baf) +/- ATGL- and HSL-inhibitor for 6 h. Data are presented as mean (n=4) + SEM. *, $p \leq 0.05$. Expression profiles were determined using the 2^{-ddCt} method.

7. Discussion: Autophagy in lipase-deficient macrophages

LDs store neutral lipids, such as TGs, steryl esters and retinyl esters. These stored lipids can be used in times of need to generate energy, membrane components and signaling lipids. TGs are the most abundant form of stored neutral lipid in white adipose and many other tissues. Until recently, the breakdown of TGs and CEs of LDs was exclusively attributed to the actions of cytosolic lipases. However in 2009 Singh *et al.* (96) demonstrated that LDs are engulfed into double-membrane vesicles and termed this process macrolipophagy, also called lipophagy, deriving from autophagy of lipids. During this process, portions of large LDs or entire small LDs are sequestered by a double-membrane autophagosome. Autophagosomes fuse with lysosomes to form autolysosomes in which the substrates of the autophagosome and the hydrolytic enzymes of the lysosome are mixed for cargo degradation. Lipid breakdown leads to release of FAs into the cytoplasm for mitochondrial β-oxidation for the generation of ATP to maintain cellular energy homeostasis. (97)

In WAT of *A0* mice, HSL inhibition resulted in more than 95% reduction of neutral TG hydrolase activity (59), indicating that other lipases play only a quantitatively minor role in fat cell lipolysis. We have previously reported that macrophages from *A0* and *H0* mice showed reduced *in vitro* neutral TG hydrolase activity. (14, 29) In contrast to *A0* macrophages, however, *H0* macrophages lack TG accumulation. We generated *A0H0* mice and investigated macrophage lipid metabolism in order to (i) analyze the contribution of ATGL and HSL to TG mobilization in macrophages and to (ii) elucidate if autophagy might be a rescue mechanism to produce energy substrates. In all experiments, macrophages were cultivated in LPDS to exclude any effects that may originate from exogenous lipid loading.

Neutral CE hydrolase activity was unchanged in *A0* macrophages but significantly reduced in *H0* and *A0H0* macrophages with an identical decrease in both genotypes, indicating that decreased CE hydrolase activity in *A0H0* macrophages was only due to the lack of HSL. TC concentrations, however, were comparable in macrophages from all genotypes. This finding is in agreement with a previous study, in which we demonstrated lack of CE accumulation in *H0* macrophages.

(14) We concluded that additional enzymes must exist that cooperate with HSL to regulate intracellular CE levels *in vivo*. Moreover, LAL could possibly assist in the breakdown of CE via lipophagy.

H0 macrophages have reduced TG hydrolase activity but failed to accumulate TGs. (14) This result is in accordance with previous data showing DG but no TG accumulation in WAT of *H0* mice. (16) Reduced TG hydrolase activity and TG accumulation in essentially all cells and tissues of *A0* mice demonstrated that ATGL is crucial for TG hydrolysis. (24, 29) Neutral TG hydrolase activity was reduced by 82% in WAT of *A0* mice. (24) In accordance with (59), we observed markedly reduced TG hydrolase activity and an accumulation of TG-rich LDs in *A0H0* macrophages. Visualization of LDs by electron and fluorescence microscopy revealed a substantial amount of LDs in *A0* and *A0H0* macrophages. Interestingly, however, we observed comparable TG concentrations in *A0H0* and *A0* macrophages. One might speculate that the absence of ATGL results in intracellular TG concentrations that cannot be further increased by the additional lack of HSL. In *A0* macrophages, HSL contributes to TG hydrolase activity, resulting in reduced but still substantial TG hydrolase activity. Since macrophages lacking both ATGL and HSL show 73% reduced TG hydrolase activity, we conclude that ATGL and HSL are the major cytoplasmic lipases required for TG hydrolysis in macrophages. Candidate enzymes, which are expressed in murine macrophages and might be responsible for the residual TG hydrolase activity in *A0H0* macrophages, are HL (155), LPL (156-158), and carboxylesterase (Ces)1d. (159) Lack of HL resulted in reduced atherosclerosis in ApoE- and lecithin:cholesterol acyltransferase-deficient mice. (160, 161) This enzyme, however, is only produced by macrophages present in aortic lesions (161) and might therefore only play a minor role as TG hydrolase in peritoneal macrophages. However, *A0H0* macrophages, although isolated from the peritoneum, mimic a foam cell-like phenotype due to a TG-rich LD accumulation which could lead to HL expression. Macrophage expression of LPL promotes foam cell formation and atherosclerosis *in vivo*. (156-158) Anyhow, both HL and LPL are extracellular lipases, which facilitate the entry of lipids into the cell by the hydrolysis of TG (and PLs) in circulating lipoproteins. Thus, these enzymes are unlikely responsible for mobilization of lipids stored in cytoplasmic LDs. Ces1d (previously called Ces3 or

TGH) is mainly expressed in adipose tissue, where it showed little TG hydrolase activity; (159) it is expressed in macrophages at low levels.

Especially during starvation, autophagy contributes to energy and building block supply. Thus, along with lipolysis, autophagy is one of two conserved responses to fasting. The role of autophagy in the breakdown of lipids in lipolytically active macrophages has not been investigated so far. Since lipolysis is markedly diminished in *A0H0* macrophages and these cells might have a fasting-like phenotype due to reduced intracellular FA concentrations, we hypothesized that autophagy might be induced. We observed a substantial amount of the autophagy marker LC3-II in macrophages from all genotypes, indicating that autophagy in macrophages is a consistently induced mechanism for degradation of intracellular material. Since the autophagosome is an intermediate structure in the dynamic pathway, the number of autophagosomes observed at any specific time point is the result of the balance between the rate of their generation and their conversion into autolysosomes. (162) For the determination of cellular autophagic activity the measurement of autophagic flux is more reliable although techniques for assessing autophagic flux are limited. (162) We used bafilomycin A1 as a potent and specific inhibitor of vacuolar H^+-ATPase, which prevents maturation of autophagic vacuoles by inhibiting fusion between autophagosomes and lysosomes. (163) As a result, LC3-II degradation is blocked and its accumulation can be monitored. (164) The differences in the amount of LC3-II between samples in the absence or presence of bafilomycin A1 represent the amount of LC3 that is degraded in lysosomes. (165-167) p62 also accumulates when autophagy is inhibited, and decreased levels can be observed when autophagy is induced. (162, 168, 169) Comparable with macrophages from all other genotypes, loss of both HSL and ATGL in macrophages resulted in increased protein expression of LC3-II after incubating the cells with bafilomycin A1, indicating an increased number of autophagosomes that cannot be degraded anymore. In analogy, p62 expression was also elevated in macrophages from all genotypes compared to untreated cells. Although not significantly different, the increase in p62 protein expression prior and after bafilomycin A1 treatment was more pronounced in Wt than A0H0 macrophages. Incubation with chloroquine, another inhibitor of autophagy, resulted in comparable p62 expression between Wt and *A0H0*

macrophages. Thus, our results indicate that autophagic flux is intact in macrophages with defective lipolysis. p62 does not accumulate in *A0H0* macrophages after treatment with bafilomycin A1 to the same extent as compared to Wt macrophages. A possible explanation might be the one given by Klionsky *et al.* (170) that a clear correlation between increases in LC3-II and decreases in p62 is sometimes missing. Thus, although analysis of p62 can assist in assessing the impairment of autophagy or autophagic flux, the authors recommend using p62 only in combination with other methods such as LC3-II turnover to monitor flux. In addition, Puissant *et al.* (171) highlight the controversies and misinterpretations of p62 expression as a marker of autophagic flux because p62 is subject to complex regulation at both the transcriptional and post-translational levels. We therefore used another independent method to measure lysosomal function in macrophages. Dequenching of DQ-BSA is used to monitor the fusion of endosomes and amphisomes with lysosomes, thereby serving as a measure of a functional lysosomal activity. (172) We observed increased amount of dequenched DQ-BSA in *A0H0* macrophages, providing evidence that deficiency of ATGL and HSL in macrophages is not associated with defective lysosomal activity. Together with increased mature cathepsin B expression, these findings rather demonstrate that *A0H0* macrophages have elevated lysosomal proteolytic activity.

Autophagy was previously shown to regulate hepatic lipid stores *in vivo*. (96) This previously unknown link between autophagy and lipid metabolism (termed lipophagy) was demonstrated by increased TG and DG concentrations *in vitro* and *in vivo,* and decreased TG breakdown in autophagy-inhibited conditions. Moreover, it has been shown that components of the autophagic pathway associate with LDs. (96) Ouimet *et al.* (151) have recently reported that autophagy also contributes to the intracellular breakdown of CE in macrophage-derived foam cells that have been loaded with modified LDL. Cytoplasmic LD-associated CEs delivered to lysosomes are degraded by LAL-dependent lipolysis, thereby generating FC for efflux to extracellular acceptors. Since acid CE hydrolase activity (resembling LAL activity) is comparable between lipase-deficient and Wt macrophages, CE accumulation does not occur, and "fatty lysosomes" as observed in *L0* macrophages (data not shown) are absent in macrophages from cytosolic lipase-deficient mice. Without changes in cytosolic CE content no

adaptive response by LAL might take place. Is degradation of cytosolic LDs by lipophagy an active mechanism for generating FAs as energy substrate in *A0H0* macrophages? Markedly reduced acid TG hydrolase activity in *A0* and *A0H0* macrophages argue against this hypothesis. Unaltered LAL protein content despite decreased TG hydrolase activity in *A0* and *A0H0* macrophages may imply a distinct regulation of TG and CE hydrolysis by LAL, suggesting a possible involvement of unknown co-activator(s). To assess whether inhibition of autophagy affects turnover of lipids stored in LDs we performed lipid flux experiments in the absence and presence of bafilomycin A1. Treatment with bafilomycin A1, however, failed to affect FA incorporation, metabolism, and release, indicating that inhibition of autophagy does not mediate turnover of LDs in macrophages. Even under conditions of defective lipolysis, inhibition of autophagy did not reduce lipid turnover, indicating that peritoneal macrophages do not rely on autophagic LD degradation.

The data provide conclusive evidence that ATGL-mediated TG breakdown is the crucial step of TG hydrolysis in macrophages. We demonstrate that loss of ATGL reaches a maximal TG accumulation capacity in macrophages, resulting in comparable intracellular TG levels between *A0* and *A0H0* macrophages. Increased cathepsin B abundance together with increased LC3-II and reduced p62 protein expression and increased dequenching of DQ-BSA suggest increased autophagic flux and lysosomal proteolysis in *A0H0* macrophages. In fact, we observed that starvation-induced autophagy did not decrease but rather increase intracellular TG content in macrophages. This is in consistence with a recent study of FA trafficking under nutrient deprivation in mouse embryonic fibroblasts. (173) The authors demonstrated that FAs generated by autophagy replenish intracellular LDs and that FAs have to be mobilized by intracellular lipases such as ATGL and HSL before being used for mitochondrial respiration. Results from this study together with our findings suggest that autophagy and lipolysis are not necessarily alternative but co-dependent mechanisms to fuel cellular metabolic needs. In *A0H0* macrophages, autophagy but not lipophagy might be triggered as a compensatory mechanism to degrade proteins and cell organelles to circumvent and balance the reduced availability of energy substrates.

8. References

1. Young, S.G., and Zechner, R., Biochemistry and pathophysiology of intravascular and intracellular lipolysis. Genes Dev, 2013. 27(5): p. 459-84.
2. Havel, R.J., Lipoprotein biosynthesis and metabolism. Ann N Y Acad Sci, 1980. 348: p. 16-29.
3. Brasaemle, D.L., Thematic review series: adipocyte biology. The perilipin family of structural lipid droplet proteins: stabilization of lipid droplets and control of lipolysis. J Lipid Res, 2007. 48(12): p. 2547-59.
4. Korn, E.D., Clearing factor, a heparin-activated lipoprotein lipase. II. Substrate specificity and activation of coconut oil. J Biol Chem, 1955. 215(1): p. 15-26.
5. Vaughan, M., Berger, J.E., and Steinberg, D., Hormone-Sensitive Lipase and Monoglyceride Lipase Activities in Adipose Tissue. J Biol Chem, 1964. 239: p. 401-9.
6. Kassan, A., Herms, A., Fernandez-Vidal, A., Bosch, M., Schieber, N.L., Reddy, B.J., Fajardo, A., Gelabert-Baldrich, M., Tebar, F., Enrich, C., et al., Acyl-CoA synthetase 3 promotes lipid droplet biogenesis in ER microdomains. J Cell Biol, 2013. 203(6): p. 985-1001.
7. Jenkins, C.M., Mancuso, D.J., Yan, W., Sims, H.F., Gibson, B., and Gross, R.W., Identification, cloning, expression, and purification of three novel human calcium-independent phospholipase A2 family members possessing triacylglycerol lipase and acylglycerol transacylase activities. J Biol Chem, 2004. 279(47): p. 48968-75.
8. Villena, J.A., Roy, S., Sarkadi-Nagy, E., Kim, K.H., and Sul, H.S., Desnutrin, an adipocyte gene encoding a novel patatin domain-containing protein, is induced by fasting and glucocorticoids: ectopic expression of desnutrin increases triglyceride hydrolysis. J Biol Chem, 2004. 279(45): p. 47066-75.
9. Zimmermann, R., Strauss, J.G., Haemmerle, G., Schoiswohl, G., Birner-Gruenberger, R., Riederer, M., Lass, A., Neuberger, G., Eisenhaber, F., Hermetter, A., et al., Fat mobilization in adipose tissue is promoted by adipose triglyceride lipase. Science, 2004. 306(5700): p. 1383-6.
10. Osuga, J., Ishibashi, S., Oka, T., Yagyu, H., Tozawa, R., Fujimoto, A., Shionoiri, F., Yahagi, N., Kraemer, F.B., Tsutsumi, O., et al., Targeted disruption of hormone-sensitive lipase results in male sterility and adipocyte hypertrophy, but not in obesity. Proc Natl Acad Sci U S A, 2000. 97(2): p. 787-92.
11. Schweiger, M., Eichmann, T.O., Taschler, U., Zimmermann, R., Zechner, R., and Lass, A., Measurement of lipolysis. Methods Enzymol, 2014. 538: p. 171-93.
12. Holm, C., Molecular mechanisms regulating hormone-sensitive lipase and lipolysis. Biochem Soc Trans, 2003. 31(Pt 6): p. 1120-4.
13. Zimmermann, R., Haemmerle, G., Wagner, E.M., Strauss, J.G., Kratky, D., and Zechner, R., Decreased fatty acid esterification compensates for the reduced lipolytic activity in hormone-sensitive lipase-deficient white adipose tissue. J Lipid Res, 2003. 44(11): p. 2089-99.
14. Buchebner, M., Pfeifer, T., Rathke, N., Chandak, P.G., Lass, A., Schreiber, R., Kratzer, A., Zimmermann, R., Sattler, W., Koefeler, H., et al., Cholesteryl ester hydrolase activity is abolished in HSL-/- macrophages but

unchanged in macrophages lacking KIAA1363. J Lipid Res, 2010. 51(10): p. 2896-908.
15. Escary, J.L., Choy, H.A., Reue, K., and Schotz, M.C., Hormone-sensitive lipase overexpression increases cholesteryl ester hydrolysis in macrophage foam cells. Arterioscler Thromb Vasc Biol, 1998. 18(6): p. 991-8.
16. Haemmerle, G., Zimmermann, R., Hayn, M., Theussl, C., Waeg, G., Wagner, E., Sattler, W., Magin, T.M., Wagner, E.F., and Zechner, R., Hormone-sensitive lipase deficiency in mice causes diglyceride accumulation in adipose tissue, muscle, and testis. J Biol Chem, 2002. 277(7): p. 4806-15.
17. Sekiya, M., Osuga, J., Nagashima, S., Ohshiro, T., Igarashi, M., Okazaki, H., Takahashi, M., Tazoe, F., Wada, T., Ohta, K., et al., Ablation of neutral cholesterol ester hydrolase 1 accelerates atherosclerosis. Cell Metab, 2009. 10(3): p. 219-28.
18. Lass, A., Zimmermann, R., Haemmerle, G., Riederer, M., Schoiswohl, G., Schweiger, M., Kienesberger, P., Strauss, J.G., Gorkiewicz, G., and Zechner, R., Adipose triglyceride lipase-mediated lipolysis of cellular fat stores is activated by CGI-58 and defective in Chanarin-Dorfman Syndrome. Cell Metab, 2006. 3(5): p. 309-19.
19. Eichmann, T.O., Kumari, M., Haas, J.T., Farese, R.V., Jr., Zimmermann, R., Lass, A., and Zechner, R., Studies on the substrate and stereo/regioselectivity of adipose triglyceride lipase, hormone-sensitive lipase, and diacylglycerol-O-acyltransferases. J Biol Chem, 2012. 287(49): p. 41446-57.
20. Gruber, A., Cornaciu, I., Lass, A., Schweiger, M., Poeschl, M., Eder, C., Kumari, M., Schoiswohl, G., Wolinski, H., Kohlwein, S.D., et al., The N-terminal region of comparative gene identification-58 (CGI-58) is important for lipid droplet binding and activation of adipose triglyceride lipase. J Biol Chem, 2010. 285(16): p. 12289-98.
21. Granneman, J.G., Moore, H.P., Granneman, R.L., Greenberg, A.S., Obin, M.S., and Zhu, Z., Analysis of lipolytic protein trafficking and interactions in adipocytes. J Biol Chem, 2007. 282(8): p. 5726-35.
22. Granneman, J.G., Moore, H.P., Krishnamoorthy, R., and Rathod, M., Perilipin controls lipolysis by regulating the interactions of AB-hydrolase containing 5 (Abhd5) and adipose triglyceride lipase (Atgl). J Biol Chem, 2009. 284(50): p. 34538-44.
23. Gandotra, S., Le Dour, C., Bottomley, W., Cervera, P., Giral, P., Reznik, Y., Charpentier, G., Auclair, M., Delepine, M., Barroso, I., et al., Perilipin deficiency and autosomal dominant partial lipodystrophy. N Engl J Med, 2011. 364(8): p. 740-8.
24. Haemmerle, G., Lass, A., Zimmermann, R., Gorkiewicz, G., Meyer, C., Rozman, J., Heldmaier, G., Maier, R., Theussl, C., Eder, S., et al., Defective lipolysis and altered energy metabolism in mice lacking adipose triglyceride lipase. Science, 2006. 312(5774): p. 734-7.
25. Haemmerle, G., Moustafa, T., Woelkart, G., Buttner, S., Schmidt, A., van de Weijer, T., Hesselink, M., Jaeger, D., Kienesberger, P.C., Zierler, K., et al., ATGL-mediated fat catabolism regulates cardiac mitochondrial function via PPAR-alpha and PGC-1. Nat Med, 2011. 17(9): p. 1076-85.
26. Lammers, B., Chandak, P.G., Aflaki, E., Van Puijvelde, G.H., Radovic, B., Hildebrand, R.B., Meurs, I., Out, R., Kuiper, J., Van Berkel, T.J., et al.,

Macrophage adipose triglyceride lipase deficiency attenuates atherosclerotic lesion development in low-density lipoprotein receptor knockout mice. Arterioscler Thromb Vasc Biol, 2011. 31(1): p. 67-73.
27. Aflaki, E., Balenga, N.A., Luschnig-Schratl, P., Wolinski, H., Povoden, S., Chandak, P.G., Bogner-Strauss, J.G., Eder, S., Konya, V., Kohlwein, S.D., et al., Impaired Rho GTPase activation abrogates cell polarization and migration in macrophages with defective lipolysis. Cell Mol Life Sci, 2011. 68(23): p. 3933-47.
28. Aflaki, E., Radovic, B., Chandak, P.G., Kolb, D., Eisenberg, T., Ring, J., Fertschai, I., Uellen, A., Wolinski, H., Kohlwein, S.D., et al., Triacylglycerol accumulation activates the mitochondrial apoptosis pathway in macrophages. J Biol Chem, 2011. 286(9): p. 7418-28.
29. Chandak, P.G., Radovic, B., Aflaki, E., Kolb, D., Buchebner, M., Frohlich, E., Magnes, C., Sinner, F., Haemmerle, G., Zechner, R., et al., Efficient phagocytosis requires triacylglycerol hydrolysis by adipose triglyceride lipase. J Biol Chem, 2010. 285(26): p. 20192-201.
30. Aflaki, E., Doddapattar, P., Radovic, B., Povoden, S., Kolb, D., Vujic, N., Wegscheider, M., Koefeler, H., Hornemann, T., Graier, W.F., et al., C16 ceramide is crucial for triacylglycerol-induced apoptosis in macrophages. Cell Death Dis, 2012. 3: p. e280.
31. Radovic, B., Aflaki, E., and Kratky, D., Adipose triglyceride lipase in immune response, inflammation, and atherosclerosis. Biol Chem, 2012. 393(9): p. 1005-11.
32. Lass, A., Zimmermann, R., Oberer, M., and Zechner, R., Lipolysis - a highly regulated multi-enzyme complex mediates the catabolism of cellular fat stores. Prog Lipid Res, 2011. 50(1): p. 14-27.
33. Oberer, M., Boeszoermenyi, A., Nagy, H.M., and Zechner, R., Recent insights into the structure and function of comparative gene identification-58. Curr Opin Lipidol, 2011. 22(3): p. 149-58.
34. Ghosh, A.K., Ramakrishnan, G., Chandramohan, C., and Rajasekharan, R., CGI-58, the causative gene for Chanarin-Dorfman syndrome, mediates acylation of lysophosphatidic acid. J Biol Chem, 2008. 283(36): p. 24525-33.
35. Montero-Moran, G., Caviglia, J.M., McMahon, D., Rothenberg, A., Subramanian, V., Xu, Z., Lara-Gonzalez, S., Storch, J., Carman, G.M., and Brasaemle, D.L., CGI-58/ABHD5 is a coenzyme A-dependent lysophosphatidic acid acyltransferase. J Lipid Res, 2010. 51(4): p. 709-19.
36. McMahon, D., Dinh, A., Kurz, D., Shah, D., Han, G.S., Carman, G.M., and Brasaemle, D.L., Comparative gene identification 58/alpha/beta hydrolase domain 5 lacks lysophosphatidic acid acyltransferase activity. J Lipid Res, 2014. 55(8): p. 1750-1761.
37. Radner, F.P., Streith, I.E., Schoiswohl, G., Schweiger, M., Kumari, M., Eichmann, T.O., Rechberger, G., Koefeler, H.C., Eder, S., Schauer, S., et al., Growth retardation, impaired triacylglycerol catabolism, hepatic steatosis, and lethal skin barrier defect in mice lacking comparative gene identification-58 (CGI-58). J Biol Chem, 2010. 285(10): p. 7300-11.
38. Brown, J.M., Betters, J.L., Lord, C., Ma, Y., Han, X., Yang, K., Alger, H.M., Melchior, J., Sawyer, J., Shah, R., et al., CGI-58 knockdown in mice causes hepatic steatosis but prevents diet-induced obesity and glucose intolerance. J Lipid Res, 2010. 51(11): p. 3306-15.

39. Lord, C.C., and Brown, J.M., Distinct roles for alpha-beta hydrolase domain 5 (ABHD5/CGI-58) and adipose triglyceride lipase (ATGL/PNPLA2) in lipid metabolism and signaling. Adipocyte, 2012. 1(3): p. 123-131.
40. Zierler, K.A., Zechner, R., and Haemmerle, G., Comparative gene identification-58/alpha/beta hydrolase domain 5: more than just an adipose triglyceride lipase activator? Curr Opin Lipidol, 2014. 25(2): p. 102-9.
41. Caviglia, J.M., Betters, J.L., Dapito, D.H., Lord, C.C., Sullivan, S., Chua, S., Yin, T., Sekowski, A., Mu, H., Shapiro, L., et al., Adipose-selective overexpression of ABHD5/CGI-58 does not increase lipolysis or protect against diet-induced obesity. J Lipid Res, 2011. 52(11): p. 2032-42.
42. Zierler, K.A., Jaeger, D., Pollak, N.M., Eder, S., Rechberger, G.N., Radner, F.P., Woelkart, G., Kolb, D., Schmidt, A., Kumari, M., et al., Functional cardiac lipolysis in mice critically depends on comparative gene identification-58. J Biol Chem, 2013. 288(14): p. 9892-904.
43. Badin, P.M., Loubiere, C., Coonen, M., Louche, K., Tavernier, G., Bourlier, V., Mairal, A., Rustan, A.C., Smith, S.R., Langin, D., et al., Regulation of skeletal muscle lipolysis and oxidative metabolism by the co-lipase CGI-58. J Lipid Res, 2012. 53(5): p. 839-48.
44. Xie, P., Kadegowda, A.K., Ma, Y., Guo, F., Han, X., Wang, M., Groban, L., Xue, B., Shi, H., Li, H., et al., Muscle-specific deletion of comparative gene identification-58 (CGI-58) causes muscle steatosis but improves insulin sensitivity in male mice. Endocrinology, 2015. 156(5): p. 1648-58.
45. Brown, J.M., Chung, S., Das, A., Shelness, G.S., Rudel, L.L., and Yu, L., CGI-58 facilitates the mobilization of cytoplasmic triglyceride for lipoprotein secretion in hepatoma cells. J Lipid Res, 2007. 48(10): p. 2295-305.
46. Caviglia, J.M., Sparks, J.D., Toraskar, N., Brinker, A.M., Yin, T.C., Dixon, J.L., and Brasaemle, D.L., ABHD5/CGI-58 facilitates the assembly and secretion of apolipoprotein B lipoproteins by McA RH7777 rat hepatoma cells. Biochim Biophys Acta, 2009. 1791(3): p. 198-205.
47. Guo, F., Ma, Y., Kadegowda, A.K., Betters, J.L., Xie, P., Liu, G., Liu, X., Miao, H., Ou, J., Su, X., et al., Deficiency of liver Comparative Gene Identification-58 causes steatohepatitis and fibrosis in mice. J Lipid Res, 2013. 54(8): p. 2109-20.
48. Lord, C.C., Betters, J.L., Ivanova, P.T., Milne, S.B., Myers, D.S., Madenspacher, J., Thomas, G., Chung, S., Liu, M., Davis, M.A., et al., CGI-58/ABHD5-derived signaling lipids regulate systemic inflammation and insulin action. Diabetes, 2012. 61(2): p. 355-63.
49. Cantley, J.L., Yoshimura, T., Camporez, J.P., Zhang, D., Jornayvaz, F.R., Kumashiro, N., Guebre-Egziabher, F., Jurczak, M.J., Kahn, M., Guigni, B.A., et al., CGI-58 knockdown sequesters diacylglycerols in lipid droplets/ER-preventing diacylglycerol-mediated hepatic insulin resistance. Proc Natl Acad Sci U S A, 2013. 110(5): p. 1869-74.
50. Xie, P., Guo, F., Ma, Y., Zhu, H., Wang, F., Xue, B., Shi, H., Yang, J., and Yu, L., Intestinal Cgi-58 deficiency reduces postprandial lipid absorption. PLoS One, 2014. 9(3): p. e91652.
51. Akiyama, M., Sakai, K., Takayama, C., Yanagi, T., Yamanaka, Y., McMillan, J.R., and Shimizu, H., CGI-58 is an alpha/beta-hydrolase within lipid transporting lamellar granules of differentiated keratinocytes. Am J Pathol, 2008. 173(5): p. 1349-60.

52. Uchida, Y., Cho, Y., Moradian, S., Kim, J., Nakajima, K., Crumrine, D., Park, K., Ujihara, M., Akiyama, M., Shimizu, H., et al., Neutral lipid storage leads to acylceramide deficiency, likely contributing to the pathogenesis of Dorfman-Chanarin syndrome. J Invest Dermatol, 2010. 130(10): p. 2497-9.
53. Radner, F.P., and Fischer, J., The important role of epidermal triacylglycerol metabolism for maintenance of the skin permeability barrier function. Biochim Biophys Acta, 2014. 1841(3): p. 409-15.
54. Ou, J., Miao, H., Ma, Y., Guo, F., Deng, J., Wei, X., Zhou, J., Xie, G., Shi, H., Xue, B., et al., Loss of abhd5 promotes colorectal tumor development and progression by inducing aerobic glycolysis and epithelial-mesenchymal transition. Cell Rep, 2014. 9(5): p. 1798-811.
55. Miao, H., Ou, J., Ma, Y., Guo, F., Yang, Z., Wiggins, M., Liu, C., Song, W., Han, X., Wang, M., et al., Macrophage CGI-58 deficiency activates ROS-inflammasome pathway to promote insulin resistance in mice. Cell Rep, 2014. 7(1): p. 223-35.
56. Miao, H., Ou, J., Zhang, X., Chen, Y., Xue, B., Shi, H., Gan, L., Yu, L., and Liang, H., Macrophage CGI-58 deficiency promotes IL-1beta transcription by activating the SOCS3-FOXO1 pathway. Clin Sci (Lond), 2015. 128(8): p. 493-506.
57. Xie, P., Zeng, X., Xiao, J., Sun, B., and Yang, D., Transgenic CGI-58 expression in macrophages alleviates the atherosclerotic lesion development in ApoE knockout mice. Biochim Biophys Acta, 2014. 1841(12): p. 1683-90.
58. Subramanian, V., Rothenberg, A., Gomez, C., Cohen, A.W., Garcia, A., Bhattacharyya, S., Shapiro, L., Dolios, G., Wang, R., Lisanti, M.P., et al., Perilipin A mediates the reversible binding of CGI-58 to lipid droplets in 3T3-L1 adipocytes. J Biol Chem, 2004. 279(40): p. 42062-71.
59. Schweiger, M., Schreiber, R., Haemmerle, G., Lass, A., Fledelius, C., Jacobsen, P., Tornqvist, H., Zechner, R., and Zimmermann, R., Adipose triglyceride lipase and hormone-sensitive lipase are the major enzymes in adipose tissue triacylglycerol catabolism. J Biol Chem, 2006. 281(52): p. 40236-41.
60. Sahu-Osen, A., Montero-Moran, G., Schittmayer, M., Fritz, K., Dinh, A., Chang, Y.F., McMahon, D., Boeszoermenyi, A., Cornaciu, I., Russell, D., et al., CGI-58/ABHD5 is phosphorylated on Ser239 by protein kinase A: control of subcellular localization. J Lipid Res, 2015. 56(1): p. 109-21.
61. Lu, X., Yang, X., and Liu, J., Differential control of ATGL-mediated lipid droplet degradation by CGI-58 and G0S2. Cell Cycle, 2010. 9(14): p. 2719-25.
62. Hofer, P., Boeszoermenyi, A., Jaeger, D., Feiler, U., Arthanari, H., Mayer, N., Zehender, F., Rechberger, G., Oberer, M., Zimmermann, R., et al., Fatty acid-binding proteins interact with comparative gene identification-58 linking lipolysis with lipid ligand shuttling. J Biol Chem, 2015.
63. Walther, T.C., and Farese, R.V., Jr., Lipid droplets and cellular lipid metabolism. Annu Rev Biochem, 2012. 81: p. 687-714.
64. Bickel, P.E., Tansey, J.T., and Welte, M.A., PAT proteins, an ancient family of lipid droplet proteins that regulate cellular lipid stores. Biochim Biophys Acta, 2009. 1791(6): p. 419-40.

65. Yen, C.L., Stone, S.J., Koliwad, S., Harris, C., and Farese, R.V., Jr., Thematic review series: glycerolipids. DGAT enzymes and triacylglycerol biosynthesis. J Lipid Res, 2008. 49(11): p. 2283-301.
66. Zechner, R., Zimmermann, R., Eichmann, T.O., Kohlwein, S.D., Haemmerle, G., Lass, A., and Madeo, F., FAT SIGNALS--lipases and lipolysis in lipid metabolism and signaling. Cell Metab, 2012. 15(3): p. 279-91.
67. Greenberg, A.S., Coleman, R.A., Kraemer, F.B., McManaman, J.L., Obin, M.S., Puri, V., Yan, Q.W., Miyoshi, H., and Mashek, D.G., The role of lipid droplets in metabolic disease in rodents and humans. J Clin Invest, 2011. 121(6): p. 2102-10.
68. Cohen, J.C., Horton, J.D., and Hobbs, H.H., Human fatty liver disease: old questions and new insights. Science, 2011. 332(6037): p. 1519-23.
69. Welte, M.A., Expanding Roles for Lipid Droplets. Curr Biol, 2015. 25(11): p. R470-R481.
70. Anand, A.N., and Lorenz, M.W., Age-dependent changes of fat body stores and the regulation of fat body lipid synthesis and mobilisation by adipokinetic hormone in the last larval instar of the cricket, Gryllus bimaculatus. J Insect Physiol, 2008. 54(10-11): p. 1404-12.
71. Zimmermann, R., Lass, A., Haemmerle, G., and Zechner, R., Fate of fat: the role of adipose triglyceride lipase in lipolysis. Biochim Biophys Acta, 2009. 1791(6): p. 494-500.
72. Schweiger, M., Lass, A., Zimmermann, R., Eichmann, T.O., and Zechner, R., Neutral lipid storage disease: genetic disorders caused by mutations in adipose triglyceride lipase/PNPLA2 or CGI-58/ABHD5. Am J Physiol Endocrinol Metab, 2009. 297(2): p. E289-96.
73. Jordans, G.H., The familial occurrence of fat containing vacuoles in the leukocytes diagnosed in two brothers suffering from dystrophia musculorum progressiva (ERB.). Acta Med Scand, 1953. 145(6): p. 419-23.
74. Lefevre, C., Jobard, F., Caux, F., Bouadjar, B., Karaduman, A., Heilig, R., Lakhdar, H., Wollenberg, A., Verret, J.L., Weissenbach, J., et al., Mutations in CGI-58, the gene encoding a new protein of the esterase/lipase/thioesterase subfamily, in Chanarin-Dorfman syndrome. Am J Hum Genet, 2001. 69(5): p. 1002-12.
75. Voeltz, G.K., Rolls, M.M., and Rapoport, T.A., Structural organization of the endoplasmic reticulum. EMBO Rep, 2002. 3(10): p. 944-50.
76. Berridge, M.J., The endoplasmic reticulum: a multifunctional signaling organelle. Cell Calcium, 2002. 32(5-6): p. 235-49.
77. Braakman, I., and Bulleid, N.J., Protein folding and modification in the mammalian endoplasmic reticulum. Annu Rev Biochem, 2011. 80: p. 71-99.
78. Fagone, P., and Jackowski, S., Membrane phospholipid synthesis and endoplasmic reticulum function. J Lipid Res, 2009. 50 Suppl: p. S311-6.
79. Hetz, C.A., and Soto, C., Stressing out the ER: a role of the unfolded protein response in prion-related disorders. Curr Mol Med, 2006. 6(1): p. 37-43.
80. Fedoroff, N., Redox regulatory mechanisms in cellular stress responses. Ann Bot, 2006. 98(2): p. 289-300.
81. Feldman, D.E., Chauhan, V., and Koong, A.C., The unfolded protein response: a novel component of the hypoxic stress response in tumors. Mol Cancer Res, 2005. 3(11): p. 597-605.

82. Fonseca, S.G., Gromada, J., and Urano, F., Endoplasmic reticulum stress and pancreatic beta-cell death. Trends Endocrinol Metab, 2011. 22(7): p. 266-74.
83. Gorlach, A., Klappa, P., and Kietzmann, T., The endoplasmic reticulum: folding, calcium homeostasis, signaling, and redox control. Antioxid Redox Signal, 2006. 8(9-10): p. 1391-418.
84. He, B., Viruses, endoplasmic reticulum stress, and interferon responses. Cell Death Differ, 2006. 13(3): p. 393-403.
85. Chaudhari, N., Talwar, P., Parimisetty, A., Lefebvre d'Hellencourt, C., and Ravanan, P., A molecular web: endoplasmic reticulum stress, inflammation, and oxidative stress. Front Cell Neurosci, 2014. 8: p. 213.
86. Dicks, N., Gutierrez, K., Michalak, M., Bordignon, V., and Agellon, L.B., Endoplasmic reticulum stress, genome damage, and cancer. Front Oncol, 2015. 5: p. 11.
87. Cannon, G.J., and Swanson, J.A., The macrophage capacity for phagocytosis. J Cell Sci, 1992. 101 (Pt 4): p. 907-13.
88. Schumann, J., It is all about fluidity: Fatty acids and macrophage phagocytosis. Eur J Pharmacol, 2015.
89. Underhill, D.M., and Goodridge, H.S., Information processing during phagocytosis. Nat Rev Immunol, 2012. 12(7): p. 492-502.
90. Bosedasgupta, S., and Pieters, J., Inflammatory stimuli reprogram macrophage phagocytosis to macropinocytosis for the rapid elimination of pathogens. PLoS Pathog, 2014. 10(1): p. e1003879.
91. Martin, C.J., Peters, K.N., and Behar, S.M., Macrophages clean up: efferocytosis and microbial control. Curr Opin Microbiol, 2014. 17: p. 17-23.
92. Zhang, J., Autophagy and Mitophagy in Cellular Damage Control. Redox Biol, 2013. 1(1): p. 19-23.
93. Vural, A., and Kehrl, J.H., Autophagy in macrophages: impacting inflammation and bacterial infection. Scientifica (Cairo), 2014. 2014: p. 825463.
94. Kabeya, Y., Mizushima, N., Ueno, T., Yamamoto, A., Kirisako, T., Noda, T., Kominami, E., Ohsumi, Y., and Yoshimori, T., LC3, a mammalian homologue of yeast Apg8p, is localized in autophagosome membranes after processing. EMBO J, 2000. 19(21): p. 5720-8.
95. Tanida, I., and Waguri, S., Measurement of autophagy in cells and tissues. Methods Mol Biol, 2010. 648: p. 193-214.
96. Singh, R., Kaushik, S., Wang, Y., Xiang, Y., Novak, I., Komatsu, M., Tanaka, K., Cuervo, A.M., and Czaja, M.J., Autophagy regulates lipid metabolism. Nature, 2009. 458(7242): p. 1131-5.
97. Liu, K., and Czaja, M.J., Regulation of lipid stores and metabolism by lipophagy. Cell Death Differ, 2013. 20(1): p. 3-11.
98. Pearson, G.L., Mellett, N., Chu, K.Y., Cantley, J., Davenport, A., Bourbon, P., Cosner, C.C., Helquist, P., Meikle, P.J., and Biden, T.J., Lysosomal acid lipase and lipophagy are constitutive negative regulators of glucose-stimulated insulin secretion from pancreatic beta cells. Diabetologia, 2014. 57(1): p. 129-39.
99. Ilhan, F., and Kalkanli, S.T., Atherosclerosis and the role of immune cells. World J Clin Cases, 2015. 3(4): p. 345-52.

100. Libby, P., Ridker, P.M., and Hansson, G.K., Progress and challenges in translating the biology of atherosclerosis. Nature, 2011. 473(7347): p. 317-25.
101. Rader, D.J., and Daugherty, A., Translating molecular discoveries into new therapies for atherosclerosis. Nature, 2008. 451(7181): p. 904-13.
102. McLaren, J.E., Michael, D.R., Ashlin, T.G., and Ramji, D.P., Cytokines, macrophage lipid metabolism and foam cells: implications for cardiovascular disease therapy. Prog Lipid Res, 2011. 50(4): p. 331-47.
103. Tomkin, G.H., and Owens, D., The chylomicron: relationship to atherosclerosis. Int J Vasc Med, 2012. 2012: p. 784536.
104. Lagace, T.A., PCSK9 and LDLR degradation: regulatory mechanisms in circulation and in cells. Curr Opin Lipidol, 2014. 25(5): p. 387-93.
105. Ono, K., Current concept of reverse cholesterol transport and novel strategy for atheroprotection. J Cardiol, 2012. 60(5): p. 339-43.
106. Buckley, M.L., and Ramji, D.P., The influence of dysfunctional signaling and lipid homeostasis in mediating the inflammatory responses during atherosclerosis. Biochim Biophys Acta, 2015. 1852(7): p. 1498-1510.
107. Hoefer, I.E., Steffens, S., Ala-Korpela, M., Back, M., Badimon, L., Bochaton-Piallat, M.L., Boulanger, C.M., Caligiuri, G., Dimmeler, S., Egido, J., et al., Novel methodologies for biomarker discovery in atherosclerosis. Eur Heart J, 2015.
108. O'Neill, F., Riwanto, M., Charakida, M., Colin, S., Manz, J., McLoughlin, E., Khan, T., Klein, N., Kay, C.W., Patel, K., et al., Structural and functional changes in HDL with low grade and chronic inflammation. Int J Cardiol, 2015. 188: p. 111-6.
109. Bryan, M.T., Duckles, H., Feng, S., Hsiao, S.T., Kim, H.R., Serbanovic-Canic, J., and Evans, P.C., Mechanoresponsive networks controlling vascular inflammation. Arterioscler Thromb Vasc Biol, 2014. 34(10): p. 2199-205.
110. Tousoulis, D., Simopoulou, C., Papageorgiou, N., Oikonomou, E., Hatzis, G., Siasos, G., Tsiamis, E., and Stefanadis, C., Endothelial dysfunction in conduit arteries and in microcirculation. Novel therapeutic approaches. Pharmacol Ther, 2014. 144(3): p. 253-67.
111. Koenen, R.R., and Weber, C., Therapeutic targeting of chemokine interactions in atherosclerosis. Nat Rev Drug Discov, 2010. 9(2): p. 141-53.
112. Weber, C., and Noels, H., Atherosclerosis: current pathogenesis and therapeutic options. Nat Med, 2011. 17(11): p. 1410-22.
113. Zernecke, A., and Weber, C., Chemokines in atherosclerosis: proceedings resumed. Arterioscler Thromb Vasc Biol, 2014. 34(4): p. 742-50.
114. Moore, K.J., Sheedy, F.J., and Fisher, E.A., Macrophages in atherosclerosis: a dynamic balance. Nat Rev Immunol, 2013. 13(10): p. 709-21.
115. Tabas, I., Macrophage death and defective inflammation resolution in atherosclerosis. Nat Rev Immunol, 2010. 10(1): p. 36-46.
116. Witztum, J.L., and Lichtman, A.H., The influence of innate and adaptive immune responses on atherosclerosis. Annu Rev Pathol, 2014. 9: p. 73-102.
117. Silvestre-Roig, C., de Winther, M.P., Weber, C., Daemen, M.J., Lutgens, E., and Soehnlein, O., Atherosclerotic plaque destabilization: mechanisms, models, and therapeutic strategies. Circ Res, 2014. 114(1): p. 214-26.

118. Moore, K.J., and Tabas, I., Macrophages in the pathogenesis of atherosclerosis. Cell, 2011. 145(3): p. 341-55.
119. Lusis, A.J., Atherosclerosis. Nature, 2000. 407(6801): p. 233-41.
120. Libby, P., Inflammation in atherosclerosis. Nature, 2002. 420(6917): p. 868-74.
121. Libby, P., Aikawa, M., and Schonbeck, U., Cholesterol and atherosclerosis. Biochim Biophys Acta, 2000. 1529(1-3): p. 299-309.
122. Tabas, I., Consequences and therapeutic implications of macrophage apoptosis in atherosclerosis: the importance of lesion stage and phagocytic efficiency. Arterioscler Thromb Vasc Biol, 2005. 25(11): p. 2255-64.
123. Heine, G.H., Ortiz, A., Massy, Z.A., Lindholm, B., Wiecek, A., Martinez-Castelao, A., Covic, A., Goldsmith, D., Suleymanlar, G., London, G.M., et al., Monocyte subpopulations and cardiovascular risk in chronic kidney disease. Nat Rev Nephrol, 2012. 8(6): p. 362-9.
124. Chinetti-Gbaguidi, G., Colin, S., and Staels, B., Macrophage subsets in atherosclerosis. Nat Rev Cardiol, 2015. 12(1): p. 10-7.
125. Verreck, F.A., de Boer, T., Langenberg, D.M., Hoeve, M.A., Kramer, M., Vaisberg, E., Kastelein, R., Kolk, A., de Waal-Malefyt, R., and Ottenhoff, T.H., Human IL-23-producing type 1 macrophages promote but IL-10-producing type 2 macrophages subvert immunity to (myco)bacteria. Proc Natl Acad Sci U S A, 2004. 101(13): p. 4560-5.
126. Mosser, D.M., The many faces of macrophage activation. J Leukoc Biol, 2003. 73(2): p. 209-12.
127. Murray, P.J., and Wynn, T.A., Protective and pathogenic functions of macrophage subsets. Nat Rev Immunol, 2011. 11(11): p. 723-37.
128. Gordon, S., Alternative activation of macrophages. Nat Rev Immunol, 2003. 3(1): p. 23-35.
129. Mantovani, A., Sica, A., Sozzani, S., Allavena, P., Vecchi, A., and Locati, M., The chemokine system in diverse forms of macrophage activation and polarization. Trends Immunol, 2004. 25(12): p. 677-86.
130. Martinez, F.O., Gordon, S., Locati, M., and Mantovani, A., Transcriptional profiling of the human monocyte-to-macrophage differentiation and polarization: new molecules and patterns of gene expression. J Immunol, 2006. 177(10): p. 7303-11.
131. Anderson, C.F., Gerber, J.S., and Mosser, D.M., Modulating macrophage function with IgG immune complexes. J Endotoxin Res, 2002. 8(6): p. 477-81.
132. Finn, A.V., Nakano, M., Polavarapu, R., Karmali, V., Saeed, O., Zhao, X., Yazdani, S., Otsuka, F., Davis, T., Habib, A., et al., Hemoglobin directs macrophage differentiation and prevents foam cell formation in human atherosclerotic plaques. J Am Coll Cardiol, 2012. 59(2): p. 166-77.
133. Boyle, J.J., Johns, M., Kampfer, T., Nguyen, A.T., Game, L., Schaer, D.J., Mason, J.C., and Haskard, D.O., Activating transcription factor 1 directs Mhem atheroprotective macrophages through coordinated iron handling and foam cell protection. Circ Res, 2012. 110(1): p. 20-33.
134. Kadl, A., Meher, A.K., Sharma, P.R., Lee, M.Y., Doran, A.C., Johnstone, S.R., Elliott, M.R., Gruber, F., Han, J., Chen, W., et al., Identification of a novel macrophage phenotype that develops in response to atherogenic phospholipids via Nrf2. Circ Res, 2010. 107(6): p. 737-46.

135. Erbel, C., Tyka, M., Helmes, C.M., Akhavanpoor, M., Rupp, G., Domschke, G., Linden, F., Wolf, A., Doesch, A., Lasitschka, F., et al., CXCL4-induced plaque macrophages can be specifically identified by co-expression of MMP7+S100A8+ in vitro and in vivo. Innate Immun, 2015. 21(3): p. 255-65.
136. Porcheray, F., Viaud, S., Rimaniol, A.C., Leone, C., Samah, B., Dereuddre-Bosquet, N., Dormont, D., and Gras, G., Macrophage activation switching: an asset for the resolution of inflammation. Clin Exp Immunol, 2005. 142(3): p. 481-9.
137. Lee, S., Huen, S., Nishio, H., Nishio, S., Lee, H.K., Choi, B.S., Ruhrberg, C., and Cantley, L.G., Distinct macrophage phenotypes contribute to kidney injury and repair. J Am Soc Nephrol, 2011. 22(2): p. 317-26.
138. Gleissner, C.A., Shaked, I., Little, K.M., and Ley, K., CXC chemokine ligand 4 induces a unique transcriptome in monocyte-derived macrophages. J Immunol, 2010. 184(9): p. 4810-8.
139. Knowles, J.W., and Maeda, N., Genetic modifiers of atherosclerosis in mice. Arterioscler Thromb Vasc Biol, 2000. 20(11): p. 2336-45.
140. Zadelaar, S., Kleemann, R., Verschuren, L., de Vries-Van der Weij, J., van der Hoorn, J., Princen, H.M., and Kooistra, T., Mouse models for atherosclerosis and pharmaceutical modifiers. Arterioscler Thromb Vasc Biol, 2007. 27(8): p. 1706-21.
141. Davignon, J., Apolipoprotein E and atherosclerosis: beyond lipid effect. Arterioscler Thromb Vasc Biol, 2005. 25(2): p. 267-9.
142. Tenger, C., and Zhou, X., Apolipoprotein E modulates immune activation by acting on the antigen-presenting cell. Immunology, 2003. 109(3): p. 392-7.
143. Clausen, B.E., Burkhardt, C., Reith, W., Renkawitz, R., and Forster, I., Conditional gene targeting in macrophages and granulocytes using LysMcre mice. Transgenic Res, 1999. 8(4): p. 265-77.
144. Brown, J.M., Chung, S., Sawyer, J.K., Degirolamo, C., Alger, H.M., Nguyen, T., Zhu, X., Duong, M.N., Wibley, A.L., Shah, R., et al., Inhibition of stearoyl-coenzyme A desaturase 1 dissociates insulin resistance and obesity from atherosclerosis. Circulation, 2008. 118(14): p. 1467-75.
145. Sattler, W., Puhl, H., Hayn, M., Kostner, G.M., and Esterbauer, H., Determination of fatty acids in the main lipoprotein classes by capillary gas chromatography: BF3/methanol transesterification of lyophilized samples instead of Folch extraction gives higher yields. Anal Biochem, 1991. 198(1): p. 184-90.
146. Mayer, N., Schweiger, M., Romauch, M., Grabner, G.F., Eichmann, T.O., Fuchs, E., Ivkovic, J., Heier, C., Mrak, I., Lass, A., et al., Development of small-molecule inhibitors targeting adipose triglyceride lipase. Nat Chem Biol, 2013. 9(12): p. 785-7.
147. Pfaffl, M.W., Horgan, G.W., and Dempfle, L., Relative expression software tool (REST) for group-wise comparison and statistical analysis of relative expression results in real-time PCR. Nucleic Acids Res, 2002. 30(9): p. e36.
148. Livak, K.J., and Schmittgen, T.D., Analysis of relative gene expression data using real-time quantitative PCR and the 2(-Delta Delta C(T)) Method. Methods, 2001. 25(4): p. 402-8.
149. Bolte, S., and Cordelieres, F.P., A guided tour into subcellular colocalization analysis in light microscopy. J Microsc, 2006. 224(Pt 3): p. 213-32.

150. Tischner, D., Manzl, C., Soratroi, C., Villunger, A., and Krumschnabel, G., Necrosis-like death can engage multiple pro-apoptotic Bcl-2 protein family members. Apoptosis, 2012. 17(11): p. 1197-209.
151. Ouimet, M., Franklin, V., Mak, E., Liao, X., Tabas, I., and Marcel, Y.L., Autophagy regulates cholesterol efflux from macrophage foam cells via lysosomal acid lipase. Cell Metab, 2011. 13(6): p. 655-67.
152. Martinez, F.O., Sica, A., Mantovani, A., and Locati, M., Macrophage activation and polarization. Front Biosci, 2008. 13: p. 453-61.
153. Kosteli, A., Sugaru, E., Haemmerle, G., Martin, J.F., Lei, J., Zechner, R., and Ferrante, A.W., Jr., Weight loss and lipolysis promote a dynamic immune response in murine adipose tissue. J Clin Invest, 2010. 120(10): p. 3466-79.
154. Baitsch, D., Bock, H.H., Engel, T., Telgmann, R., Muller-Tidow, C., Varga, G., Bot, M., Herz, J., Robenek, H., von Eckardstein, A., et al., Apolipoprotein E induces antiinflammatory phenotype in macrophages. Arterioscler Thromb Vasc Biol, 2011. 31(5): p. 1160-8.
155. Gonzalez-Navarro, H., Nong, Z., Freeman, L., Bensadoun, A., Peterson, K., and Santamarina-Fojo, S., Identification of mouse and human macrophages as a site of synthesis of hepatic lipase. J Lipid Res, 2002. 43(5): p. 671-5.
156. Babaev, V.R., Fazio, S., Gleaves, L.A., Carter, K.J., Semenkovich, C.F., and Linton, M.F., Macrophage lipoprotein lipase promotes foam cell formation and atherosclerosis in vivo. J Clin Invest, 1999. 103(12): p. 1697-705.
157. Babaev, V.R., Patel, M.B., Semenkovich, C.F., Fazio, S., and Linton, M.F., Macrophage lipoprotein lipase promotes foam cell formation and atherosclerosis in low density lipoprotein receptor-deficient mice. J Biol Chem, 2000. 275(34): p. 26293-9.
158. Van Eck, M., Zimmermann, R., Groot, P.H., Zechner, R., and Van Berkel, T.J., Role of macrophage-derived lipoprotein lipase in lipoprotein metabolism and atherosclerosis. Arterioscler Thromb Vasc Biol, 2000. 20(9): p. E53-62.
159. Soni, K.G., Lehner, R., Metalnikov, P., O'Donnell, P., Semache, M., Gao, W., Ashman, K., Pshezhetsky, A.V., and Mitchell, G.A., Carboxylesterase 3 (EC 3.1.1.1) is a major adipocyte lipase. J Biol Chem, 2004. 279(39): p. 40683-9.
160. Mezdour, H., Jones, R., Dengremont, C., Castro, G., and Maeda, N., Hepatic lipase deficiency increases plasma cholesterol but reduces susceptibility to atherosclerosis in apolipoprotein E-deficient mice. J Biol Chem, 1997. 272(21): p. 13570-5.
161. Nong, Z., Gonzalez-Navarro, H., Amar, M., Freeman, L., Knapper, C., Neufeld, E.B., Paigen, B.J., Hoyt, R.F., Fruchart-Najib, J., and Santamarina-Fojo, S., Hepatic lipase expression in macrophages contributes to atherosclerosis in apoE-deficient and LCAT-transgenic mice. J Clin Invest, 2003. 112(3): p. 367-78.
162. Mizushima, N., Yoshimori, T., and Levine, B., Methods in mammalian autophagy research. Cell, 2010. 140(3): p. 313-26.
163. Yamamoto, A., Tagawa, Y., Yoshimori, T., Moriyama, Y., Masaki, R., and Tashiro, Y., Bafilomycin A1 prevents maturation of autophagic vacuoles by inhibiting fusion between autophagosomes and lysosomes in rat hepatoma cell line, H-4-II-E cells. Cell Struct Funct, 1998. 23(1): p. 33-42.

164. Tanida, I., Minematsu-Ikeguchi, N., Ueno, T., and Kominami, E., Lysosomal turnover, but not a cellular level, of endogenous LC3 is a marker for autophagy. Autophagy, 2005. 1(2): p. 84-91.
165. Klionsky, D.J., Abeliovich, H., Agostinis, P., Agrawal, D.K., Aliev, G., Askew, D.S., Baba, M., Baehrecke, E.H., Bahr, B.A., Ballabio, A., et al., Guidelines for the use and interpretation of assays for monitoring autophagy in higher eukaryotes. Autophagy, 2008. 4(2): p. 151-75.
166. Mizushima, N., and Yoshimori, T., How to interpret LC3 immunoblotting. Autophagy, 2007. 3(6): p. 542-5.
167. Rubinsztein, D.C., Cuervo, A.M., Ravikumar, B., Sarkar, S., Korolchuk, V., Kaushik, S., and Klionsky, D.J., In search of an "autophagomometer". Autophagy, 2009. 5(5): p. 585-9.
168. Bjorkoy, G., Lamark, T., Pankiv, S., Overvatn, A., Brech, A., and Johansen, T., Monitoring autophagic degradation of p62/SQSTM1. Methods Enzymol, 2009. 452: p. 181-97.
169. Komatsu, M., Waguri, S., Koike, M., Sou, Y.S., Ueno, T., Hara, T., Mizushima, N., Iwata, J., Ezaki, J., Murata, S., et al., Homeostatic levels of p62 control cytoplasmic inclusion body formation in autophagy-deficient mice. Cell, 2007. 131(6): p. 1149-63.
170. Klionsky, D.J., Abdalla, F.C., Abeliovich, H., Abraham, R.T., Acevedo-Arozena, A., Adeli, K., Agholme, L., Agnello, M., Agostinis, P., Aguirre-Ghiso, J.A., et al., Guidelines for the use and interpretation of assays for monitoring autophagy. Autophagy, 2012. 8(4): p. 445-544.
171. Puissant, A., Fenouille, N., and Auberger, P., When autophagy meets cancer through p62/SQSTM1. Am J Cancer Res, 2012. 2(4): p. 397-413.
172. Ha, S.D., Ham, B., Mogridge, J., Saftig, P., Lin, S., and Kim, S.O., Cathepsin B-mediated autophagy flux facilitates the anthrax toxin receptor 2-mediated delivery of anthrax lethal factor into the cytoplasm. J Biol Chem, 2010. 285(3): p. 2120-9.
173. Rambold, A.S., Cohen, S., and Lippincott-Schwartz, J., Fatty acid trafficking in starved cells: regulation by lipid droplet lipolysis, autophagy, and mitochondrial fusion dynamics. Dev Cell, 2015. 32(6): p. 678-92.